

ALMA MATER STUDIORUM - UNIVERSITÀ DI BOLOGNA

SCUOLA DI INGEGNERIA E ARCHITETTURA

DIPARTIMENTO DEI

CORSO DI LAUREA in AUTOMATION ENGINEERING

TESI DI LAUREA

in

Industrial Robotics

**Condition Monitoring of a Belt-Based Transmission System
for Comau Racer3 Robots**

CANDIDATO

Roberta Tanzariello

RELATORE:

Chiar.mo Prof. Claudio Melchiorri

CORRELATORE/CORRELATORI

Ing. Marco Robusti

Anno Accademico 2016/2017

Sessione II

To my Mother and Alberto.

Condition Monitoring of a Belt-Based
Transmission System for Comau
Racer3 Robots

*In fin dei conti, non temete i momenti difficili.
Il meglio scaturisce da lì.*

Rita Levi Montalcini

ACKNOWLEDGEMENTS

I acknowledge and thank my Advisor Claudio Melchiorri for the opportunity given through the AlmaTong Project, my Co-Advisor Marco Robusti and the all team *PD Cost Engineering* of Comau Kunshan for all the advise, insight and discussion over my intership that has led to the completion of the work.

Special Thanks to Aldo Maria Bottero, Gagliano Alberto and the *Performance Engineering Team* for their knowledge shared and the support provided in the high frequency acquisition. I would like to thank all the PD department of Comau Italy for the assistance and conversation about the development of the test plan.

Additional thanks to Zhou Shaohua for the support in the installation of the FTP connection, Kuai Peng Loki and Cheng Yu for the simulation of the fault. Special thanks to Davide Miceli, Luca Menzio and the all team of Innovation Specialists for the collaboration and the support given in the implementation of the Automatic Acquisition.

ABSTRACT

This project has been developed in collaboration with Comau Robotics S.p.a and the main goal is the development in China of an Health Monitoring Process using vibration analysis. This project is connected to the activity of Cost Reduction carried out by the *PD Cost Engineering Department* in China.

The Project is divided in two part:

1. Data Acquisition
2. Data Analysis

An Automatic Acquisition of the *moni.log* file is carried out and is discussed in Chapter 1. As for the Data Analysis is concerned a data driven approach is considered and developed in frequency domain through the FFT transform and in time domain using the Wavelet transform.

In Chapter 2 a list of the techniques used nowadays for the Signal Analysis and the Vibration Monitoring is shown in time domain, frequency domain and time-frequency domain.

In Chapter 3 the state of art of the Condition Monitoring of all the possible machinery part is carried out from the evaluation of the spectrum of the current and speed.

In Chapter 4 are evaluated disturbances that are not related to a fault but belong to a normal behaviour of the system acting on the measured forces. Motor Torque Ripple and Output Noise Resolution are disturbance dependent on velocity and are mentioned in comparison to the one related to the configuration of the Robot.

In Chapter 5 a particular study case is assigned: the noise problem due to belt-based power transmission system of the axis three of a Racer 3 Robot in Endurance test. The chapter presents the test plan done including all the simulations.

In Chapter 6 all the results are shown demonstrating how the vibration analysis carried out from an external sensor can be confirmed looking at the spectral content of the speed and the current.

In the last Chapter the final conclusions and a possible development of this thesis are presented considering both a a Model of Signal and a Model Based approach.

Questo progetto è stato sviluppato in collaborazione di Comau S.p.A e l'obiettivo è lo sviluppo di un "Health Monitoring Process" usando l'analisi vibrazionale è inoltre connesso all'attività di riduzione dei costi portata avanti in Cina dal *PD Cost Engineering Department*.

Il progetto è diviso in due parti:

1. Acquisizione dei dati
2. Analisi dei dati

L'**Acquisizione Automatica** del file moni.log è discussa nel Capitolo 1. Un approccio di tipo **data driven** è stato usato per l'analisi dei dati e sviluppato nel dominio della frequenza secondo trasformata FFT e in dominio tempo frequenza usando la trasformata Wavelet.

Nel Capitolo 2 è riportato un elenco di tutte le tecniche usate oggi per l'analisi del segnale e il monitoraggio delle vibrazioni nel dominio del tempo, della frequenza o tempo frequenza.

Nel Capitolo 3 lo stato dell'arte riguardo il monitoraggio di componenti meccanici è sviluppato dall'analisi dello spettro di corrente e velocità.

Nel Capitolo 4 sono considerati disturbi non connessi a guasti ma appartenenti al comportamento nominale del sistema e che agiscono sulle **Forze**. "Motor Torque Ripple" e "Output Noise Resolution" sono disturbi che dipendono dalla velocità al contrario di quelli che dipendono dalla configurazione del Robot.

Nel Capitolo 5 è stato assegnato e sviluppato il problema di un rumore nella trasmissione dell'asse tre del Robot Racer 3 in Endurance Test. Il Capitolo riporta il progetto dei test condotti e le rispettive simulazioni.

Nel Capitolo 6 sono riportati e commentati tutti i risultati con l'intento di dimostrare come l'analisi della vibrazione fatta da un sensore esterno può essere confermata dallo spettro di corrente e velocità.

Nell'ultimo capitolo sono riportati le conclusioni finali e i possibili sviluppi della tesi basati sul Modello e sul Modello del segnale.

LIST OF FIGURE

Figure 1.1 Timings of action for maintenance	1
Figure 1.2 An integrated approach to CBM/PHM design.....	3
Figure 1.3 CBM/PHM online and offline phase.....	3
Figure 1.4 Part of the DFMEA considered in the project	4
Figure 1.4 Not Automatic Acquisition for the Collection of Moni.log.....	5
Figure 1.5 Map of the cells connected	6
Figure 1.6 Racer Family Robots	6
Figure 1.7 WinC5G interface	7
Figure 1.8 Automatic Acquisition performed.....	7
Figure 1.9 Features displayed during the Automatic Acquisition	8
Figure 2.1 Skewness, a measure of the symmetry of a distribution	11
Figure 2.2 The Kurtosis, a measure of the size of the side lobes of a distribution	12
Figure 2.3 Matrix representation of the DFT (note the rotating and imaginary part).....	14
Figure 2.4 Signal schematic classification	15
Figure 2.5 Time-frequency resolution of: (a) Short-Time-Fourier-Transform (STFT) and (b) Wavelet Transform (WT).....	17
Figure 2.6 Mother Wavelet with (a) large scale and (b) small scale	19
Figure 2.7 Subband Algorithm.....	21
Figure 2.8 The Haar Wavelet.....	23
Figure 3.1 FFT analysis-unbalance.....	27
Figure 3.2 Phase relationship-static unbalance	27
Figure 3.3 Phase relationship-couple unbalance	28
Figure 3.4 A belt driven fan/blower with an overhung rotor – the phase is measured in the axial direction	28
Figure 3.5 A belt-driven fan/blower – vibration	29
Figure 3.6 Eccentric rotor	29
Figure 3.7 An FFT of a bent shaft with bend near the shaft center	30
Figure 3.8 Note the 180 ° phase different in the axial direction.....	30
Figure 3.9 Angular misalignment	32
Figure 3.10 FFT of angular misalignment.....	32
Figure 3.11 Angular misalignment confirmed by phase analysis.....	33
Figure 3.12 Parallel misalignment.....	33
Figure 3.13 FFT of parallel misalignment	34
Figure 3.14 Radial phase shift of 180° is observed across the coupling	34
Figure 3.15 loose internal assembly graph	35
Figure 3.16 Loose fit.....	35
Figure 3.17 Mechanical looseness graph	36
Figure 3.18 Mechanical looseness	36
Figure 3.19 Structure looseness.....	37
Figure 3.20 Structure looseness graph.....	37
Figure 3.21 Characteristic frequencies of the bearing of axis 3.....	39
Figure 3.22 Small defect in the raceways of a bearing	40
Figure 3.23 More obvious wear in the form of pits	40
Figure 3.24 Wear is now clearly visible over the breath of the bearing	41
Figure 3.25 Severely damaged bearing in final stage of wear	41
Figure 3.26 Graph of a gearbox spectrum.....	42

Figure 3.27 Gear tooth wear	43
Figure 3.28 Gear tooth load	43
Figure 3.29 Gear eccentricity and backlash	44
Figure 3.30 Gear Misalignment.....	45
Figure 3.31 Gears-cracked.....	45
Figure 3.31 Sub-harmonic belt frequencies	46
Figure 3.32 Misalignment types (the pigeon toe and angle are classified as angular misalignment).....	47
Figure 3.33 Vibration due to sheave misalignment	47
Figure 3.34 Vibration due to sheave misalignment	48
Figure 3.35 High 1x with <i>FP</i> sidebands.....	50
Figure 3.36 All harmonics with <i>FP</i> sidebands.....	50
Figure 3.37 Rotor bar pass frequency	51
Figure 3.38 Eccentric Rotor	52
Figure 3.39 Stator defects	52
Figure 3.40 Synchronous motors	53
Figure 4.1 Dependence of the torque ripple on the angular position and current	58
Figure 4.2a Speed response to the torque disturbance.....	60
Figure 4.2b Control Scheme	60
Figure 4.3 TRC effect on ax 3 of a NJ 420-3.0 manipulator.....	61
Figure 4.4 Load Accelerator with TRC not active and active on a NJ4 175-2.5 manipulator	62
Figure 4.5 Basic adaptive copensator for sinusoidal disturbances	63
Figure 4.6 Feed forward disturbance compensation	64
Figure 4.7 The complete architecture of the adaptive compensator	64
Figure 5.1 Vibration power of the signal coming from the sensor	69
Figure 5.2 Vibration power versus velocity.....	69
Figure 6.1: Experimental test bed for displacement sensor	70
Figure 6.2: Experimental test bed for Accelerometer.....	71
Figure 6.3: CMOS type Micro Laser Distance Sensor HG-C.....	72
Figure 6.4: The interface TracerDAQ Pro	72
Figure 6.5.a and Figure 6.5.b: Position of the accelerometer in case of Axial and Radial vibration respectively.....	73
Figure 6.6: Axial vibration in term of voltage in nominal case 25% of the maximum speed.....	73
Figure 6.7: Axial vibration in Matlab environment 25% of the maximum speed	74
Figure 6.8: Belt-Transmission Based transmission.....	75
Figure 6.9 Angular Misalignment	76
Figure 6.10 Addition of Spacers for the simulation of the Angular Misalignment.....	76
Figure 6.11 FFT in case of Angular Misalignment	76
Figure 6.12 Parallel Misalignment.....	77
Figure 6.13 FFT in case of Parallel Misalignment.....	77
Figure 6.14 Limitations in space considered for the simulation of the fault Unbalance	78
Figure 6.15 FFT of the fault Unbalance	79
Figure 6.16 Simulation of Loseness.....	79
Figure 6.17 FFT in case of Loseness.....	80
Figure 6.19. Damaged Belt	80
Figure 6.20 Application of a Damaged Belt.....	80
Figure 6.21 Transversal Vibration in Nominal case.....	81
Figure 6.22 Transversal Vibration in case of fault.....	82
Figure 6.23 Reference Speed of the Motor.....	82

Figure 6.24 Time interval with Constant Velocity	82
Figure 6.25 Trace of the entire vibration obtained at constant velocity	83
Figure 6.26 Points from which the vibration is recorded.....	83
Figure 6.26 Delta of the entire vibration obtained at constant velocity.....	84
Figure 6.27 Delta of the first vibration obtained at constant velocity	85
Figure 6.28 Delta of the second vibration obtained at constant velocity.....	85
Figure 6.29 Haar 8 level wavelet transform used for the temporal analysis	86
Figure 6.30 Interval of time between vibration confirmed.....	86
Figure 6.31 Mass added for the simulation of Unbalance	87
Figure 6.32 FFT in case of Unbalance	87
Figure 6.32 Comparison in the spectrum of the speed with 5% of the maximum speed.....	88
Figure 6.33 Comparison in the spectrum of the speed with 75% of the maximum speed.....	88
Figure 6.34 Comparison in the spectrum of the voltage with 5% of the maximum speed	89
Figure 6.35 FFT in case of Internal Assembly Loseness.....	89
Figure 6.36 FFT of the voltage in case of Internal Assembly Loseness at 25% of the maximum speed: different rate are considered	90
Figure 6.37 FFT of the speed in case of Internal Assembly Loseness at 25% of the maximum speed	90

LIST OF TABLES

Table 1 Domain selection for diagnostic information.....	25
Table 2 Frequencies of the belt at different speed of the motor	66
Table 3 Frequencies of the Driver and Driven Pulley at different speed of the motor	66
Table 4 Inertia of the different components.....	68
Table 5 Resonance frequency and Tensioning frequency of the belt.....	68

CONTENTS

Acknowledgements	iii
Abstract	iv
List of Figure.....	vi
List of Tables	ix
1 Introduction to Structural Health Monitoring and Condition Based Monitoring.....	1
1.1 Introduction	1
1.2 Structural Health Monitoring Process	2
1.3 Scope of the Project.....	4
2 Vibration Monitoring and Signature Analysis	9
2.1 Signal Processing in Time domain	9
2.2 Signal Processing in Frequency domain.....	13
2.3 Signal Processing in Time-Frequency domain	14
2.3.1 Non-stationary signal processing.....	15
3 Condition Based Monitoring of Rotating Machine using Vibration Analysis.....	24
3.1 Introduction	24
3.2 Unbalance	25
3.3 Eccentric rotor	28
3.4 Bent Shaft.....	29
3.5 Misalignment.....	30
3.5.1 Angular misalignment	31
3.5.2 Parallel misalignment.....	33
3.6 Mechanical looseness	34
3.6.1 Internal assembly looseness	34
3.6.2 Looseness between machine to base plate	35
3.6.3 Structure looseness.....	36
3.7 Rolling element Bearing	37
3.8 Gearing defects.....	41
3.9 Belt defects	45
3.10 Electrical Problems	48
3.10.1 Rotor problems	49
4 Condition Based Monitoring of Disturbance acting on the measured Force	54
4.1 Velocity independent disturbance	54
4.2 Velocity dependent disturbance	56

4.2.1	Resolver output noise	56
4.2.2	Motor torque ripple	57
5	Case Study: Abnormal noise on Axis 3 due to a belt-based Power Transmission System	66
5.1	Belt Based Power transmission	66
5.1.1	Frequency Analysis	66
5.1.2	Temporal Analysis	68
6	Experimental Results.....	70
6.1	Experimental Set Up	70
6.1.1	High frequency acquisition from a signal controller	71
6.1.2	Acquisition from a displacement sensor	71
6.1.3	Acquisition from an accelerometer.....	73
6.2	Test Plan.....	74
6.2.1	NOMINAL CASE	75
6.2.2	ANGULAR MISALIGNMENT.....	75
6.2.3	PARALLEL MISALIGNMENT.....	77
6.2.4	EXCESSIVE LOAD UNBALANCE.....	78
6.2.5	INTERNAL ASSEMBLY LOSENESS	79
6.2.6	TOOTH SHEAR.....	80
6.3	Testing Result	81
6.3.1	Tooth shear	81
6.3.2	UNBALANCE.....	86
6.3.3	INTERNAL ASSEMBLY LOSENESS	89
7	Conclusions and Future Work	91
7.1	Conclusions	91
7.2	Future Work	91
	References	93
	Appendix.....	95

1 INTRODUCTION TO STRUCTURAL HEALTH MONITORING AND CONDITION BASED MONITORING

1.1 INTRODUCTION

Maintenance is a combination of science, art, and philosophy. The rationalization of maintenance requires a deep insight into what maintenance really is. Efficient maintenance is a matter of having the right resources in the right place at the right time. Maintenance can be defined as the total activities carried out in order to restore or renew an item to working condition, if fault is there. Maintenance is also defined as combination of action carried out to return an item to or restore it to an acceptable condition. The classification of maintenance according to timings of action for maintenance is shown in Figure 1.

Timing of Action	Maintenance
Operating to failure	Shutdown or breakdown
Fixed time based	Preventive
Condition based	Predictive or Diagnostic

Figure 1.1 Timings of action for maintenance

Every machine component behaves as an individual. Failure can take place earlier or later than recommended in case of preventive maintenance. It can be improved by condition based maintenance. Condition-based maintenance is defined as **“maintenance work initiated as a result of knowledge of the condition of an item from routine or continuous checking.”** It is carried out in response to a significant deterioration in a unit as indicated by a change in a monitored parameter of the unit condition or performance. Condition reports arise from human observations, checks, and tests, or from fixed instrumentation or alarm systems grouped under the name condition monitoring. It is here that one can make use of predictive maintenance by using a technique called signature analysis. Signature analysis technique is intended to continually monitor the health of the

Introduction to Structural Health Monitoring and Condition Based Monitoring
equipment by recording systematic signals or information derived from the form of mechanical vibrations, noise signals, acoustic and thermal emissions, change in chemical compositions, smell, pressure, relative displacement, and so on.

Condition-based maintenance differs from both failure maintenance and fixed-time replacement. It requires monitoring of some condition-indicating parameter of the unit being maintained. This contrasts with failure maintenance, which implies that no successful condition monitoring is undertaken and with fixed-time replacement which is based on statistical failure data for a type of unit. In general, condition based maintenance is more efficient and adaptable than either of the other maintenance actions. On indication of deterioration, that unit can be scheduled for shutdown at a time chosen in advance of failure, yet, if the production policy dictates, the unit can be run to failure. Alternatively, the amount of unnecessary preventive replacement can be reduced, while if the consequences of failure are sufficiently dire, the condition monitoring can be employed to indicate possible impending failure well before it becomes a significant probability.

The trend monitoring method for one or group of similar machines is possible if sufficient data of monitored parameters are available. It relates the condition of machine(s) directly to the monitored parameters. On the other hand, condition checking method is employed for a wide range of diagnostics instruments apart from human senses. Some of the recent developments in the form of CBM are proactive maintenance, reliability centered maintenance (RCM) and total productive maintenance (TPM).

1.2 STRUCTURAL HEALTH MONITORING PROCESS

Prognostic and health management refers specifically to the phase involved with predicting future behaviour, including remaining useful life (RUL), in terms of current operating state and the scheduling of required maintenance action to maintain system health. Detecting a component fault or incipient failure for a critical dynamic system and predicting its remaining useful life necessitate a series of studies that are intended to familiarize the CBM/PHM designer with the physics of the failure mechanisms associated with the particular system/component. Failure modes and effects criticality analysis (FMECA) forms the foundation for a good

Introduction to Structural Health Monitoring and Condition Based Monitoring
 CBM/PHM design. A FMECA study decides the severity of candidate failure mode, their frequency of occurrence and their testability. In fig. 1.2 the main modules of an integrated approach to CBM/PHM system design with the system-based components of the architecture: the feedback loops are intended to optimize the approach and complete the data collection and analysis steps that are essential inputs to the development of the fault diagnostic and prognostic algorithm.

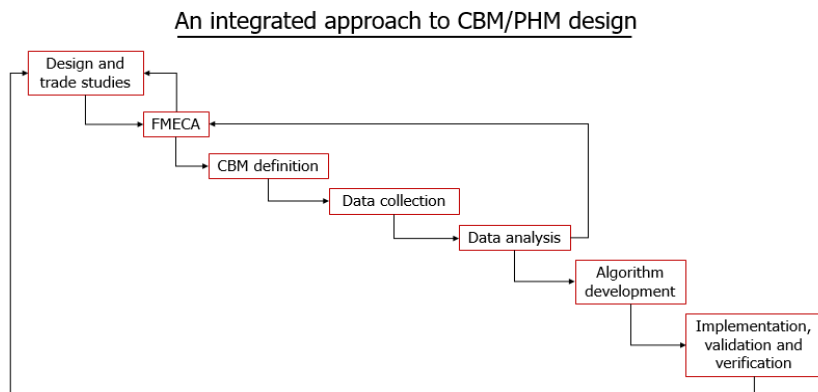


Figure 1.2 An integrated approach to CBM/PHM design

In Figure 1.3 is possible to identify a preliminary offline phase and an online phase of CBM/PHM. The online phase included obtaining machinery data from sensors, signal preprocessing, extracting the features that are the most useful for determining the current status or fault condition of the machinery, fault detection and classification, prediction of fault evolution and scheduling of required maintenance.

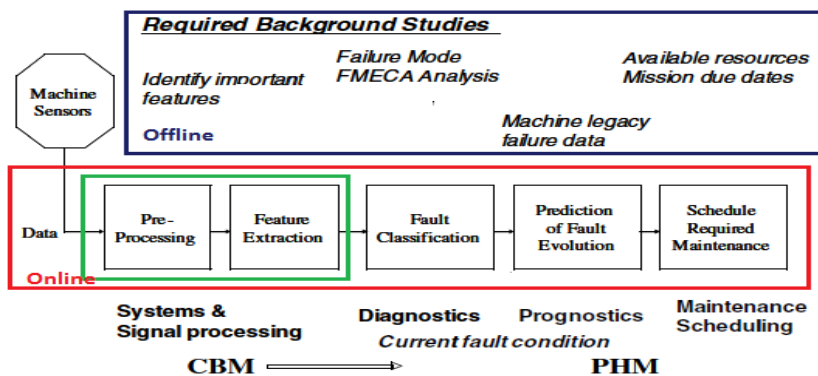


Figure 1.3 CBM/PHM online and offline phase

Introduction to Structural Health Monitoring and Condition Based Monitoring

The offline phase consists of the required background studies that must be performed offline prior to implementation of the online CBM phase and include determination of which features are the most important for machine condition assessment, the FMECA, the collection of machine legacy fault data to allow useful prediction of fault evolution, and the specification of available personnel resources to perform maintenance actions.

Failure mode and effect analysis (FMEA)

Understanding the physics of failure mechanisms constitute the cornerstone of good CBM/PHM system design. FMECA study attempts to relate failure events to their root causes. Towards this goal it addresses issues of identifying failure modes, their severity, frequency of occurrence, and testability; fault symptoms that are suggestive of the system's behavior under fault conditions; and the sensors/monitoring apparatus required to monitor and track the system's fault-symptomatic behaviors.

In this project the DFMEA of the transmission of axis 3 of the Racer 3 is taken under consideration for the development of the test plan described in Chapter 5. In Fig. 1.4 only a part of the file is visible.

Item #	Function/ Requirements	Potential Failure Mode	Potential Effect(s) of Failure	SEV	CLASS	Potential Cause(s)/ Mechanism(s) of Failure
CR82391704 REDUCER HARMONIC DRIVE SHF-20-80-2A-GR-SP	Transmit motion from axis 3 motor	No or difficult output shaft rotation	Working cycle not correctly accomplished. Dynamic performances compromised.	7	K	Centring diameters too tight (forced mounting)
				7		Insufficient lubrication
CR82391705 PULLEY GT3 Z= 45	Transmit motion from axis 3 motor	Irregular or no motion transmission	Working cycle not correctly accomplished. Precision decline. Greater current absorption.	7		Pulley contact against fixed parts
				7		Keyway slot machined not respecting geometrical tolerances.
CR82391706 PULLEY GT3 Z= 40	Transmit motion from axis 3 motor	Irregular or no motion transmission	Working cycle not correctly accomplished. Precision decline. Greater current absorption.	7		Pulley contact against fixed parts
				7		Keyway slot machined not respecting geometrical tolerances
TMC00000005954 BELT GATES 426-3MGT WIDTH=6	Transmit motion from axis 3 motor	Belt breakage or wearing	Working cycle not correctly accomplished. Precision decline	7	K	Pulley teeth profile not respected
				7		Insufficient mounting tension (resonance)
				7		Parallel misalignment between supporting pulleys
				7	K	Parallelism error between axis-3 motor's and reducer's fixing planes on arm CR82391701. Induce angular misalignment.
			Working cycle not accomplished	8		Excessive mounting tension till transmission block

Figure 1.4 Part of the DFMEA considered in the project

1.3 SCOPE OF THE PROJECT

The activity carried out during my internship in Comau Robotics Kunshan starts from the construction of an automatic system of acquisition as already done in Italy in order to perform a systematic monitoring of the robots.

Introduction to Structural Health Monitoring and Condition Based Monitoring

The file to be acquired automatically is called *moni.log* and contains inside all the information regarding current, velocity and acceleration for each joint of the manipulator.

In order to understand the common faults or alarm for each robot I started my activity recording all the fault with the *lastmoni.log* associated in an excel file. All the other information are also specified (Date, Type of test, Cycle number/ Time, Observed data, Type of failure, Axis, Component, Observed effect, Occurrence, Future effect, Action taken). The *lastmoni.log* are taken manually by ethernet cable.

Date	Robot	Time	Axis	Component	Observed effect	Occurrence	Future effect	Action taken
14/03/2017	Robot 3			robot 3				
15/03/2017	Robot 3			robot 3				
17/04/2017	Robot 3 340367			robot 3				
17/04/2017	Robot 3 340367			robot 3				
17/04/2017	Robot 3 340380			robot 3				
14/03/2017	Robot 3 340331	1274-22:34	2450	robot 3	Validation Error for Regressor Estimation			
14/03/2017	Robot 3 340333			robot 3	Robot 3 340333			
14/03/2017	Robot 3	12:13	242	robot 3	Robot 3 340333			
14/03/2017	Robot 3	1:0:13	7	robot 3	Robot 3 340333			
15/03/2017	Robot 3 340333			robot 3	Robot 3 340333			
15/03/2017	Robot 3 340366			robot 3	Robot 3 340366			
15/03/2017	Robot 3 340380			robot 3	Robot 3 340380			
15/03/2017	Robot 3 340380	1:0:38	12	robot 3	Robot 3 340380			

Figure 1.4 Not Automatic Acquisition for the Collection of *Moni.log*

To start an automatic acquisition we set an FTP connection in order to make all the robots visible and controllable by remote first introducing Internet in all the cells and then setting properly the Subnet Mask and the Gateway from the Touch Pendant of the Robots. In the following picture is shown the map of all the cells connected divided according to the test going on: MFG-Manufacturing and Sign Off area. Endurance testing and Validation Testing for components.

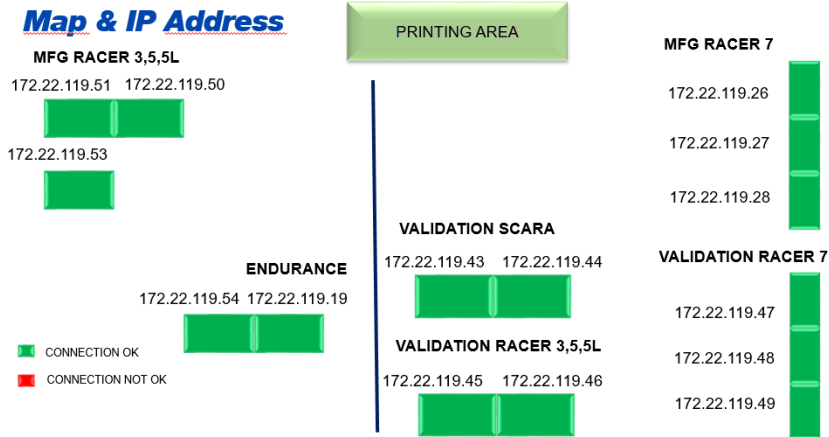


Figure 1.5 Map of the cells connected

The Robots considered for the acquisition are the Racer Family (Racer 3, 5 and 5L) Racer Plus 7-1.4, 7-1.0 see Figure 1.6 and the Scara Robot (Rebel). The vibration analysis is performed instead on the Racer 3 robot in chapters 6.

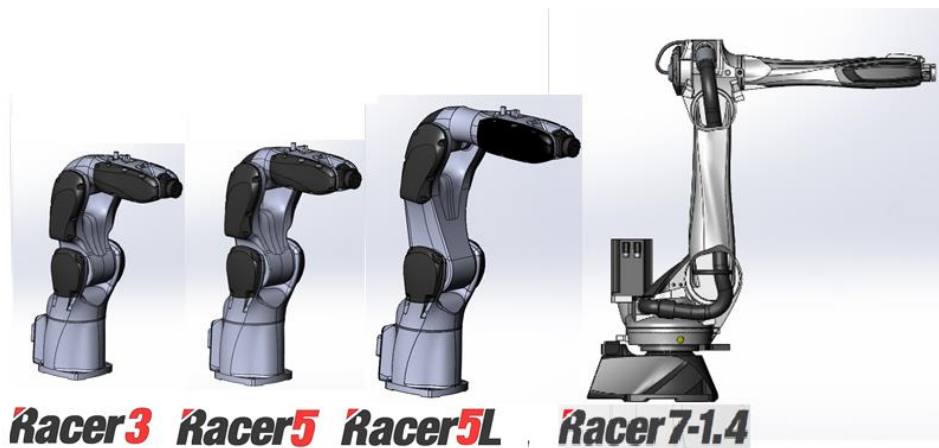


Figure 1.6 Racer Family Robots

The WinC5G is the PC interface for the C5G Robot Controller. From the terminal is possible to see the actual status of the Robot. Is possible also to have the access to the program active the last moni.log, the history of the error and the alarm happened.



Figure 1.7 WinC5G interface

Without changing the standard run in program is possible to acquire automatically all the lastmoni.log from all the robots in the plant. The Software Moni Collector used is provided by Innovation Specialists in Comau Italy.

Results		Messages					
	id_cycle	dt_logged	id_sys	file_name	robot_program	cycle_time	
1	2	2017-04-26 07:27:01.000	3200627	R1C_3200627_Racer3_170426_072701.log	Racer3	131.736	
2	7	2017-05-15 15:56:57.000	2222613	CNTRLC5G_2222613_RACER-7-1.4--7_170515_155657.log	RACER-7-1.4--7	277.76	
3	13	2017-07-24 14:22:55.000	2200002	R1C_2200002_Rebel-S6-0.60_170724_142255.log	Rebel-S6-0.60	116.28	
4	12	2017-07-24 14:34:22.000	2200002	R1C_2200002_Rebel-S6-0.60_170724_143422.log	Rebel-S6-0.60	116.276	
5	11	2017-07-24 14:49:39.000	2200002	R1C_2200002_Rebel-S6-0.60_170724_144939.log	Rebel-S6-0.60	116.364	
6	10	2017-07-24 14:53:28.000	2200002	R1C_2200002_Rebel-S6-0.60_170724_145328.log	Rebel-S6-0.60	116.368	
7	9	2017-07-24 15:12:35.000	2200002	R1C_2200002_Rebel-S6-0.60_170724_151235.log	Rebel-S6-0.60	116.328	
8	8	2017-07-24 16:02:15.000	2200002	R1C_2200002_Rebel-S6-0.60_170724_160215.log	Rebel-S6-0.60	116.376	
9	6	2017-07-25 10:56:15.000	2200002	R1C_2200002_Rebel-S6-0.60_170725_105615.log	Rebel-S6-0.60	116.384	
10	5	2017-07-25 11:00:04.000	2200002	R1C_2200002_Rebel-S6-0.60_170725_110004.log	Rebel-S6-0.60	116.496	
11	4	2017-07-25 11:03:54.000	2200002	R1C_2200002_Rebel-S6-0.60_170725_110354.log	Rebel-S6-0.60	116.488	
12	3	2017-07-25 11:26:50.000	2200002	R1C_2200002_Rebel-S6-0.60_170725_112650.log	Rebel-S6-0.60	116.396	
13	1	2017-07-25 17:43:06.000	2200011	R1C_2200011_Rebel-S6-0.60c_170725_174306.log	Rebel-S6-0.60c	101.896	
14	15	2017-07-25 17:49:45.000	2200011	R1C_2200011_Rebel-S6-0.60c_170725_174945.log	Rebel-S6-0.60c	101.864	
15	16	2017-07-25 17:53:05.000	2200011	R1C_2200011_Rebel-S6-0.60c_170725_175305.log	Rebel-S6-0.60c	102.044	

Figure 1.8 Automatic Acquisition performed

Is so also possible to control defined features in real time as shown in Fig. 1.9.

fk_cycle	ax	f_s_ax	t_s_ax	rms_ax	mean_ax	str_ax	inv_ax	fit_ax	i_peak_ax	i_max_err_ax	p_avg_ax	p_max_ax
12	1	0.07	0.00	1.71	0.0011	827.842532684	238	0.0	0.01181	0.676546812	0.0098	0.00525
13	1	0	0	0	0	2292.372367397	117	0	0	0	0	0
13	2	0	0	0	0	1269.037067175	303	0	0	0	0	0
13	3	0	0	0	0	902.055407174	103	0	0	0	0	0
13	4	0	0	0	0	827.955467701	282	0	0	0	0	0
15	1	0.26...	0.01...	0.00...	0.0692...	2028.136510611	196	0.0...	0.05103...	10.6080472...	0.0003...	0.00440...
15	2	0.41...	0.01...	0.00...	0.4647...	1235.357356023	249	0.0...	0.01461...	4.700931907	0.0285...	0.07004...
15	3	0.04...	0.00...	0.00...	0.2116...	807.072117209	100	0.0...	0	5.532020688	0.0004...	0.00103...
15	4	0.02...	0.00...	0.00...	0.0525...	829.594623059	62	0.0...	0.00589...	0.940480605	0.0005...	0.00114...
16	1	0.21...	0.01...	0.00...	0.0637...	2026.871028662	198	0.0...	0.02577...	8.78311348	0.0057...	0.01184...
16	2	0.24...	0.01...	0.00...	1.4136...	1235.352697404	246	0.0...	0.02767...	4.709700346	0.0025...	0.02655...
16	3	0.04...	0.00...	0.00...	0.1949...	807.056199193	100	0.0...	0	5.532020688	0.0032...	0.00200...
16	4	-1	0.00...	0.00...	0.0153...	829.589635849	62	0.0...	0.03353...	0.933283396	0.0093...	0.03273...

Features

Figure 1.9 Features displayed during the Automatic Acquisition

2 VIBRATION MONITORING AND SIGNATURE ANALYSIS

The word signature has been coined to designate signal patterns which characterize the state or condition of a system from which they are acquired. Signatures are extensively used as a diagnostic tool for mechanical system. In many cases, some kind of signal processing is undertaken on those signals in order to enhance or extract specific features of such vibration signatures. It is very important to consider the type and range of transducers used as pickup for capturing vibration signal. Signature-based diagnostic makes extensive use of signal processing techniques involving one or more methods to deal with the problem of improvement in the signal to noise ratio. Vibration-based monitoring techniques have been widely used for detection and diagnosis of bearing defects for several decades. These methods have traditionally been applied, separately in time and frequency domains. A time-domain analysis focuses principally on statistical characteristics of vibration signal such as peak level, standard deviation, skewness, kurtosis, and crest factor. A frequency domain approach uses Fourier methods to transform the time-domain signal to the frequency domain, where further analysis is carried out, using both the time and space domain according to the Multi-resolution Analysis.

2.1 SIGNAL PROCESSING IN TIME DOMAIN

To use information from CBM/PHM sensors for diagnosis, one must know how to compute statistical moments, which we describe in this section. The fourth moment, kurtosis, has been found to be especially useful to capture the bang-bang types of motion owing to loose or broken components.

Given a random variable, its n th moment is computed using the ensemble average

$$E(x^P) = \int x^P f(x) dx$$

With $f(x)$ the probability density function (PDF). If a random variable is ergodic, then its ensemble averages can be approximated by its time averages.

Moments about Zero and Energy

Given a discrete time series x_k , the pth moment over the time interval [1, N] is given by

$$\frac{1}{N} \sum_{k=1}^N x_k^p$$

The first moment is the (sample) mean value

$$\bar{x} = \frac{1}{N} \sum_{k=1}^N x_k$$

And the second moment is the moment of the inertia

$$\frac{1}{N} \sum_{k=1}^N x_k^2$$

As N become larger, these better approximate the corresponding ensemble averages. The energy of the time series over the time interval [1, N] is given by

$$\sum_{k=1}^N x_k^2$$

And the root mean square value (RMS) is

$$\sqrt{\frac{1}{N} \sum_{k=1}^N x_k^2}$$

Moments about the Mean.

Given a time series x_k , the pth moment about the mean over the time interval [1, N] is given by

$$\frac{1}{N} \sum_{k=1}^N (x_k - \bar{x})^p$$

The second moment about the mean is the sample variance

$$\sigma^2 = \frac{1}{2} \sum_{k=1}^N (x_k - \bar{x})^2$$

Where σ is the standard deviation. Unfortunately, the sample variance is a biased estimate of the true ensemble variance, so in statistics one often uses instead the unbiased variance:

$$s^2 = \frac{1}{N-1} \sum_{k=1}^N (x_k - \bar{x})^2$$

The third moment about the mean contains information about the symmetry of a distribution. A commonly used measure of symmetry is the skewness

$$\frac{1}{N\sigma^3} \sum_{k=1}^N (x_k - \bar{x})^3$$

Skewness vanishes for symmetry distributions and is positive (negative) if the distribution develop along tail to the right (left) of the mean $E(x)$. It measures the amount of spread of the distribution in either direction from the mean. Both probability density functions (PDF) of Fig 2.1 have the same mean and standard deviation. The one on the left is positively skewed. The one on the right is negatively skewed.

Also useful define the kurtosis, as

$$\frac{1}{N\sigma^4} \sum_{k=1}^N (x_k - \bar{x})^4 - 3$$



Figure 2.1 Skewness, a measure of the symmetry of a distribution

The kurtosis measures the contribution of the tails of the distribution, as illustrated in Fig. 2.2. The PDF on the right has higher kurtosis than the one on the left.

It is more peaked at the center, and it has fatter tails. It is possible for a distribution to have the same mean, variance and skew and not have the same kurtosis measurement.

Correlation, Covariance, Convolution

The (auto)correlation is given by

$$R_x = \frac{1}{N} \sum_{k=1}^N x_k x_{k+n}$$

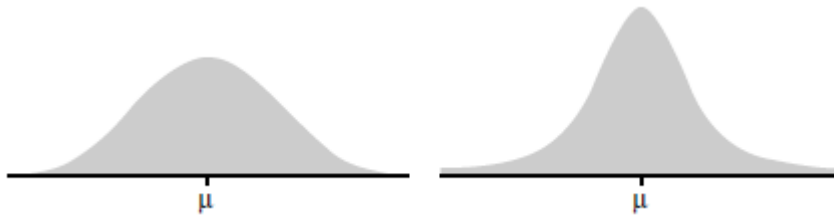


Figure 2.2 The Kurtosis, a measure of the size of the side lobes of a distribution

Note that $NR_x(0)$ is the energy. The (auto)covariance is given as

$$P_x(n) = \frac{1}{N} \sum_{k=1}^N (x_k - \bar{x})(x_{k+n} - \bar{x})$$

Note that $P_x(0) = \sigma^2$.

Given two time series x_k and y_k the cross correlation is

$$R_{xy}(n) = \frac{1}{N} \sum_{k=1}^N x_k y_{k+n}$$

And the cross-covariance is

$$P_{xy}(n) = \frac{1}{N} \sum_{k=1}^N (x_k - \bar{x})(y_{k+n} - \bar{y})$$

Often used in statistics in Pearson's correlation, which is defined as

$$r = \frac{\sum x_k y_k - \frac{\sum x_k \sum y_k}{N}}{\sqrt{\left[\sum x_k^2 - \frac{(\sum x_k)^2}{N} \right] \left[\sum y_k^2 - \frac{(\sum y_k)^2}{N} \right]}}$$

The discrete time convolution for N point sequences is given as

$$x * y(n) = \sum_{k=0}^{N-1} x_k y_{n-k}$$

Which is nothing more than polynomial multiplication. It is interesting to note that the correlation is expressed in terms of the convolution operator by

$$R_{xy}(n) = \frac{1}{N} \sum_{k=1}^N x_k y_{k+n} = \frac{1}{N} x(k) * y(-k)$$

2.2 SIGNAL PROCESSING IN FREQUENCY DOMAIN

Discrete Fourier Transform

The continuous infinite integrals of the Fourier transform become finite sums, usually expressed as

$$G(k) = (1/N) \sum_{n=0}^{N-1} g(n) \exp(-j2\pi kn/N)$$

$$g(n) = \sum_{k=0}^{N-1} G(k) \exp(j2\pi kn/N)$$

This version, known as the discrete Fourier transform (DFT), corresponds most closely to the Fourier series in that the forward transform is divided by the length of record N to give correctly scaled Fourier series components. If the DFT is used with other types of signals, for example transients or stationary random signals, the scaling must be adjusted accordingly as discussed below. The forward DFT operation can be understood as the matrix multiplication

$$G_k = \frac{1}{N} W_{kn} g_n$$

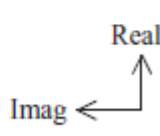
$$\begin{pmatrix} G_0 \\ G_1 \\ G_2 \\ G_3 \\ G_4 \\ G_5 \\ G_6 \\ G_7 \end{pmatrix} = \frac{1}{8} \begin{bmatrix} \uparrow & \uparrow & \uparrow & \uparrow & \uparrow & \uparrow & \uparrow & \uparrow \\ \uparrow & \nearrow & \rightarrow & \searrow & \downarrow & \swarrow & \leftarrow & \nwarrow \\ \uparrow & \rightarrow & \downarrow & \leftarrow & \uparrow & \rightarrow & \downarrow & \leftarrow \\ \uparrow & \searrow & \leftarrow & \swarrow & \downarrow & \nwarrow & \rightarrow & \swarrow \\ \uparrow & \downarrow & \uparrow & \downarrow & \uparrow & \downarrow & \uparrow & \downarrow \\ \uparrow & \swarrow & \rightarrow & \nwarrow & \downarrow & \swarrow & \leftarrow & \nwarrow \\ \uparrow & \leftarrow & \downarrow & \rightarrow & \uparrow & \leftarrow & \downarrow & \rightarrow \\ \uparrow & \nwarrow & \leftarrow & \swarrow & \downarrow & \nwarrow & \rightarrow & \swarrow \end{bmatrix} \begin{pmatrix} g_0 \\ g_1 \\ g_2 \\ g_3 \\ g_4 \\ g_5 \\ g_6 \\ g_7 \end{pmatrix}$$


Figure 2.3 Matrix representation of the DFT (note the rotating and imaginary part)

Where G_k represents the vector of N frequency components, the $G(k)$, while g_k represents the N time samples $g(n)$. W_{kn} represents a square matrix of unit vectors $\exp(-j2\pi kn/N)$ with angular orientation depending on the frequency index k (the rows) and time sample index n (the columns). This is illustrated graphically. For $k=0$ the zero frequency value $G(0)$ is simply the mean value of the time samples $g(n)$ as would be expected. For $k=1$ the unit vector rotates $-1/N$ th of a revolution for each time sample increment resulting in one complete (negative) revolution after N samples. For higher values of k rotation speed is proportionally higher. For $k=N/2$ (half the sampling frequency, the **so called 'Nyquist frequency'**) the vector turns through $-\pi$ for each time sample, but it is not possible to see in which direction it has turned. For $k>N/2$ the vector turns through less than π (in the negative direction) but is more easily interpreted as having turned through **less than π (in the opposite direction) and thus if the time signal has been low pass filtered at half the sampling frequency (as should always be the case) the second half of G_k will contain the negative frequency components ranging from minus one-half of the Nyquist frequency to just below zero.**

2.3 SIGNAL PROCESSING IN TIME-FREQUENCY DOMAIN

As previously mentioned spectral methods such as Fourier transform assume stationary signals. However, localized defects generally introduce non-stationary signal components, which cannot be properly described by ordinary spectral methods. This drawback can be overcome by the use of the short-time Fourier transform (STFT) that is a Fourier transform applied to many short time windows. However, narrow time windows mean poor frequency resolution. This trade-off

between time and frequency resolution is the main disadvantage of the STFT, which can be solved by the use of other time-frequency techniques such as Wigner-Ville distribution (WVD) and Continuous wavelet transform (CWT). The WVD provides better time-frequency resolutions compared to the STFT, but produces severe interference terms.

2.3.1 Non-stationary signal processing

Figure 2.4 depicts the classical division into different signal types, which actually is the division into stationary and non-stationary signals.

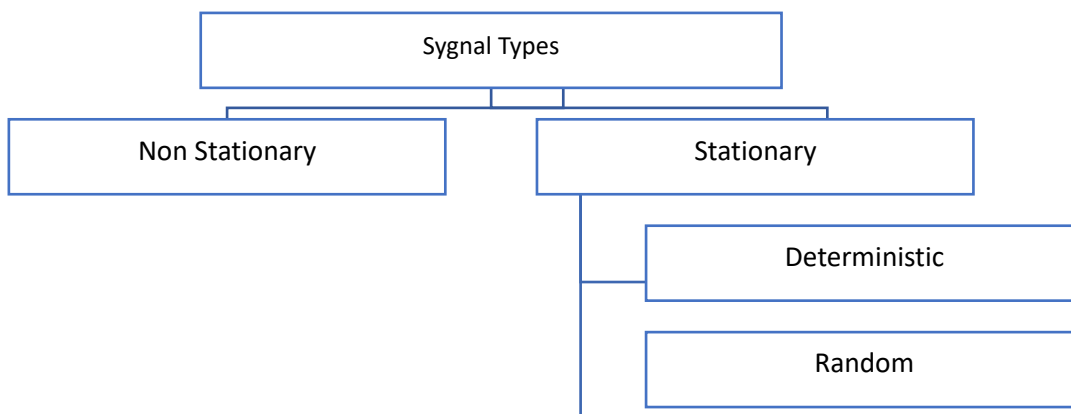


Figure 2.4 Signal schematic classification

For practical purposes it is sufficient to interpret stationary functions as being those whose average properties do not vary with time and are thus independent of the particular sample record used to determine them. While the term “non-stationary” cover all signals which do not satisfy the requirements for stationary ones.

Several signal processing techniques are applied to stationary signals in both time and frequency domain for diagnostic purpose of rotating machines, such as timesynchronous average (TSA), power spectral density (PSD) amplitude and phase demodulations and cepstrum analysis. Subsequently, the main theoretical background on timefrequency analysis is reported below highlighting the time-frequency techniques, i.e. Continuous Wavelet Transform (CWT), which overcome the well known problem of fixed time-frequency resolution of the Short Time Fourier Transform.

From the Short time Fourier Transform to Continuous Wavelet Transform
Time-frequency analysis offers an alternative method to signal analysis by presenting information in both the time domain and in frequency one.
For stationary signal the genuine approach is the well-known Fourier transform

$$X(f) = \int_{-\infty}^{+\infty} x(t)e^{-2\pi jft} dt$$

As long as we are satisfied with linear time invariant operators, the Fourier transform provides simple answer to most questions. Its richness makes it suitable for a wide range of applications such as signal transmissions or stationary signal processing. However if we are interested in transient phenomena the Fourier transform becomes a cumbersome tool. De facto, as one can see from the previous equation the Fourier coefficients $X(f)$ are obtained by inner products of $x(t)$ with sinusoidal waves $e^{2\pi jft}$ with infinite duration in time. Therefore, the global information makes it difficult to analyze any local property of $x(t)$, because any abrupt change in the time signal is spread out over the entire frequency axis. As a consequence the Fourier transform cannot be adapted to non-stationary signal.

In order to overcome this difficulty a “local frequency” parameter is introduced in the Fourier transform. So that the “local” Fourier transform looks at the signal through a window over which the signal is approximately stationary.

the Fourier transform was first adapted by Gabor to define a two dimensional time-frequency representation. Let $x(t)$ a signal which is stationary when looked through a limited extent window $g(t)$, which is centered at a certain time location τ , then the Short time Fourier Transform is defined as

$$STFT = \int_{-\infty}^{+\infty} x(t)g^*(t - \tau)e^{-2\pi jt} dt$$

Where $*$ denote the complex conjugate. Even if many properties of the Fourier transform carry over to the STFT, the signal analysis strongly depends on the choice of the window $g(t)$. In other words, the STFT may be seen as modulated filter bank. De facto, for a given frequency f the STFT filters the signal at each time

with a band pass filter having as impulse response the window function modulated to that frequency. From this dual interpretation of the STFT, some considerations about time and frequency transform resolutions can be granted. De facto, both time and frequency resolutions are linked to the energy of the window $g(t)$, therefore their product is lower bounded by the uncertainty principle, or Heisenberg inequality, which states that:

$$\Delta t \Delta f \geq \frac{1}{4\pi}$$

So, resolution in time and frequency cannot be arbitrarily small and once a window has been chosen, the time-frequency resolution is fixed over the entire time-frequency plane, since the same window is used at all frequencies, Figure 2.5 (a). In order to overcome the resolution limitation of the STFT, one can think at a filter bank in which the time resolution increases with the central frequency of the analysis filter (**Vetterli**). Therefore, the frequency resolution (Δf) is imposed to be proportional to f :

$$\frac{\Delta f}{f} = c$$

where c is a constant. In other words, the frequency response of the analysis filter is regularly spaced in a logarithmic scale. This way, Heisenberg inequality is still satisfied, but the frequency resolution becomes arbitrarily good at high frequencies and the time resolution become arbitrarily good at low frequency as well Fig. 2.5 (b).

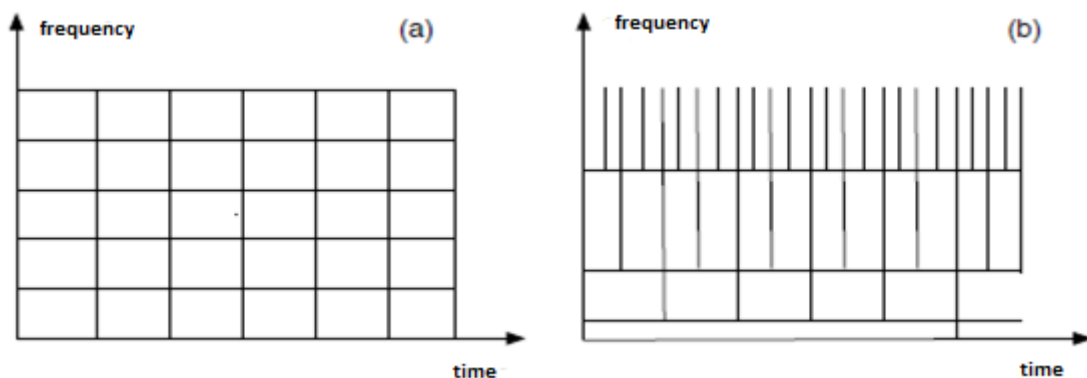


Figure 2.5 Time-frequency resolution of: (a) Short-Time-Fourier-Transform (STFT) and (b) Wavelet Transform (WT)

the above idea of multiresolution analysis is followed in CWT and overcome the limitation of the STFT and is defined as follows (S. Mallat, 1999):

$$CWT(s, \tau) = \int_{-\infty}^{+\infty} x(t) \psi_s^* \left(\frac{t - \tau}{s} \right) dt$$

Where s and τ are the scale factor and the translation parameter respectively

while $\psi_s(t)$ is called the mother wavelet

$$\psi_s(t) = \frac{1}{\sqrt{s}} \psi\left(\frac{t}{s}\right)$$

The term $1/\sqrt{s}$ of the right end side of equation is used for energy normalization. Some considerations about the time-frequency resolution of the CWT can be obtained by analyzing the Fourier transform of the mother wavelet ψ

$$F \left\{ \frac{1}{\sqrt{s}} \psi \left(\frac{t}{s} \right) \right\} = \psi(sf)$$

Therefore, if $\psi(t)$ has a “bandwidth” Δf with a central frequency f_0 , $\psi(st)$ has a “bandwidth” $\Delta f / s$ with a central frequency f_0/s .

The link between scale and frequency is straightforward, de facto as the scale increases the wavelet becomes spread out in time and so only long-time behavior of the signal is taken into account. On the contrary as the scale decreases the wavelet becomes shrunked in time and only short-time behavior of the signal is taken into account. In other words, large scales mean global views, while very small scales mean detailed views. Figure 2.6 plots a mother wavelet for two different values of the scale parameter s .

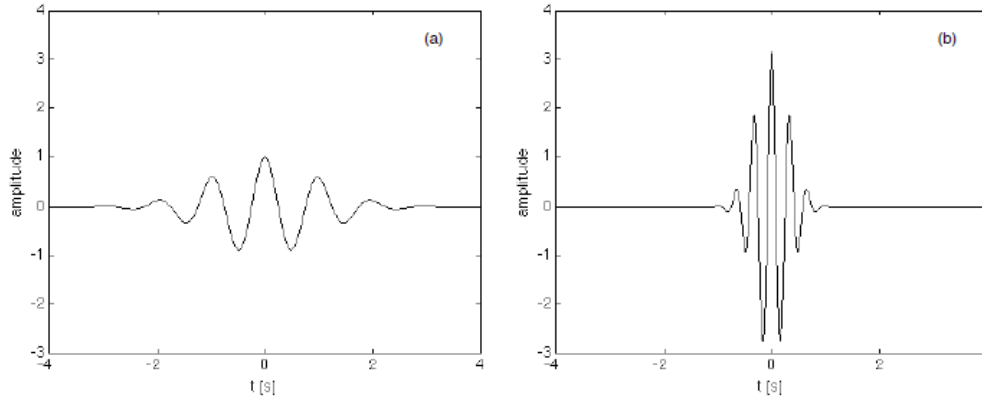


Figure 2.6 Mother Wavelet with (a) large scale and (b) small scale

There are a number of basis functions that can be used as the mother wavelet for Wavelet Transformation. Since the mother wavelet produces all wavelet functions used in the transformation through translation and scaling, it determines the characteristics of the resulting Wavelet Transform. Therefore, the details of the particular application should be taken into account and the appropriate mother wavelet should be chosen in order to use the Wavelet Transform effectively.

Discrete Wavelet Transform

It turned out quite remarkably that instead of using all possible scales only dyadic scales can be utilized without any information loss. Mathematically this procedure is described by the discrete wavelet transform (DWT) which is expressed as:

$$DW(j, k) = \sqrt{2^j} \int_{-\infty}^{+\infty} f(t) \psi^*(2^j t - k) dt$$

where $DW(j, k)$ are the wavelet transforms coefficients given by a two-dimensional matrix, j is the scale that represents the frequency domain aspects of the signal and k represents the time shift of the mother wavelet. $f(t)$ is the signal that is analyzed and ψ the mother wavelet used for the analysis (ψ^* is the complex conjugate of ψ). The inverse discrete wavelet transform can be expressed as (Kostropoulos, 1992):

$$f(t) = c \sum_j \sum_k DW(j, k) \psi_{j,k}(t)$$

where c is a constant depending only on ψ . Practically DWT is realized by the algorithm known as Mallat's algorithm or sub-band coding algorithm (Mallat, 1989).

The DWT of a signal x is calculated by passing it through a series of filters. First the samples are passed through a low pass filter l_d with impulse response h resulting in a convolution of the two. The signal is also decomposed simultaneously using a high-pass filter h_d . The output from the high-pass filter gives the detail coefficients and the output from the low-pass filter gives the approximation coefficients. The two filters h, g are not arbitrarily chosen but are related to each other and they are known as a quadrature mirror filter.

Thus, the extracted signal coefficients from the HP filter and after down sampling are called the detail coefficients of the first level (D_1) (Bicker, 2016). These coefficients contain the high frequency information of the original signal, while, the coefficients that are extracted from the LP filter and after the down sampling process are called the approximation coefficients of the first level (A_1). The low frequency information of the signal is hidden in these coefficients. This can be expressed mathematically as (Vivas et al., 2013):

$$y_{high}[k] = \sum_n x[n] * g[2k - n]$$

$$y_{low}[k] = \sum_n x[n] * h[2k - n]$$

where $y_{high}[k]$ and $y_{low}[k]$ are the outputs of the high-pass and low-pass filters respectively, after down-sampling by 2. After obtaining the first level of decomposition, the above procedure can be repeated again to decompose cA_1 into another approximation and detail coefficients. This procedure can be continued successively until a pre-defined certain level up to which the decomposition is required to be found. At each decomposition level, the corresponding detail and approximation coefficients have specific frequency bandwidths given by

1. $[0 - F_s/2^{l+1}]$ for the approximation coefficients (A_l)
2. $[F_s/2^{l+1} - F_s/2^l]$ for the detailed one (D_l)

where F_s is the sampling frequency (Sawicki et al., 2009, Vivas et al., 2013). However, at every level, the filtering and down-sampling will result in half the number of samples (half the time resolution) and half the frequency band (double the frequency resolution). Also, due to the consecutive down sampling by 2, the total number of samples in the analyzed signal must be a power of 2 (Ghods and Lee, 2014). By concatenating all coefficients starting from the last level of decomposition, the DWT of the original signal is then produced, and it will have the same number of samples as the original signal. The number of decomposition levels is identified by the lowest frequency band needed to be traced, and a higher number of decomposition levels are required if very low frequency band is investigated. However, the highest decomposition level that can be achieved is up to that the individual details consist of a single sample (Misiti et al., 1997).

Since half the frequencies of the signal have now been removed, half the samples can be discarded according to Nyquist's rule. The filter outputs are then sub-sampled by 2. This decomposition has halved the time resolution since only half of each filter output characterizes the signal. However, each output has half the frequency band of the input so the frequency resolution has been doubled. The approximation is then itself split into a second-level approximation and detail and the process is repeated as many times as it is desirable. This procedure can be repeated as many times as desirable by the user resulting in N levels of decomposition.

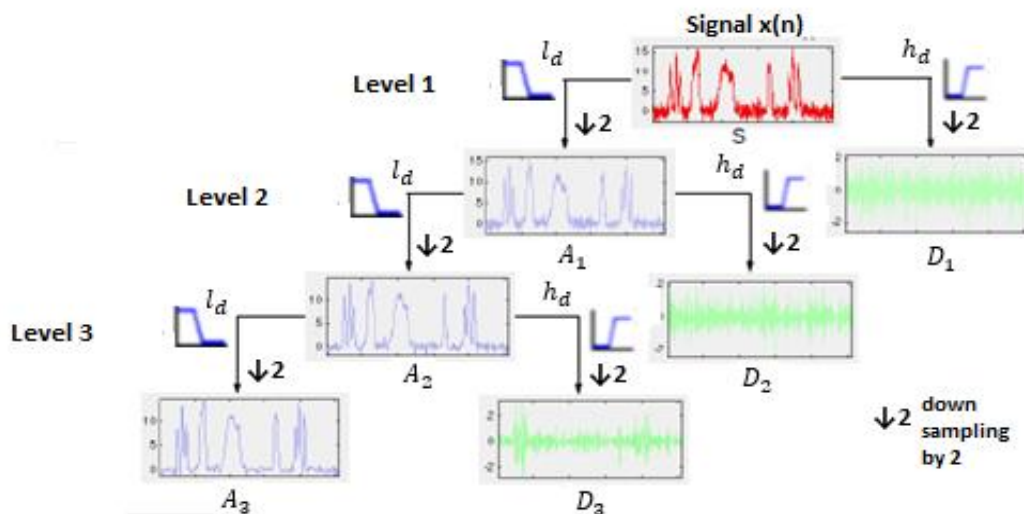


Figure 2.7 Subband Algorithm

The number of decomposition levels N is related to the sampling frequency of the signal being analyzed (f_s). In order to get an approximation signal containing frequencies below frequency f , the number of decomposition levels that has to be considered is given by (Antonino-Daviu, Jover, Riera, Arkkio, & Roger-Folch, 2007)

$$N = \text{int}\left(\frac{\log\left(\frac{f_s}{f}\right)}{\log(2)}\right)$$

Haar Wavelet

Haar functions have been used from 1910 when they were introduced by the Hungarian mathematician Alfred Haar. The Haar transform is one of the earliest examples of what is known now as a compact, dyadic, orthonormal wavelet transform. The Haar function, being an odd rectangular pulse pair, is the simplest and oldest orthonormal wavelet with compact support. Thanks to their useful features and possibility to provide a local analysis of signals, the Haar functions appear very attractive in many applications as for example, image coding, edge extraction, and binary logic design.

In mathematics is a sequence of rescaled “square-shaped” functions which together form a wavelet family or basis. The technical disadvantage of the Haar wavelet is that it is not continuous, and therefore not differentiable. This property can however be an advantage for the analysis of signals with sudden transitions, such as **monitoring of tool failure in machines**. The Haar wavelet’s mother function $\psi(t)$ can be described as:

$$\psi(t) = \begin{cases} 1 & 0 \leq t < 1/2 \\ -1 & \frac{1}{2} \leq t < 1 \\ 0 & \text{otherwise} \end{cases}$$

Its scaling function $\phi(t)$ can be described as:

$$\phi(t) = \begin{cases} 1 & 0 \leq t < 1 \\ 0 & \text{otherwise} \end{cases}$$

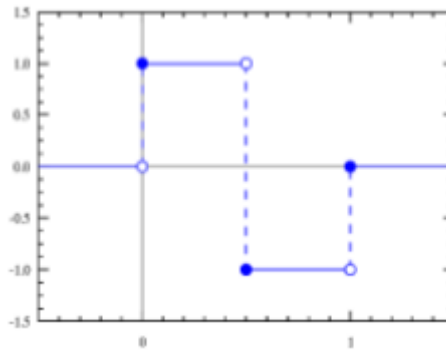


Figure 2.8 The Haar Wavelet

Haar properties

The Haar wavelet has several notable properties:

1. Any continuous real function with compact support can be approximated uniformly by linear combinations of $\phi(t)$, $\phi(2t)$, $\phi(4t)$, $\phi(2^n t)$,..... **and** their shifted functions. This extends to those function spaces where any function therein can be approximated by continuous functions.
2. Any continuous real function on $[0, 1]$ can be approximated uniformly on $[0, 1]$ by linear combinations of the constant function 1, $\psi(t)$, $\psi(2t)$, $\psi(4t)$, $\psi(2^n t)$ and their shifted functions.
3. Orthogonality in the form Here $\delta_{i,j}$ represents the Kronecker delta. The **dual function of $\psi(t)$ is $\psi(t)$ itself**

$$\int_{-\infty}^{+\infty} 2^{\frac{n+n_1}{2}} \psi(2^n t - k) \psi(2^{n_1} t - k_1) dt = \delta_{n,n_1} \delta_{k,k_1}$$

3 CONDITION BASED MONITORING OF ROTATING MACHINE USING VIBRATION ANALYSIS

3.1 INTRODUCTION

Using vibration analysis the condition of a machine can be constantly monitored. Detailed analysis can be made to determine the health of a machine and identify any faults that may be arising or that already exist. Commonly witnessed machinery faults diagnosed by vibration analysis are:

- Unbalance
- Bent Shaft
- Eccentricity
- Misalignment
- Looseness
- Belt drive problems
- Gear defect
- Bearing defect
- Electrical faults
- Shaft cracks
- Rotor rubs

In this chapter each one of the cases is discussed in order to see how they manifest in vibration analysis.

Guideline for Domain Selection

The following table indicates when Frequency, Phase and Time should be examined for diagnostic information.

Application/Problem	Spectrum FFT	Phase	Time Waveform
Unbalance	X	X	

Condition Based Monitoring of Rotating Machine using Vibration Analysis

Misalignment	X	X	
Resonance	X	X	X
Rolling Element Bearing	X		X
Sleeve Bearing	X	X	X
Gears	X		X
Electrical	X		X
Looseness	X	X	X
Flow Problems	X		
Very low Frequency			X
Cyclic Vibration			X
Variable Speed	X		X

Table 1 Domain selection for diagnostic information

3.2 UNBALANCE

The International Standards Organisation (ISO) define unbalance as:

That condition, which exists in a rotor when vibratory, force or motion is imparted to its bearing as a result of centrifugal forces.

It may also be defined as: The uneven distribution of mass about a rotor's rotating centerline. There are two new terminologies used: one is rotating centerline and the other is geometric centerline.

The rotating centerline is defined as the axis about which the rotor would rotate if not constrained by its bearing (also called Principal inertia axis or PIA). The geometric centerline (GCL) is the physical centerline of the rotor. When the two centerline are coincident, then the rotor will be in a state of balance. When they are apart, the rotor will be unbalanced. There are three type of unbalance:

1. Static unbalance
2. Couple unbalance (PIA and GCL intersect)
3. Dynamic unbalance (PIA and GCL do not touch or coincide)

Unbalance (imbalance) causes excitation by forces rotating at the shaft speed when the local centre of mass (CoM) of the cross-section is not at the centre of rotation. The response depends on whether the inertias on the shaft are localized

Condition Based Monitoring of Rotating Machine using Vibration Analysis

or distributed axially, and whether the shaft is running below or above its first critical speed. If the shaft is short and the inertia localized, there will basically be a radial force rotating at shaft speed, which excites vibrations primarily in the two radial directions, but very little axially. Where the radial stiffness of the shaft and bearing supports is high, the response vibration will be stiffness controlled, and so in terms of displacement it will be proportional to the unbalance force $M\omega^2 e$, where M is the mass of the rotor, e is the radial displacement of the CoM of the rotor from the centre of rotation, and ω is the rotational speed of the shaft. The shaft is most often axisymmetric, but the bearing supports usually have different stiffnesses in the horizontal and vertical directions, so that the vibration response will be different in the two directions. Even in this simplest of cases, the stiffness of the bearings is usually nonlinear, in particular for fluid film bearings, but even for rolling element bearings, so even though the unbalance force is only at shaft speed, the response will be distorted to some extent from sinusoidal, and so the spectrum of the response will contain harmonics of the shaft speed. Where the inertia of the rotor is distributed axially, the CoM of each section is not necessarily the same, and thus the radial unbalance force changes in amplitude and direction along the rotor. If the rotor is rigid, all the unbalance forces can be combined into an equivalent single unbalance force at the global CoM of the rotor and a moment about some axis through the CoM. Thus the overall response is a combination of radial (cylindrical) motion and rocking (conical) motion, once again with circles distorted to ellipses if the horizontal and vertical support stiffnesses are different, and generating higher harmonics if the bearing stiffnesses are nonlinear. Such rocking motions can give axial responses, even if the elemental unbalance forces are purely radial.

Static unbalance

For all type of unbalance, the FFT spectrum will show a predominant 1xrpm frequency of vibration. Vibration amplitude at the 1 x rpm frequency will vary proportional to the square of rotational speed. It is always present and normally dominates the vibration spectrum (Figure 3.1).

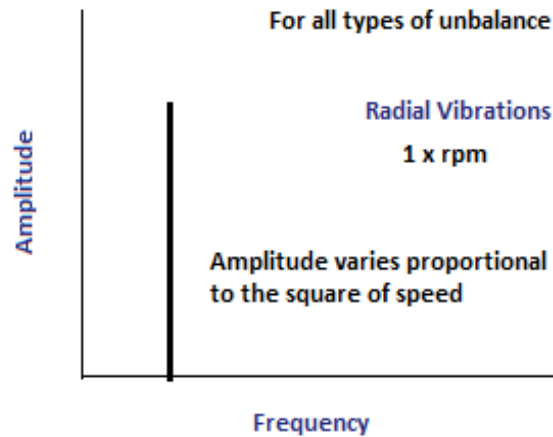


Figure 3.1 FFT analysis-unbalance

Static unbalance will be in-phase and steady (15-20°). If the pickup is moved from the vertical (V in the figure) to the horizontal (H direction) the phase will shift by 90° (+-30°). If we move the pickup from one bearing to another in the same plane (vertical or horizontal). The phase will remain the same, if the fault is static unbalance (Figure 3.2).

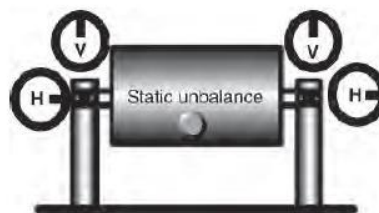


Figure 3.2 Phase relationship-static unbalance

Couple unbalance

In a couple unbalance (Figure 3.3) the fft spectrum again displays a single 1x rpm frequency peak the amplitude at the 1x varies proportional to the square of the speed. This defect may cause high axial and radial vibrations. Couple unbalance tends to be 180° out of phase on the same shaft. Note that almost a 180° phase difference exists between two bearings in the horizontal plane. The same is observed in the vertical plane. It is advisable to perform an operational deflection shape (ODS) analysis to check if couple unbalance is present in a system.

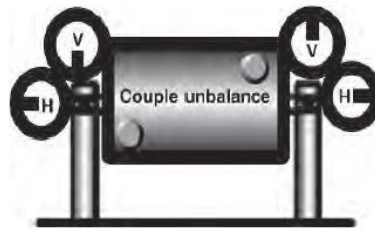


Figure 3.3 Phase relationship-couple unbalance

Unbalance – overhung rotors

In this case, the FFT spectrum displays a single $1x$ rpm peak as well, and the amplitude again varies proportional to the square of the shaft speed. It may cause high axial and radial vibrations. The axial phase on the two bearings will seem to be in phase whereas the radial phase tends to be unsteady. Overhung rotors can have both a static and couple unbalance and must be tested and fixed using analyzers or balancing equipment (Figure 3.4).

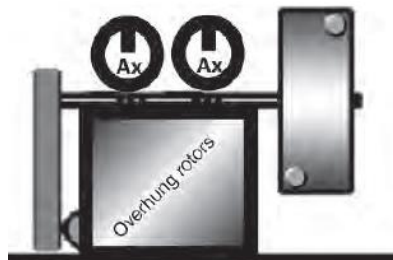


Figure 3.4 A belt driven fan/blower with an overhung rotor – the phase is measured in the axial direction

3.3 ECCENTRIC ROTOR

Eccentricity occurs when the center of rotation is at an offset from the geometric centerline of a sheave, gear, bearing, motor armature or any other rotor. The maximum amplitude occurs at $1x$ rpm of the eccentric component in a direction through the centers of the two rotors. Here the amplitude varies with the load even at constant speeds (Figure 3.5)

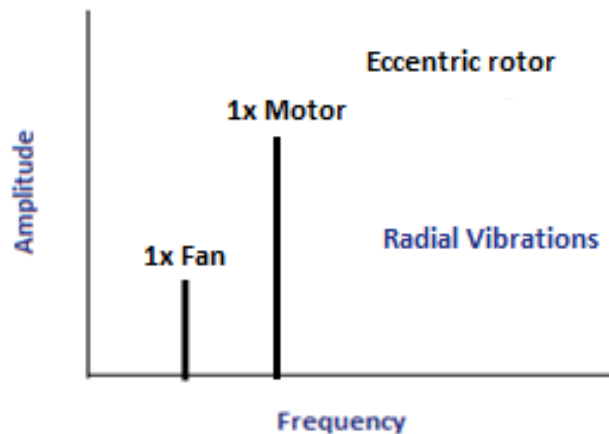


Figure 3.5 A belt-driven fan/blower – vibration

In a normal unbalance defect, when the pick up is moved from the vertical to the horizontal direction, a phase shift of 90° will be observed. However in eccentricity, the phase readings differ by 0 or 180° (each indicates the straight line motion) when measured in horizontal and vertical directions. Attempts to balance an eccentric rotor often result in reducing the vibration in one direction, but increasing it in the other radial direction (depends on the severity of the eccentricity) (Figure 3.6).

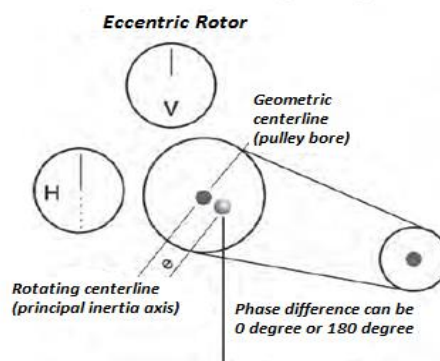


Figure 3.6 Eccentric rotor

3.4 BENT SHAFT

When a bent shaft is encountered, the vibrations is in radials as well as in the axial direction will be high. Axial vibrations may be higher than the radial vibrations. The FFT will normally have 1x, 2x components. If the:

Condition Based Monitoring of Rotating Machine using Vibration Analysis

- Amplitude of 1x rpm is dominant then the bend is near the shaft center (Figure 3.7)
- Amplitude of 2x rpm is dominant then the bend is near the shaft end.

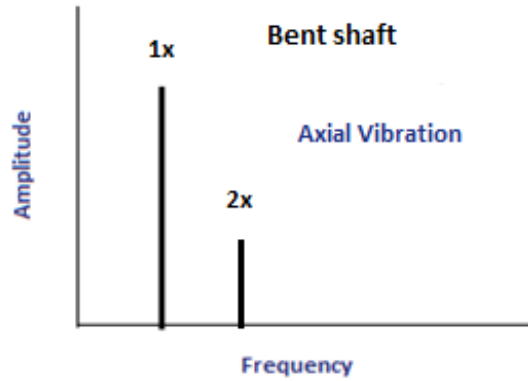


Figure 3.7 An FFT of a bent shaft with bend near the shaft center

The phase will be 180 ° apart in the axial direction and in the radial direction. This means that when the probe is moved from vertical plane to the horizontal plane, there will be no change in the phase reading (Figure 3.8).

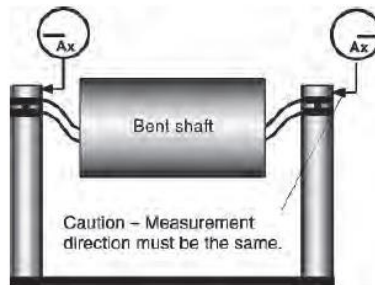


Figure 3.8 Note the 180 ° phase different in the axial direction

3.5 MISALIGNMENT

Misalignment, just like unbalance, is a major cause of machinery vibration. Some machines have been incorporated with self-aligning bearings and flexible coupling that can take quite a bit of misalignment. However, despite these, it is not uncommon to come across high vibrations due to misalignment. There are basically two types of misalignment:

Condition Based Monitoring of Rotating Machine using Vibration Analysis

1. Angular misalignment: the shaft centerline of the two shafts meets an angle with each other
2. Parallel misalignment: the shaft centerline of the two machines is parallel to each other and have an offset

When a shaft has three or more bearings, for example when two machines are coupled together, there is a potential for misalignment, which can be parallel misalignment, meaning that one of the two shafts is displaced laterally, but still parallel to the other, or angular misalignment, where the axis of one is at an angle to that of the other. Such misalignment introduces into the shafts bending deflections, which are fixed spatially, but rotating with respect to the shafts. The induced bending moments thus depend on the bending stiffness of the shaft and have to be counteracted by forces at the bearings and the foundations.

3.5.1 Angular misalignment

As shown in Figure 2.9 angular misalignment primarily subjects the driver and driven machine shafts to axial vibrations at the 1x rpm frequency. The figure is a single-pin representation, but a pure angular misalignment on a machine is rare. Thus alignment is rarely seen just 1x rpm peak. Typically, there will be high axial vibration with both 1x, 2x rpm. However, it is not unusual for 1x, 2x or 3x to dominate. These symptoms may also indicate coupling problem.

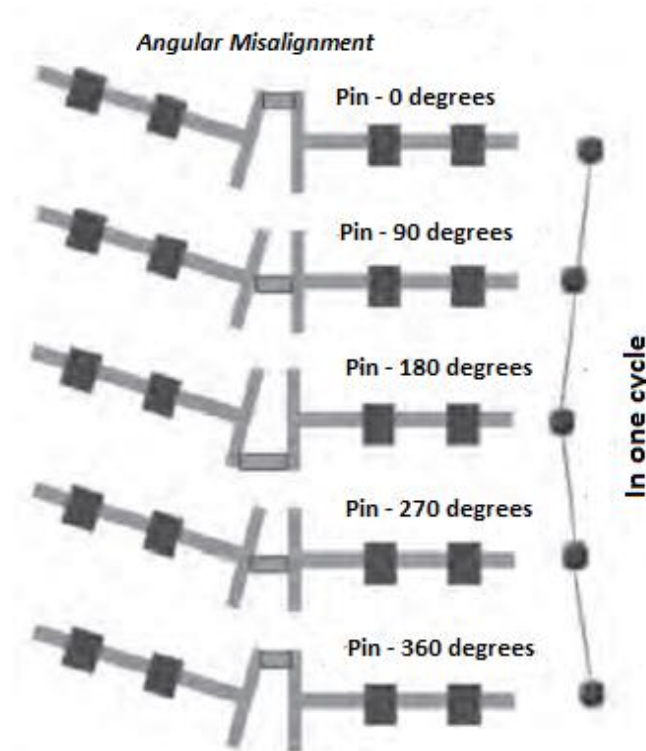


Figure 3.9 Angular misalignment

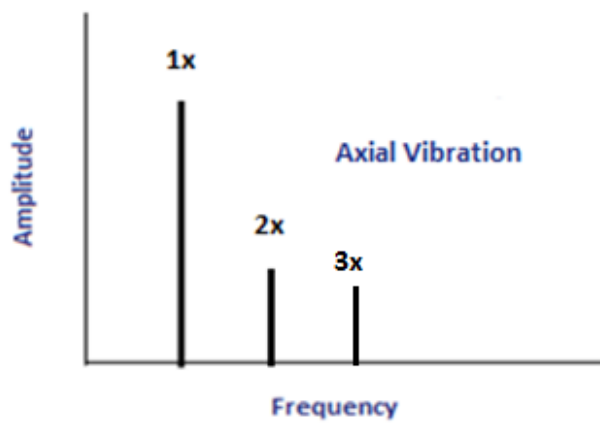


Figure 3.10 FFT of angular misalignment

A 180° phase difference will be observed when measuring the axial phase on the bearings of the two machines across the coupling (Figure 3.11).

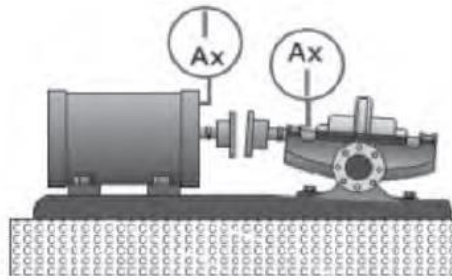


Figure 3.11 Angular misalignment confirmed by phase analysis

3.5.2 Parallel misalignment

Parallel misalignment results in 2 hits per cycle and therefore a 2x rpm vibration in the radial direction. Parallel misalignment has similar vibration symptoms compared to angular misalignment, but shows high radial vibration that approach 180° phase difference across the coupling. Pure angular Misalignment is rare and is commonly observed in conjunction with angular misalignment. Thus we will see both the 1x and 2x peaks. When the parallel misalignment is predominant, 2x is often larger than 1x, but its amplitude relative to 1x may often be dictated by the coupling type and its construction.

When either angular or parallel misalignment becomes severe, it can generate high-amplitude peaks at much higher harmonics (3x to 8x) (Figure 3.13) or even a whole series of high-frequency harmonics. Coupling construction will often significantly influence the shape of the spectrum if misalignment is severe (Figure 3.12).

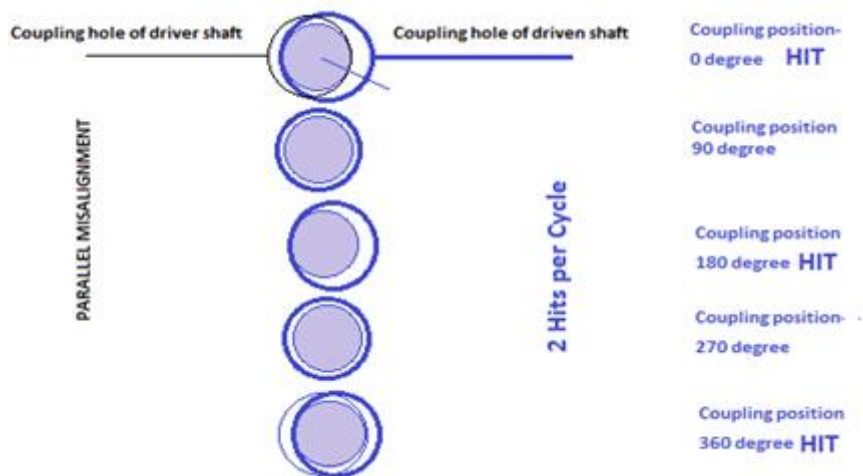


Figure 3.12 Parallel misalignment

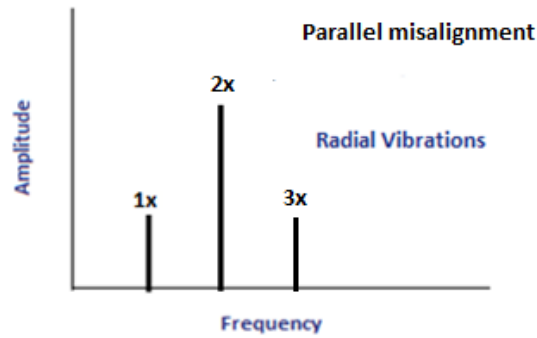


Figure 3.13 FFT of parallel misalignment

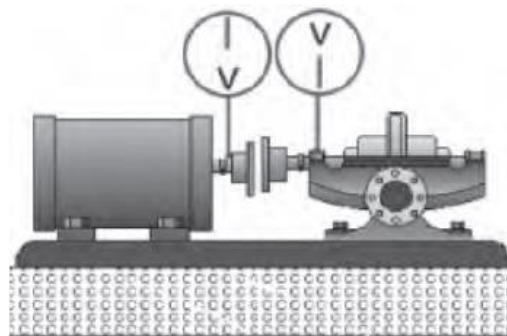


Figure 3.14 Radial phase shift of 180° is observed across the coupling

3.6 MECHANICAL LOOSENESS

If we consider any rotating machine, mechanical looseness can occur at three locations:

1. Internal looseness
2. Looseness at machine to base plate interface
3. Structure looseness

3.6.1 Internal assembly looseness

This category of looseness could be between a bearing liner in its cap, a sleeve or rolling element bearing, or an impeller on a shaft. It is normally caused by an improper fit between component parts, which will produce harmonic in the fft due to the non linear response of the loose parts to the exciting forces from the rotor. A truncation of the time waveform occurs, causing harmonics. The phase is often unstable and can vary broadly from one measurement to the next, particularly if the rotor alters its position on the shaft from one start-up to the next.

Mechanical looseness is often highly directional and may cause noticeably different readings when they are taken at 30° increments in radial direction all around the bearing housing. Also note that looseness will often cause sub-harmonic multiples at exactly ½ x or 1/3 x rpm (e.g. ½ x, 1 ½ x, 2 ½ x and further) (Figure 3.15 and 3.16).

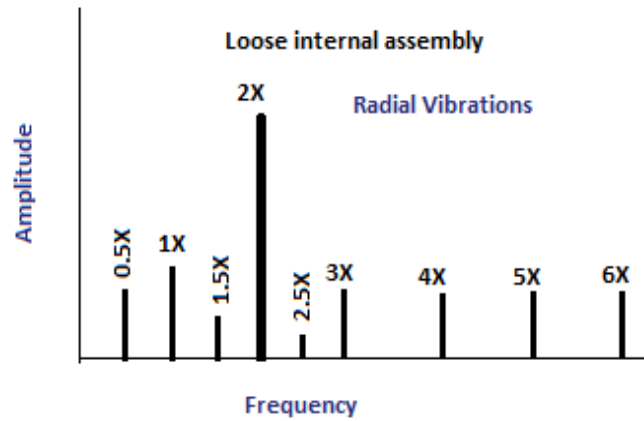


Figure 3.15 loose internal assembly graph

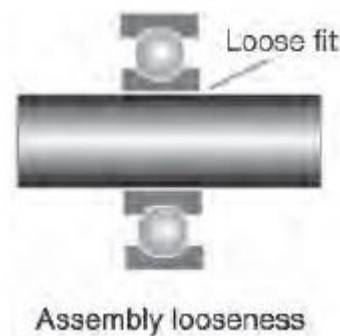


Figure 3.16 Loose fit

3.6.2 Looseness between machine to base plate

This problem is associated with loose pillow-block bolts, cracks in the frame structure or the bearing pedestal. Figures 3.17 3.18 make it evident how higher harmonics are generated due to the rocking motion of the pillow block with loose bolts.

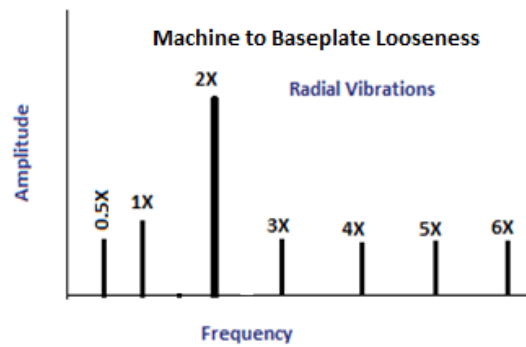


Figure 3.17 Mechanical looseness graph

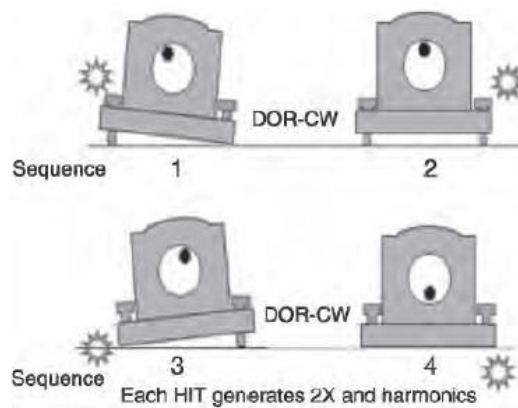


Figure 3.18 Mechanical looseness

3.6.3 Structure looseness

This type of looseness is caused by structural looseness or weaknesses in the machine's feet baseplate or foundation. It can also be caused by deteriorated grouting, loose hold-down bolts at the base and distortion of the frame or base (known as soft foot).

Phase analysis may reveal approximately 180° phase shift between vertical measurements on the machine's foot, baseplate and base itself (Figure 3.19). When the soft foot condition is suspected, an easy test to confirm for it is to loosen each bolt, one at a time and see if this brings about significant changes in the vibration. In this case, it might be necessary to re-machine the base or install shims to eliminate the distortion when the mounting bolts are tightened again.

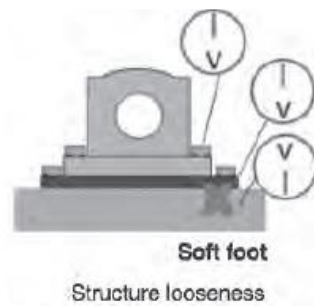


Figure 3.19 Structure looseness

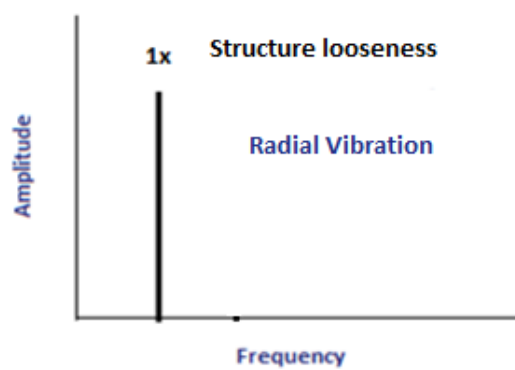


Figure 3.20 Structure looseness graph

3.7 ROLLING ELEMENT BEARING

A rolling element bearing comprises of inner and outer races, a cage and rolling elements. Defects can occur in any of the parts of the bearing and will cause high frequency vibrations. In fact the severity of the wear keep changing the vibration pattern. In most cases it is possible to identify the component of the bearing that is defective due to the specific vibration frequency that are excited. Raceways and rolling element defects are easily detected. However the same cannot be said for the defects that crop up in bearing cages. Though there are many techniques available to detect where defects are occurring, there are no established techniques to predict when the bearing defect will turn into a functional failure. In an earlier topic dealing with enveloping/demodulation, we saw how bearing defects generate both the bearing defect frequency and the ringing random vibrations that are the resonant frequencies of the bearing components. Bearing defect frequencies are not integrally harmonic to running speed. However, the following formulas are used to determine bearing defect frequencies. There is also a bearing database

Condition Based Monitoring of Rotating Machine using Vibration Analysis available in the form of commercial software that readily provides the values upon entering the requisite bearing number.

$$BPFI = \frac{Nb}{2} \left(1 + \frac{Bd}{Pd} \cos \theta \right) x rpm$$

$$BPFO = \frac{NB}{2} \left(1 - \frac{Bd}{Pd} \cos \theta \right) x rpm$$

$$FTF = \frac{1}{2} \left(1 - \frac{Bd}{Pd} \cos \theta \right) x rpm$$

$$BSF = \frac{Pd}{2Bd} \left[1 - \left(\frac{Bd}{Pd} \right)^2 (\cos \theta)^2 \right] x rpm$$

Nb= Number of Balls or Rollers

Bd=Ball/Roller diameter (inch or mm)

Pd=Bearing Pitch diameter

θ=Contact angle in degree

BPFI=Ball pass frequency inner

BPFO=Ball pass frequency outer

FTF=Fundamental train frequency

BSF=Ballspin frequency (rolling element)

It is very interesting to note that in an FFT, we find both the inner and outer race defect frequencies. Add these frequencies and then divide the result by the machine rpm – [(BPFI + BPFO) /rpm]. The answer should yield the number of rolling elements. Bearing deterioration progresses through four stages. During the initial stage, it is just a high-frequency vibration, after which bearing resonance frequencies are observed. During the third stage, discrete frequencies can be seen, and in the final stage high-frequency random noise is observed, which keeps broadening and rising in average amplitude with increased fault severity. In the following Figure the characteristic frequency of a Racer 3, 5, 5L and 7 Robot.

Condition Based Monitoring of Rotating Machine using Vibration Analysis

Robot	AX	Desc	supplier code	RPM	Hz	BPFI	BPFO	FTF	BSF	Rolling element defect frequency
Racer 3	AX3	BALL BEARING 12X28X8-6001-2RS-DIN625	6001-2RS	6000	100	495.250 Hz	304.750 Hz	38.094 Hz	198.067 Hz	396.134 Hz
Racer 5	AX3	BALL BEARING 12X28X8-6001-2RS-DIN626	6001-2RS	5985.185	99.75309	494.027 Hz	303.997 Hz	38.000 Hz	197.578 Hz	395.156 Hz
Racer 5L	AX3	BALL BEARING 12X28X8-6001-2RS-DIN627	6001-2RS	5915.556	98.59259	488.280 Hz	300.461 Hz	37.558 Hz	195.279 Hz	390.559 Hz
Racer Plus--		BALL BEARING 12X28X8-6001-2RS-DIN628	6001-2RS	3450	57.5	284.769 Hz	175.231 Hz	35.596 Hz	113.889 Hz	227.777 Hz
Racer 3	AX5	RADIAL BALL BEARINGS	61810-2RS	6120	102	1363.008 Hz	1186.992 Hz	47.480 Hz	735.331 Hz	1470.662 Hz
Racer 5	AX5	RADIAL BALL BEARINGS	61810-2RS	5100	85	1135.840 Hz	989.160 Hz	39.566 Hz	612.776 Hz	1225.551 Hz
Racer 5L	AX5	RADIAL BALL BEARINGS	61810-2RS	5100	85	1135.840 Hz	989.160 Hz	39.566 Hz	612.776 Hz	1225.551 Hz
Racer Plus--		RADIAL BALL BEARINGS	61810-2RS	5100	85	1135.840 Hz	989.160 Hz	39.566 Hz	612.776 Hz	1225.551 Hz
Racer 3	AX3	NEEDLE ROLLER BEARING	61814-2RS	6000	100	1336.812 Hz	1163.188 Hz	46.527 Hz	716.470 Hz	1432.940 Hz
Racer 5	AX3	NEEDLE ROLLER BEARING	61814-2RS	5985.185	99.75309	1333.512 Hz	1160.315 Hz	46.413 Hz	714.701 Hz	1429.402 Hz
Racer 5L	AX3	NEEDLE ROLLER BEARING	61814-2RS	5915.556	98.59259	1317.998 Hz	1146.817 Hz	45.873 Hz	706.386 Hz	1412.773 Hz
Racer Plus--		NEEDLE ROLLER BEARING	61814-2RS	3450	57.5	768.667 Hz	668.833 Hz	26.753 Hz	411.970 Hz	823.940 Hz
Racer 3	AX6	Angular contact ball bearing single row	7200B/P5	6000	100	551.888 Hz	348.112 Hz	38.679 Hz	160.494 Hz	320.989 Hz
Racer 5	AX6	Angular contact ball bearing single row	7200B/P5	5100	85	469.105 Hz	295.895 Hz	32.877 Hz	136.420 Hz	272.840 Hz
Racer 5L	AX6	Angular contact ball bearing single row	7200B/P5	5333.333	88.88889	490.567 Hz	309.433 Hz	34.381 Hz	142.662 Hz	285.323 Hz
Racer Plusno		Angular contact ball bearing single row	7200B/P5	5416.667	90.27778	498.232 Hz	314.268 Hz	34.919 Hz	144.891 Hz	289.782 Hz
Racer 3	AX5	BALL BEARING 10X26X8-6000-2RS-DIN625	6000-2RS	6120	102	452.508 Hz	261.492 Hz	37.356 Hz	176.990 Hz	353.981 Hz
Racer 5	AX5	BALL BEARING 10X26X8-6000-2RS-DIN626	6000-2RS	5100	85	377.090 Hz	217.910 Hz	31.130 Hz	147.492 Hz	294.984 Hz
Racer 5L	AX5	BALL BEARING 10X26X8-6000-2RS-DIN627	6000-2RS	5100	85	377.090 Hz	217.910 Hz	31.130 Hz	147.492 Hz	294.984 Hz
Racer Plus--		BALL BEARING 10X26X8-6000-2RS-DIN628	6000-2RS	5100	85	377.090 Hz	217.910 Hz	31.130 Hz	147.492 Hz	294.984 Hz
Racer 3	AX3	BALL BEARING 55X72X9-61811-2RS1-DIN625	61811-2RS1	6000	100	1236.241 Hz	1063.759 Hz	46.250 Hz	662.987 Hz	1325.974 Hz
Racer 5	AX3	BALL BEARING 55X72X9-61811-2RS1-DIN625	61811-2RS1	5985.185	99.75309	1233.188 Hz	1061.132 Hz	46.136 Hz	661.350 Hz	1322.700 Hz
Racer 5L	AX3	BALL BEARING 55X72X9-61811-2RS1-DIN625	61811-2RS1	5915.556	98.59259	1218.842 Hz	1048.788 Hz	45.599 Hz	653.656 Hz	1307.312 Hz
Racer PlusAX5		BALL BEARING 55X72X9-61811-2RS1-DIN625	61811-2RS1	5100	85	1050.805 Hz	904.195 Hz	39.313 Hz	563.539 Hz	1127.078 Hz

Figure 3.21 Characteristic frequencies of the bearing of axis 3

Stage 1 of bearing defect

The FFT spectrum for bearing defects can be split into four zones (A, B, C and D), where we will note the changes as bearing wear progresses.

These zones are described as:

Zone A: machine rpm and harmonics zone

Zone B: bearing defect frequencies zone (5–30 kcpm)

Zone C: bearing component natural frequencies zone (30–120 kcpm)

Zone D: high-frequency-detection (HFD) zone (beyond 120 kcpm)

The first indications of bearing wear show up in the ultrasonic frequency ranges from approximately 20–60 kHz (120–360 kcpm). These are frequencies that are evaluated by high-frequency detection techniques such as gSE (Spike Energy), SEE, PeakVue, SPM and others. As Figure 3.25 shows, the FFT in case raceways or rolling elements of the bearing do not have any visible defects during the first stage. The raceways may no longer have the shine of a new bearing and may appear dull gray.

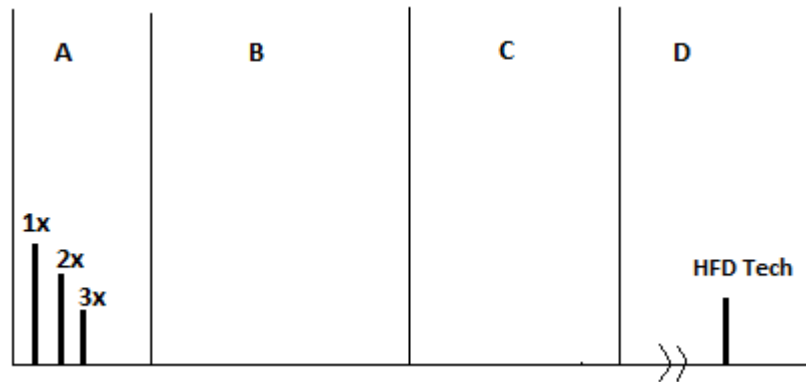


Figure 3.22 Small defect in the raceways of a bearing

Stage 2 of bearing defect

In the following stage (Figure 3.26), the fatigued raceways begin to develop minute pits. Rolling elements passing over these pits start to generate the ringing or the bearing component natural frequencies that predominantly occur in the 30–120 kcpm range. Depending on the severity, it is possible that the sideband frequencies (bearing defect frequency \pm rpm) appear above and below the natural frequency peak at the end of stage two. The high-frequency detection (HFD) techniques may double in amplitude compared to the readings during stage one.

Stage 3 of bearing defect

As we enter the third stage (Figure 3.27), the discrete bearing frequencies and harmonics are visible in the FFT. These may appear with a number of sidebands. Wear is usually now visible on the bearing and may expand through to the edge of the bearing raceway.

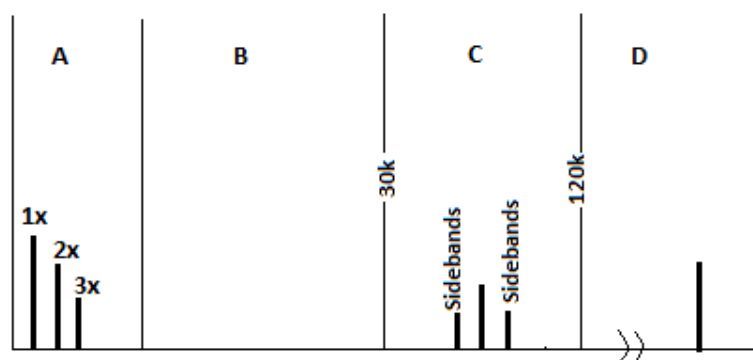


Figure 3.23 More obvious wear in the form of pits

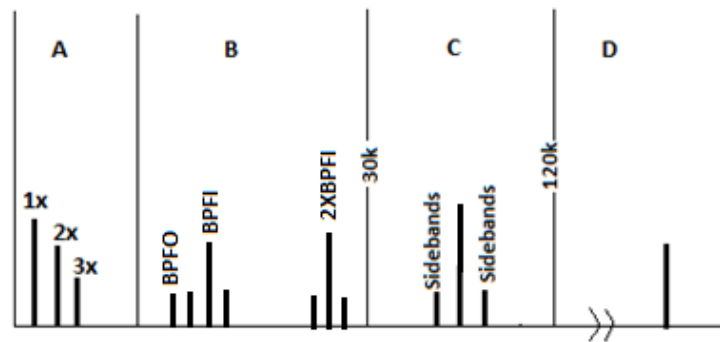


Figure 3.24 Wear is now clearly visible over the breath of the bearing

Stage 4 of bearing defect

In the final phase (Figure 3.28), the pits merge with each other, creating rough tracks and spalling of the bearing raceways or/and rolling elements. The bearing is in a severely damaged condition now. Even the amplitude of the 1× rpm component will rise. As it grows, it may also cause growth of many running speed harmonics. It can be visualized as higher clearances in the bearings allowing a higher displacement of the rotor. Discrete bearing defect frequencies and bearing component natural frequencies actually begin to merge into a random, broadband high-frequency ‘noise floor’. Initially, the average amplitude of the broad noise may be large. However, it will drop and the width of the noise will increase. In the final stage, the amplitude will rise again and the span of the noise floor also increases.

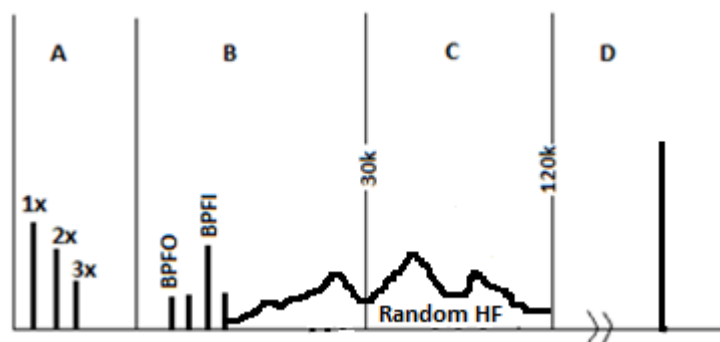


Figure 3.25 Severely damaged bearing in final stage of wear

3.8 GEARING DEFECTS

A gearbox is a piece of rotating equipment that can cause the normal low frequency harmonics in the vibration spectrum, but also show a lot of activity in the

high frequency region due to gear teeth and bearing impacts. The spectrum of any gearbox shows the 1x and 2x rpm, along with the gear mesh frequency (GMF). The GMF is calculated by the product of the number of teeth of a pinion or a gear, and its respective running speed:

$$\text{GMF} = \text{number of teeth on pinion} \times \text{pinion rpm}$$

The GMF will have running speed sidebands relative to the shaft speed to which the gear is attached. Gearbox spectrums contain a range of frequencies due to the different GMFs and their harmonics. All peaks have low amplitudes and no natural gear frequencies are excited if the gearbox is still in good condition. These contain information about gearbox faults (Figure 3.28).

Tooth wear and backlash can excite gear natural frequency along the gear mesh frequencies and their sidebands. Signal enhancement analysis enables the collection of vibrations from a single shaft inside a gearbox.

Cepstrum analysis is an excellent tool for analysing the power in each sideband family. The use of cepstrum analysis in conjunction with order analysis and **time domain averaging** can eliminate the 'smearing' of the many frequency components due to small speed variations.

As a general rule, distributed faults such as eccentricity and gear misalignment will produce sidebands and harmonics that have high amplitude close to the tooth-mesh frequency. Localized faults such as a cracked tooth produce sidebands that are spread more widely across the spectrum.

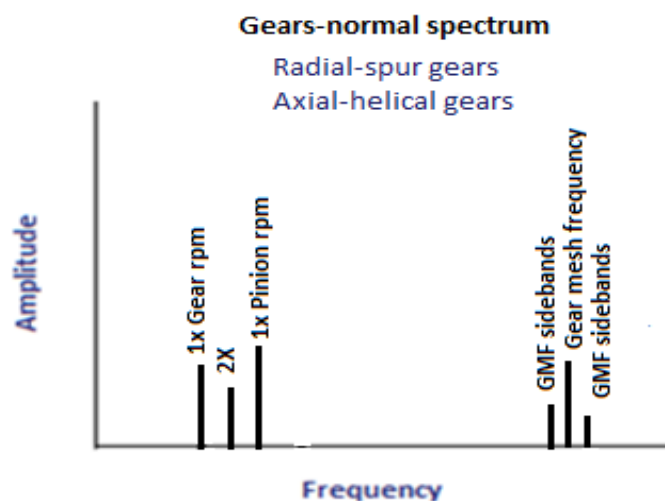


Figure 3.26 Graph of a gearbox spectrum

Gear tooth wear

An important characteristic of gear tooth wear is that gear natural frequencies are excited with sidebands around them. These are spaced with the running speed of the bad gear.

The GMF may or may not change in amplitude, although high-amplitude sidebands surrounding the GMF usually occur when wear is present. Sidebands are a better wear indicator than the GMF itself (Figure 3.29).

Gear tooth load

As the load on a gearbox increases, the GMF amplitude may also increase high GMF amplitudes do not necessary indicate a problem, particularly if sideband frequencies remain low and no gear natural frequencies are excited. It is advised that vibration analysis on a gearbox be conducted when the gearbox is transmitting maximum power (Figure 3.30).

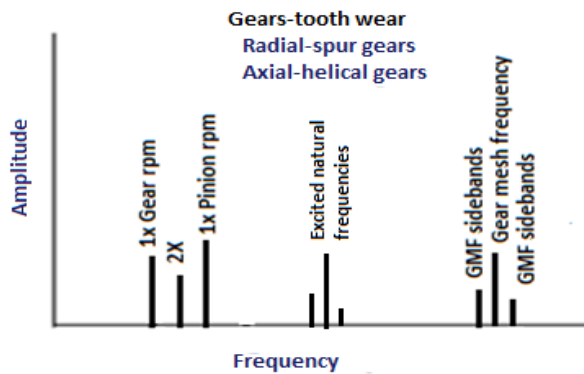


Figure 3.27 Gear tooth wear

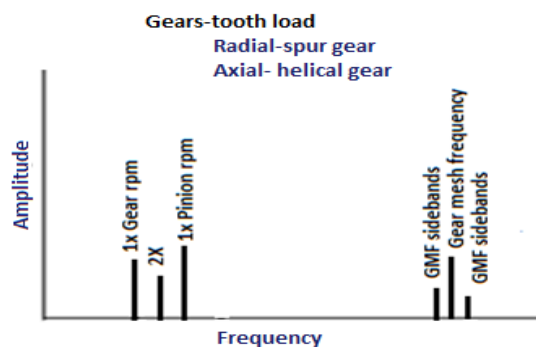


Figure 3.28 Gear tooth load

Gear eccentricity and backlash

Fairly high amplitude sidebands around the GMF often suggest gear eccentricity, backlash or non-parallel shafts. In these cases, the rotation of one gear may cause the amplitude of gear vibration to *modulate* at the running speed of the other. This can be seen in the time domain waveform. The spacing of the sideband frequencies indicates the gear with the problem. Improper backlash normally excites the GMF and gear natural frequencies. Both will have sidebands at 1xrpm. The GMF amplitudes will often decrease with increasing load if backlash is the problem (Figure 3.29).

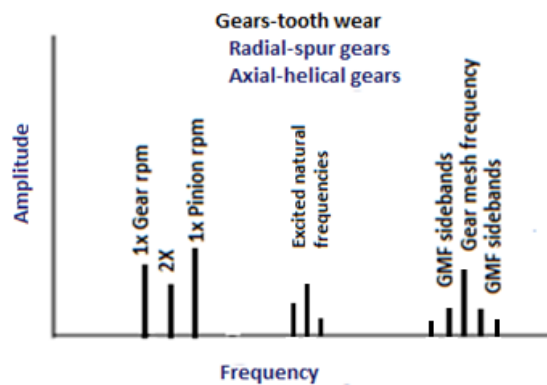


Figure 3.29 Gear eccentricity and backlash

Gear Misalignment

Gear misalignment almost always excites second order or higher GMF harmonics, which will have sidebands spaced with the running speed. It will often show only small amplitudes at 1xGMF, but much higher levels at 2x or 3xGMF. It is important to set the F-max of the FFT spectrum to more than 3xGMF (Figure 3.30).

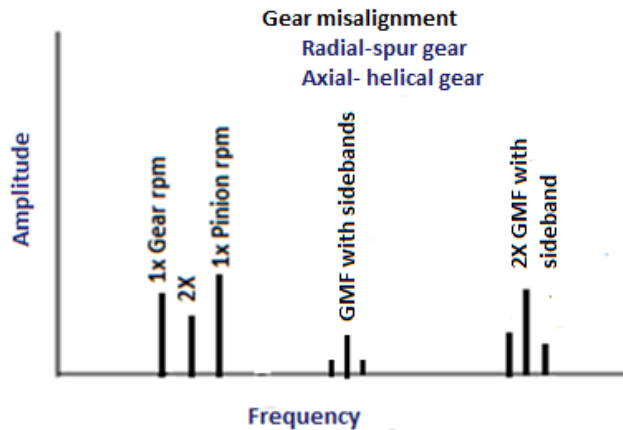


Figure 3.30 Gear Misalignment

Gears- cracked or broken tooth

A cracked or broken gear tooth will generate high amplitude at 1x rpm of this gear, plus it will excite the gear natural frequency with sidebands spaced with its running speed. It is best detected in the time domain, which will show a pronounced spike every time the problematic tooth tries to mesh with teeth on the mating gear. The time between impacts will correspond to 1/speed of the gear with the broken tooth. The amplitude the impact spike in the time waveform will often be much higher than that of the 1x gear rpm in the FFT spectrum (Figure 3.31).



Figure 3.31 Gears-cracked

3.9 BELT DEFECTS

Worn, loose, mismatched belts

Belt defect frequencies are of the sub-harmonic type. Upon analysing belt drives, it is necessary to keep the F-max low to be able to notice these peaks. When belts are worn, loose or mismatched, they may generate harmonics of the belt frequency. It is possible to obtain 3x, 4x times of belt frequency. Quite often, the 2x belt frequency is dominant. The belt frequency is given by the formula:

$$\text{Belt frequency} = \frac{\pi \times \text{pulley rpm} \times \text{pitch dia.}}{\text{belt length}}$$

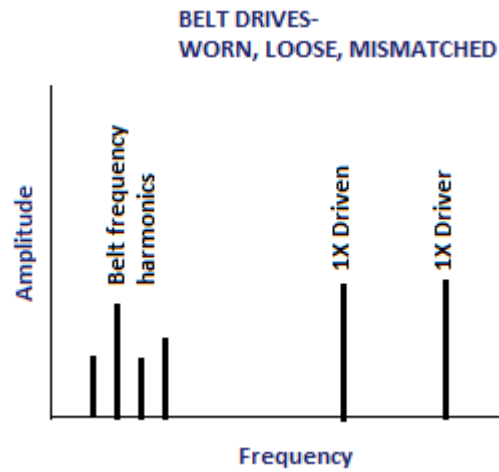


Figure 3.31 Sub-harmonic belt frequencies

With timing belt driven it is useful to know that high amplitudes at the timing belt frequency indicate wear or pulley misalignment.

Belt/sheave misalignment

The different types of misalignment possible with belt drives are shown in Figure 3.35. These conditions not only result in destructive vibration but also cause accelerated wear of both the belt and the sheaves. Misalignment of sheaves produce high vibration at 1x rpm, predominantly in the axial direction (Figure 3.33). The ratio of amplitudes of driver to driven rpm depends on the measurement position, relative mass and the frame stiffness. With sheave misalignment in fans, the highest axial vibration will be at the fan rpm. When the belt drives an overhung rotor, which is in an unbalanced condition, it will have to be resolved with phase analysis.

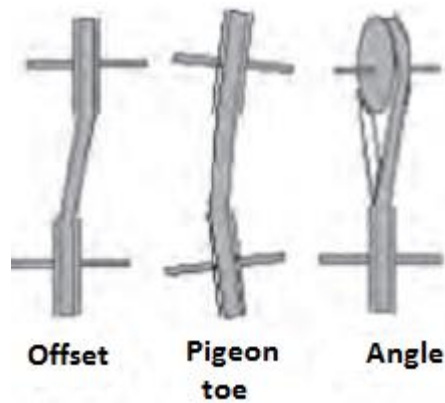


Figure 3.32 Misalignment types (the pigeon toe and angle are classified as angular misalignment)

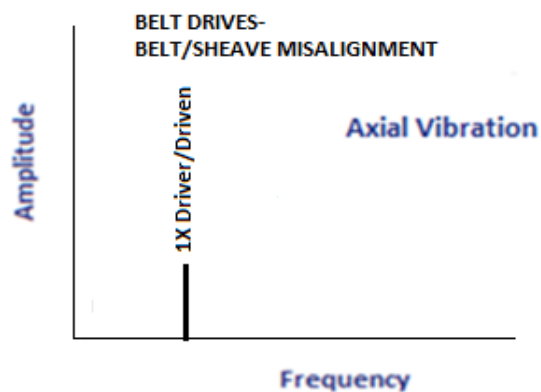


Figure 3.33 Vibration due to sheave misalignment

Belt resonance

Belt resonance (Figure 3.34) can occur if the natural frequency of the belt is close to either the motor or the driven shaft rpm. Drive belts also experience high vertical and lateral vibrations when their natural frequencies coincide with that of connected equipment. Tensioning and releasing the belt while measuring the response on sheaves or bearings can normally identify and help to rectify this situation. A common method to control vertical vibration is by using a restraining device (metal rod or idler pulley) placed perpendicular to the belt span and close to (or lightly touching) the belt. This device should be positioned roughly at one-third of the span distance from the larger pulley.

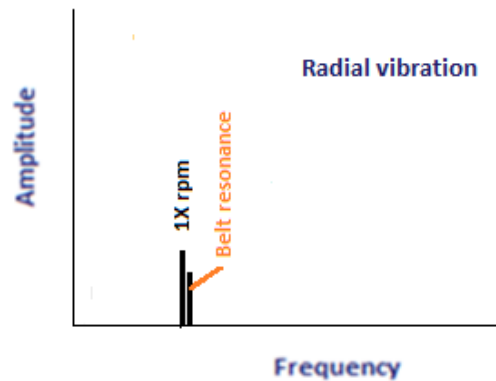


Figure 3.34 Vibration due to sheave misalignment

3.10 ELECTRICAL PROBLEMS

Vibration of electrical machines such as motors, generators can be either mechanical or electrical in nature. Electrical problem also appear in the vibration spectrum and can provide information about the nature of the defects. Electrical problems occur due to unequal magnetic forces acting on the rotor or the stator. These unequal magnetic forces may be due to

- Open or short windings of the rotor or stator
- Broken rotor bar
- Unbalanced phases
- Unequal air gap

Generally the vibration pattern emerging due to the above mentioned electrical problem will be at 1x rpm and will thus appear similar to unbalance.

A customary technique to identify these conditions is to keep the analyzer capturing the FFT spectrum in the live mode and then switching off the electrical power. If the peak disappear instantly, the source is electrical in nature. On the other hand if there is a gradual decrease in the 1x amplitude it is more likely to be a mechanical problem. This technique requires caution. If there is a time lag in the analyzer itself, it may delay the drop in vibration amplitude. It is also possible that a resonance frequency may drop quickly as the speed changes. Induction motors, which have electrical problems, will cause the vibration amplitude to hunt or swing in a cyclic manner. The following are some terms that will be required to understand vibrations due to electrical problems:

$F_L = \text{electrical line frequency (50/60 Hz)}$

$$F_s = \text{slip frequency} = \frac{2 \times F_L}{P} - \text{rpm}$$

$$F_p = \text{pole pass frequency} = F_s \times P$$

$P = \text{number of poles}$

3.10.1 Rotor problems

Normally, four kinds of problems can occur within the rotor:

1. Broken rotor bars
2. Open or shorted rotor windings
3. Bowed rotor
4. Eccentric rotor

Rotor defects

Along with the stator is a rotor, which is basically an iron following the rotating magnetic field. As the magnetic field sweeps across the conductor, it creates a voltage across the length of the rotor bar. If the bar is open-circuited, no current flows and no forces are generated. When the bar is short-circuited, a current flows. This current is proportional to the speed at which the field cuts through the conductor and the strength of the field. The field interacts with the stator field to generate a force on the rotor bar. If everything else remains the same, an equal and opposite force on the opposite side of the rotor will develop. These two forces generate the torque that drives the load. In case anything disrupts the current or magnetic fields on either side of the rotor, the two forces will become unequal. This results in a radial force, which is the cause for vibration. A cracked or broken bar can cause this category of unbalanced forces. The forces rotate with the rotor with a constant load plus a load that varies with $2 \times$ slip. Therefore, the force acting on the bearings will have frequency components at $1 \times$ rpm and $1 \times$ rpm \pm $2 \times$ slip. Thus:

- **Broken or cracked rotor bars or shorting rings** (Figure 3.35 3.36)
- **Bad joints between rotor bars and shorting rings**
- **Shorted rotor laminations**

Condition Based Monitoring of Rotating Machine using Vibration Analysis will produce high $1 \times$ running speed vibration with pole pass frequency sidebands. In addition, cracked rotor bars will often generate F_p sidebands around the 3rd, 4th and 5th running speed harmonics. Loose rotor bars are indicated by $2 \times$ line frequency ($2F_L$) sidebands surrounding the rotor bar pass frequency (RBPF) and/or its harmonics (Figure 3.37).

$$\text{RBPF} = \text{number of rotor bars} \times \text{rpm.}$$

It may often cause high levels at $2 \times$ RBPF with only a small amplitude at $1 \times$ RBPF.

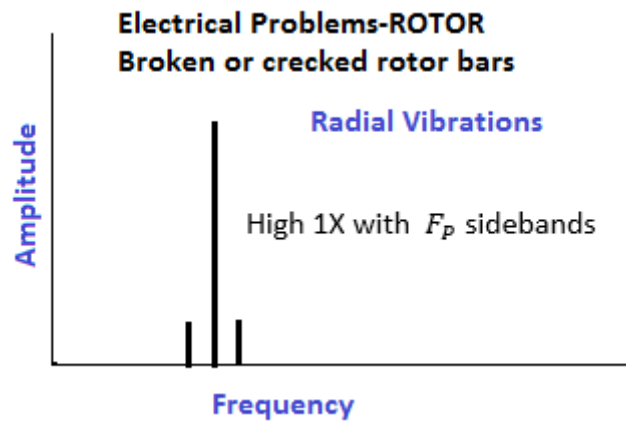


Figure 3.35 High 1x with F_p sidebands

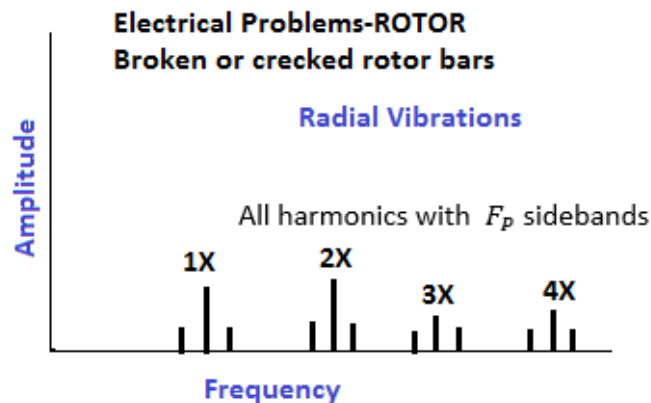


Figure 3.36 All harmonics with F_p sidebands

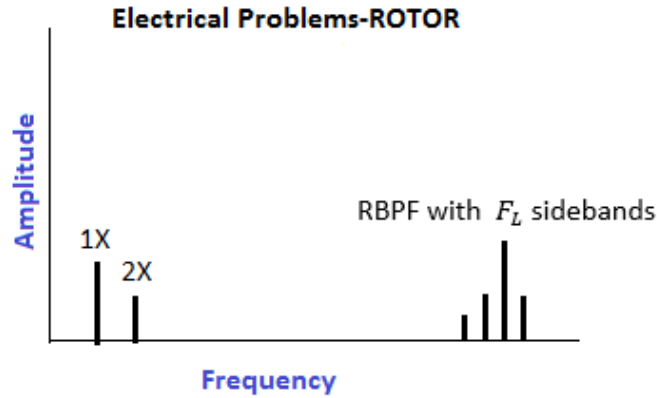


Figure 3.37 Rotor bar pass frequency

Eccentric rotor

The rotor is supposed to be concentric with respect to the stator coils. If this is not the case, a magnetic unbalance force is generated which is given by the formula

$$F = \frac{KI^2}{g^2} \left(\frac{4e}{(1-e)^2} \right)$$

where I = stator current, g = average gap between stator and rotor, e = eccentricity.

From this equation, it can be observed that an increase in current and eccentricity can generate high unbalanced magnetic forces. It is assumed that the eccentricity of the rotor will line up with the magnetic field. The closer side of the rotor will be respectively attracted to the positive pole and to the negative pole; thus the force will vary twice during a single current cycle. This can affect the bearings, and therefore it can modulate any other frequency present in the system. These effects generally cause sidebands of $\pm 2 \times$ slip frequency around the $1 \times$ rpm frequency caused by unbalance. Eccentric rotors produce a rotating variable air gap between the rotor and stator, which induces pulsating vibrations (it is a beat phenomenon between two frequencies, one is $2F_L$ and is the closest running speed harmonic). This may require a **'zoom' spectrum to separate the $2F_L$** and the run-

Condition Based Monitoring of Rotating Machine using Vibration Analysis
 ning speed harmonic. Eccentric rotors generate $2F_L$ surrounded by pole pass frequency sidebands (F_P as well as F_P sidebands around $1\times$ rpm). The pole pass frequency F_P itself appears at a low frequency (Figure 3.38).

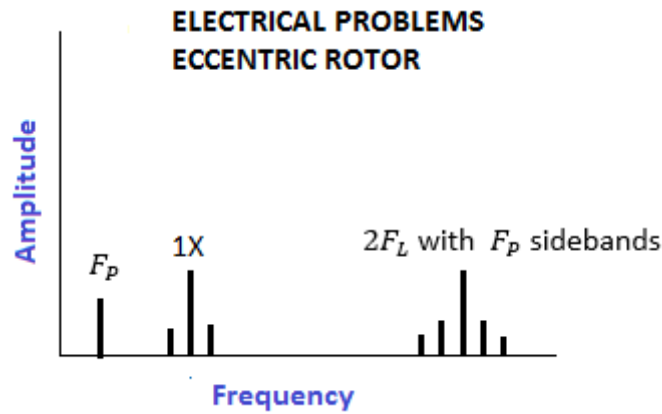


Figure 3.38 Eccentric Rotor

Stator defects

An induction motor comprises a set of stator coils, which generate a rotating magnetic field. The magnetic field causes alternating forces in the stator. If there is any looseness or a support weakness in the stator, each pole pass gives it a tug. This generates a $2\times$ line frequency ($2F_L$) also known as *loose iron*. Shorted stator laminations cause uneven and localized heating, which can significantly grow with time (Figure 3.39).

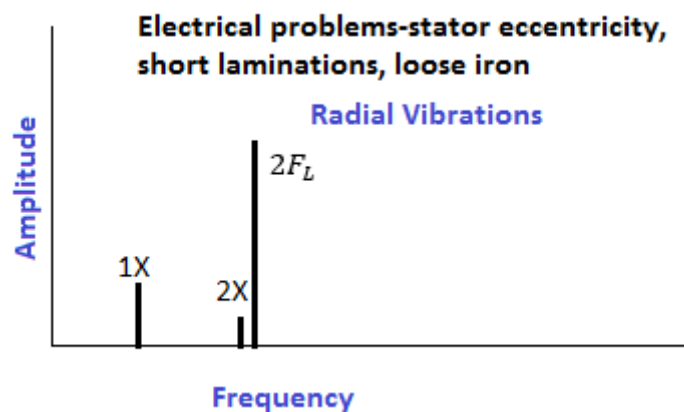


Figure 3.39 Stator defects

Synchronous Motor

Loose stator coils in synchronous motors will generate fairly high vibrations at the coil

pass frequency (CPF), defined as:

$$\text{CPF} = \text{number of stator coils} \times \text{rpm}$$

$$(\text{number of stator coils} = \text{poles} \times \text{number of coils/pole})$$

The coil pass frequency will be surrounded by $1 \times \text{rpm}$ sidebands (Figure 3.40).

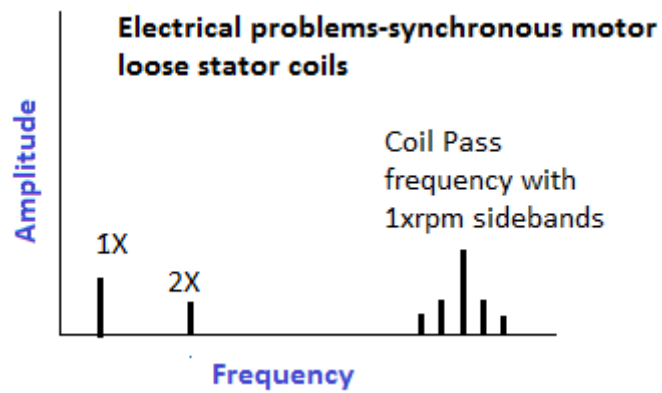


Figure 3.40 Synchronous motors

4 CONDITION BASED MONITORING OF DISTURBANCE ACTING ON THE MEASURED FORCE

The presence of disturbances in force rapidly growing with the contact velocity. These disturbances do not depend neither on contact friction and roughness of the contact surface, nor on force sensor noise. On the contrary they have to be ascribed to two prominent causes, namely arm structural elasticity due to torsional flexibility of the joints (Spong M. a., 1989), and the torque ripple of the permanent magnet brushless motor (Hanselman D., 1992). The structural elasticity is characterized by a resonance frequency, function of the arm configuration, while the torque ripple has a sinusoidal component whose frequency is proportional to the motor velocity. Both these frequencies (around a given configuration and for constant motor velocity) are clearly recognisable in the contact force spectra.

4.1 VELOCITY INDEPENDENT DISTURBANCE

The kinematic description of the robot is defined by the set of the Denavit-Hartenberg parameters. The model is therefore defined by the following equations:

$$M(q)\ddot{q} + V(q, \dot{q}) - G^{-T}\tau_t = J^T(q)f$$

$$J_m\ddot{q}_m + D_m\dot{q}_m + \tau_t = \tau_m$$

$$\tau_t = -K(G^{-1}q - q_m) - D(G^{-1}\dot{q} - \dot{q}_m)$$

$$\dot{s} = \bar{q}_m - q_m = e_m$$

$$\tau_m = K_P e_m + K_I s + K_D \dot{e}_m$$

Where vectors q and q_m are the link and motor coordinates vectors, respectively $G^{-T}\tau_t$ and τ_m are the transmitted torque vector, applied by the gearboxes to the links, and the motor torque vector, respectively, $M(q)$ is the robot generalized mass matrix, $V(q, \dot{q})$ is the vector of Coriolis, centrifugal and gravitational terms, $G = \text{diag}(G_I)$ with $|G_I| < 1$ is the matrix of transmission ratios, $J(q)$ is the 3x6 Jacobian matrix of the robot, relating the linear velocity of the tool tip, expressed in the tool reference frame, to the link coordinates velocities \dot{q} , $f = f_n = f[0 \ 0 \ 1]^T$ is

Condition Based Monitoring of Disturbance acting on the measured Force
the contact force, $J_m = \text{diag}(J_{mi})$ and $D_m = \text{diag}(D_{mi})$ are the motor inertias and the motor viscous damping matrices, respectively; K_p , K_I and K_D are the diagonal matrices collecting the proportional, integral and derivative gains of the PID motor position controller. The input output identification techniques have been adopted for computing the stiffness and damping parameters of the transmissions, namely matrices K, D, D_m . The whole identification process is described in (Campostrini, 1994) (Ferretti G., 1995).

A spectral analysis performed on force data relative to the time intervals where the motor velocities are approximately constant made it possible to classify the high frequency disturbances into two main categories:

- Velocity independent disturbance
- Velocity dependent disturbance

The following factor may be first discarded as possible sources of velocity independent oscillations:

- force sensor noise;
- support table compliance;

In particular, the spectral density of the force sensor output with the robot at rest shows a very low level noise, while no peak in the neighbourhood of the velocity independent resonance frequency is put into evidence. The velocity independent disturbances have been therefore ascribed to the arm structural elasticity, in particular to the joint torsional flexibility (mainly due to transmission gears), whose effects have been studied by means of a linearized model of the whole system around an equilibrium point (\bar{q}, \bar{q}_m) . The linearized model is derived taking into account the force sensor compliance, being the variations of the contact force amplitude δf related to the variations of the joint coordinates δq as follows:

$$\delta f = -K_s \delta z = -K_s n^T J(\bar{q}) \delta q$$

here K_s is the sensor compliance. The linearized model is therefore defined by the previous equation and by the following equations:

$$M(\bar{q}) \delta \ddot{q} + \left. \frac{\partial V(q, \dot{q})}{\partial q} \right|_{q=\bar{q}} \delta q - G^{-T} \delta \tau_t = J^T(\bar{q}) n \delta f$$

$$J_m \delta \ddot{q}_m + D_m \delta \dot{q}_m + \delta \tau_t = \delta \tau_m$$

$$\delta \tau_t = -K(G^{-1} \delta q - \delta q_m) - D(G^{-1} \delta \dot{q} - \delta \dot{q}_m)$$

$$\dot{\delta s} = \delta \bar{q}_m - \delta q_m = \delta e_m$$

$$\delta \tau_m = K_p \delta e_m + K_I \delta s + K_D \delta \dot{e}_m$$

where δx denotes the variations of the quantity x from the equilibrium value. The Coriolis and the Centrifugal term, showing a quadratic dependence on joint velocities, give no contribution to the linearized model, since an equilibrium point with $\dot{q} = \dot{q}_m = \mathbf{0}$ is considered. Since the singularities of the linearized model depend on the particular equilibrium point. The linearized model is characterized by a couple of dominant low damped complex conjugate poles, located in the different configurations. These values are in quite good agreement with the location frequency of the peaks in the force spectral densities computed from force measurement obtained by exciting, through a random offset of suitable amplitude, the motor position setpoints with the robot at rest.

4.2 VELOCITY DEPENDENT DISTURBANCE

The motor torque ripple and the resolver output noise are the main sources of the velocity dependent disturbances. Both the torque ripple and the resolver output noise have a well defined frequency characteristics, that are predicted by modeling and may be experimentally verified. (Ferretti G. M. G., 1997)

4.2.1 Resolver output noise

Resolver stator output signal are processed by Tracking Resolver to Digital Converters (TRDC) to obtain the digital value of the rotor angular position. TRDC assure steady state accuracy at constant rotating velocity in ideal condition. It is shown in (Hanselman. 1990) that non-ideal characteristics like amplitude imbalance, imperfect quadrature between the two resolver signals, and distortion of the excitation signal cause position errors that can be approximated as sinusoidal functions of $2 q_m$, while inductive harmonics determine an error ε expressed by the following Fourier series:

$$\varepsilon = \sqrt{2} K_0 \cos\left(q_m + \frac{\pi}{4}\right) - \sum_{n=1}^{\infty} K_n \sin[(n-1)q_m]$$

Therefore, when a motor is rotating at constant velocity ω_m , the resolver output is affected by harmonics of frequency multiple of ω_m . From the spectral analysis of the output of the adopted resolvers it appears that the first, second and third harmonic are those with larger amplitude, but also higher order harmonics are clearly observable. The resolver output noise enters the position regulators and thus, with possible amplification especially in the frequency range where the gain of the derivative action of the regulator is higher, it perturbs the motor current setpoint and generates a motor torque disturbance. This, in turn, reflects on the contact force.

4.2.2 Motor torque ripple

It's well known that the torque ripple in permanent magnet brushless motors constitutes one of the most significant limitations for high accuracy positioning control of mechanical systems. The disturbance, which affects in varying degrees all brushless motors, appears, in fact, as an irregularity in the generation of the torque, which shows a ripple added to the nominal torque provided by motor. The torque ripple shows components whose frequencies are linearly varying with the rotational motor speed. So, when not properly compensated, it can easily excite the mechanical resonances of the machine, causing persistent fluctuations of the manipulator tool. These phenomena can badly affect the motion and the positioning quality (Bottero A.).

4.2.2.1 The model of disturbance

The model of the torque generation is formalized in

$$\tau = N(\alpha, I_{ref}) + K_t \cdot I_{ref}$$

$$N(\alpha, I_{ref}) = \gamma(\alpha) + \delta(\alpha) \cdot K_t \cdot I_{ref}$$

Where:

- τ is the total torque generated by the motor;
- α is the electrical angle (p times the mechanical angle θ , where p is the number of the motor pole pairs);

Condition Based Monitoring of Disturbance acting on the measured Force

- I_{ref} is the output of the position controller and represents the set-point reference for the current control;
- $\gamma(\alpha)$ represents the torque disturbance, acting on the rotor, originated both by the irregularity of the air gap and by the measurement offsets in phases current sensors;
- $\delta(\alpha)$ represents the torque disturbance arising from the imperfections of profiles of back emf and currents, which are not really sinusoidal, from the unbalances of the amplitudes and non-alignment of phases. Under ideal conditions γ and δ are 0.

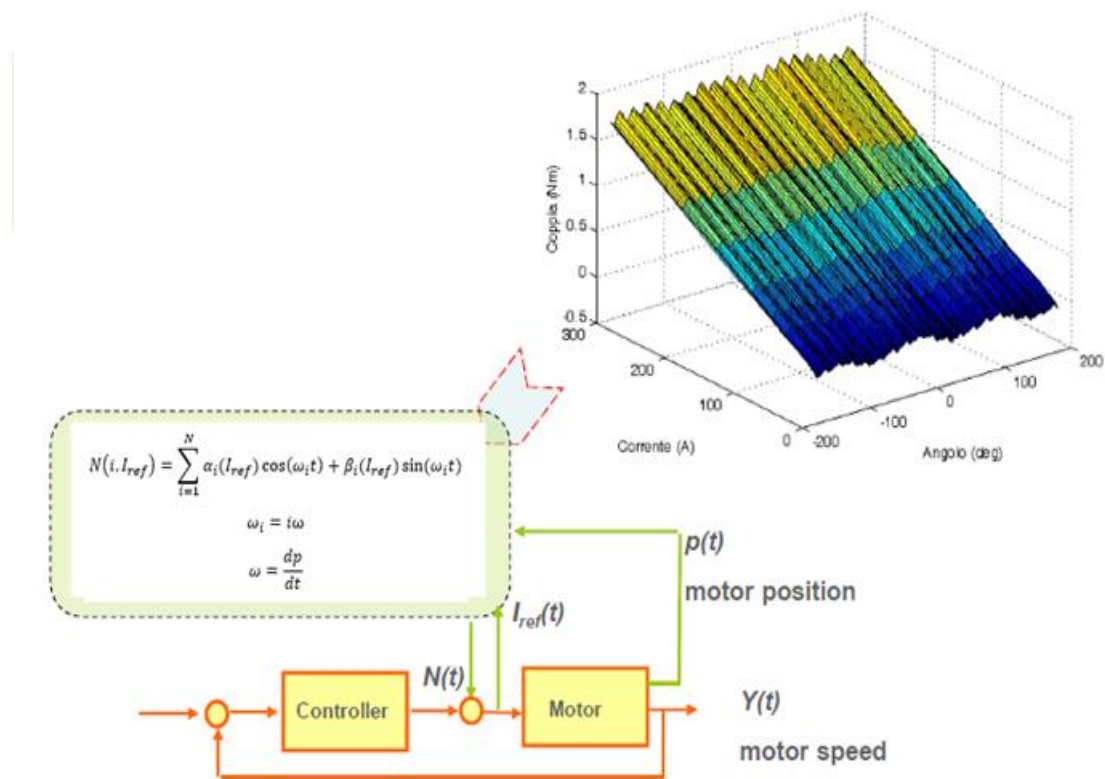


Figure 4.1 Dependence of the torque ripple on the angular position and current

Figure 4.1 shows the dependence of torque ripple $N(\alpha, I_{ref})$ on the angular position of the rotor and on the requested current/torque. If the closed loop position control was able to adjust to zero the torque ripple (ideal input noise rejection condition), the load torque transmitted to the plant could be expressed as:

$$\tau = K_t \cdot \bar{I}_{ref}$$

Condition Based Monitoring of Disturbance acting on the measured Force \bar{I}_{ref} being the current that would feed the motor with no torque “ripple”. \bar{I}_{ref} can be computed as the average value of the current set-point I_{ref} when the load torque, acting on the joint, is constant. Combining the two equations, is possible to obtain:

$$K_t \cdot \bar{I}_{ref} = \gamma(\alpha) + K_t \cdot (1 + \delta(\alpha)) \cdot I_{ref}$$

Or in an equivalent form:

$$I_{ref} = \frac{\bar{I}_{ref}}{(1 + \delta(\alpha))} - \frac{\gamma(\alpha)}{K_t \cdot (1 + \delta(\alpha))}$$

The previous equation describes the compensation of the torque disturbance: it models how the position controller output \bar{I}_{ref} should be modified in such a way that current set-point will reject

$$I_{ref} = \left(1 + \frac{\sigma(\alpha)}{K_t}\right) \cdot \bar{I}_{ref} + \frac{\rho(\alpha)}{K_t}$$

The previous equation describes the compensation of the torque disturbance: it model show the position controller output \bar{I}_{ref} should be modified in such a way that current set-point I_{ref} will ideally reject the disturbance $N(\alpha, I_{ref})$.

4.2.2.2 Disturbance action on speed control

The torque ripple $N(\alpha, I_{ref})$ in acts as a non-linear feedback disturbance on the closed loop control system. Fig. 3.2a represents the sensitivity function of the loop $S(s) = \frac{w_m(s)}{N(s)}$, as valued on the controlled output (motor rotation speed). The disturbance $N(\alpha, I_{ref})$ can be developed as a trigonometric series of functions of α . **The instantaneous frequencies of the sine and cosine components are proportional to the rotor rotation speed.** In Fig. 3.2b we can see that:

- **at high** speed, the high-frequency components of the disturbance are filtered by the inertial terms in the controlled system

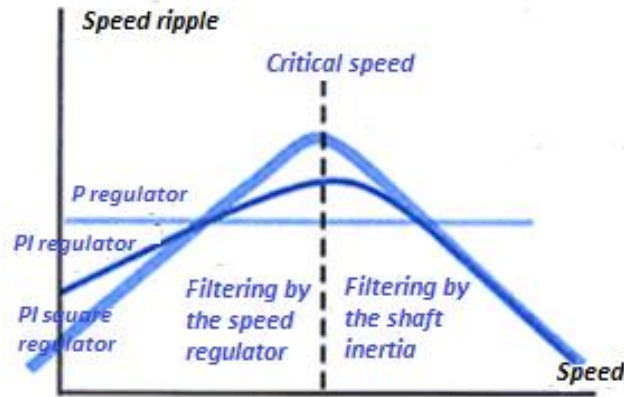


Figure 4.2a Speed response to the torque disturbance

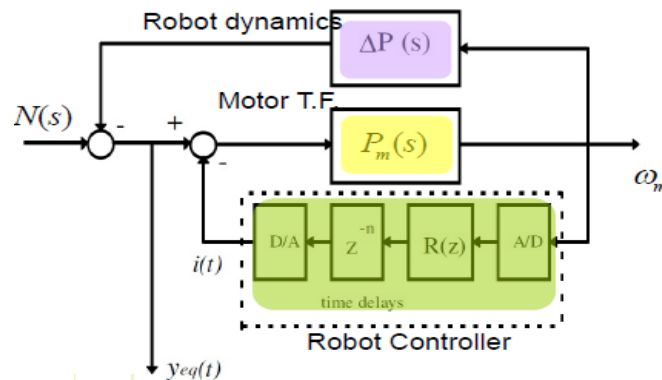


Figure 4.2b Control Scheme

- at low speed, the low-frequency components are filtered by the integral actions of the closed-loop controller;
- torque ripple components with frequency close to the limit of closed-loop control bandwidth cannot be filtered and give rise to persistent oscillation phenomena.

We understand, from Fig. 3.2a, that at extremely low speeds the closed loop control, thanks to internal integrative actions, is able to perfectly reject the torque disturbance, returning an accurate image of it.

4.2.2.3 Feed Forward Compensation

Considering the disturbance) $N(\alpha, I_{ref})$ as an additive input torque to the motor, the expression of the feedforward compensation, rejecting the ripple, is:

$$(I_{ref} - \bar{I}_{ref}) \cdot K_t = \sigma(\alpha) \cdot \bar{I}_{ref} + \rho(\alpha)$$

Condition Based Monitoring of Disturbance acting on the measured Force Function $\sigma(\alpha)$ and $\rho(\alpha)$ can be expanded in trigonometric series relative to the electric angle $\alpha = p \cdot \theta$:

$$\sigma(p \cdot \theta) = \sum_{n=1}^N B_{\sigma_n} \cdot \cos(n \cdot p \cdot \theta) + A_{\sigma_n} \cdot \sin(n \cdot p \cdot \theta)$$

$$\rho(p \cdot \theta) = \sum_{n=1}^N B_{\rho_n} \cdot \cos(n \cdot p \cdot \theta) + A_{\rho_n} \cdot \sin(n \cdot p \cdot \theta)$$

The characterization of B_{σ_n} A_{σ_n} B_{ρ_n} A_{ρ_n} based on the residual signal $K_t \cdot (I_{ref} - \bar{I}_{ref})$, allows applying the compensation of the torque ripple. The torque ripple compensator is here referred as TRC.

The term \bar{I}_{ref} is equal to the average value of set point current (the load acting on the joint is constant). The measurement process, for parameter estimation, is executed at low speed, in constant speed conditions, performing movements that correspond to some complete rotor revolutions, and for different values of \bar{I}_{ref} (constant average value of I_{ref}). The experimental results obtained with the application of TRC to medium and big sizes COMAU industrial manipulator are exemplified in the following Figure.

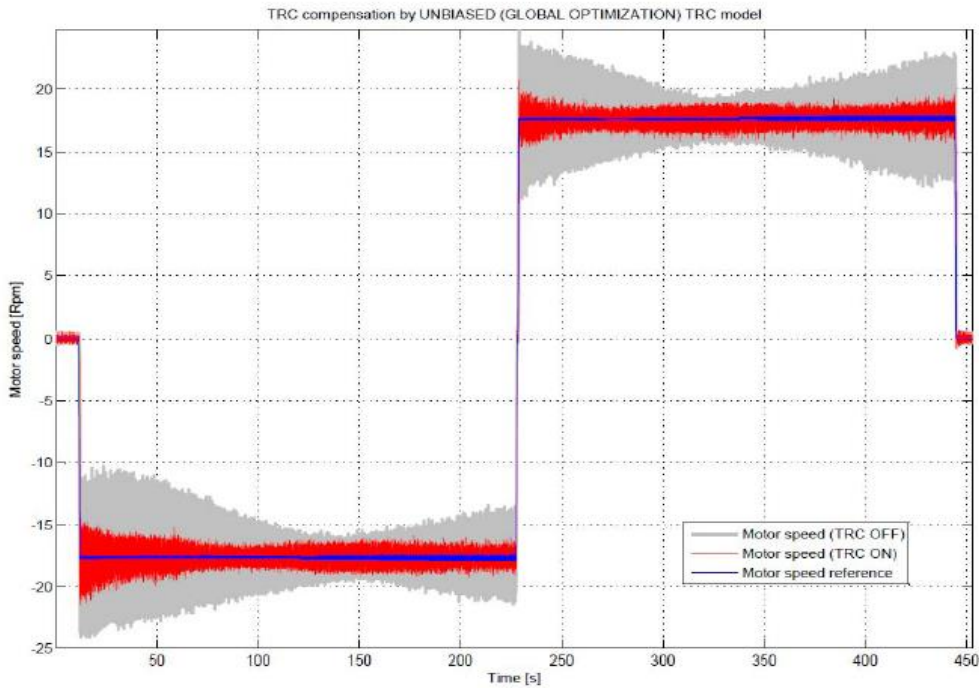


Figure 4.3 TRC effect on ax 3 of a NJ 420-3.0 manipulator

Condition Based Monitoring of Disturbance acting on the measured Force

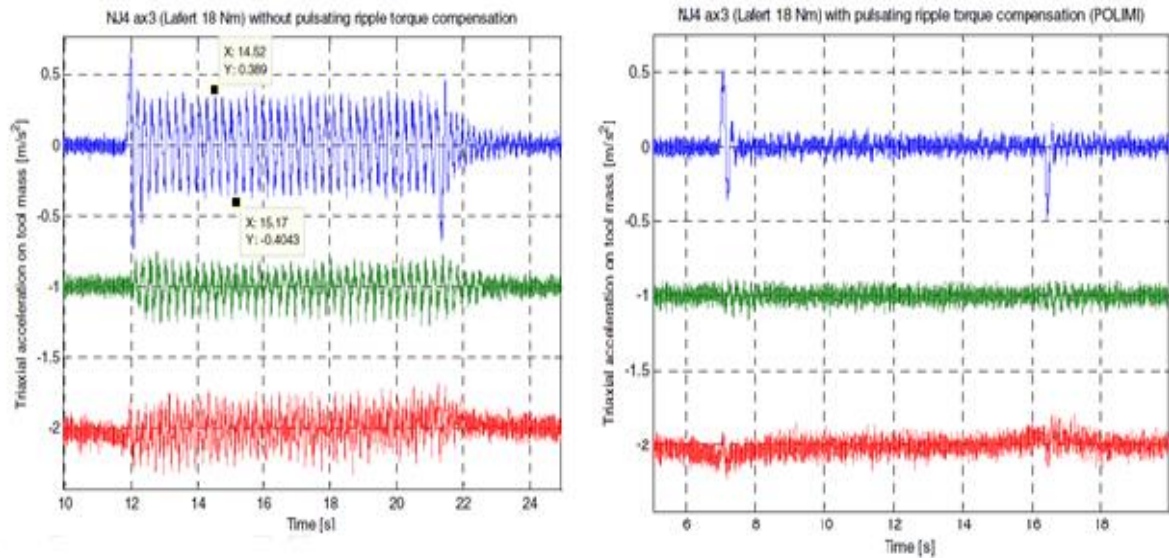


Figure 4.4 Load Accelerator with TRC not active and active on a NJ4 175-2.5 manipulator

4.2.2.4 Limits in Parameters Identification

The results obtained are very good. The efficacy was maintained over time because the torque ripple is predictable and stationary (does not seem to change with ageing of motor components or changes in operating conditions, like the temperature variation). However, the effort required for the model parameters identification (described in detail in (G. Ferretti, 1998) (G. Ferretti G. M., 1998)) from controller currents is almost prohibitive and exhibits some limits:

- an effective compensation requires series expansions of 9 terms for each motor;
- in the identification phase, 14 terms (56 parameters + 14 parameters representing the frequencies) should be estimated, for each motor;
- for a 6 axes manipulator, the activation of the feedforward compensation asks for identification of 420 parameters;
- the identification from the regulation current ($I_{ref} - \bar{I}_{ref}$), requires tests at extremely low speed (0.5 Rpm);
- this results into a 20 minutes identification phase for each motor (2 hours for 6 axes manipulator);

• due to limitations in input noises rejection capability of industrial controllers, the signal $(I_{ref} - \bar{I}_{ref})$ does not contain a “perfect copy” of the disturbance. This systematic error in the representation of the disturbance causes bias errors in the parameter estimates $B_{\sigma_n} A_{\sigma_n} B_{\rho_n} A_{\rho_n}$

4.2.2.5 Adaptive Control for Compensation Model Identification

There are several industrial applications of adaptive compensation of periodic disturbances (automotive industry, aerospace and robotics). The adaptive compensator is shown in Figure 4.5 (P. A. Ioannou) (S. Sastry, 1989).

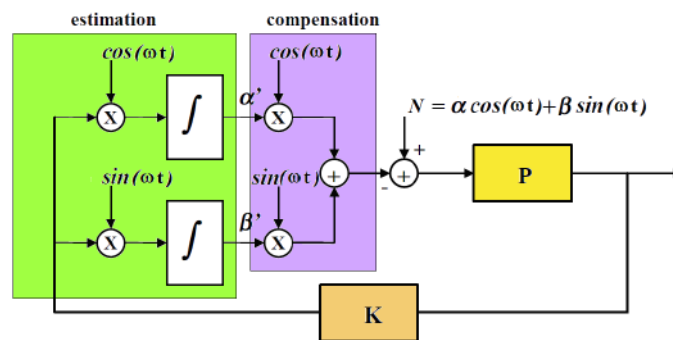


Figure 4.5 Basic adaptive compensator for sinusoidal disturbances

The adaptive compensator is a non linear controller which regulates to zero the effect of periodic disturbance $N(\omega t)$ by producing an exact copy of it, having the same structure of the signal. Fig. 3.5 shows the adaptive controller for a sinusoidal disturbance with one component and one frequency ω .

These adaptive system are defined “direct adaptive system”, since the model parameters are estimated while they are used to compensate the disturbance. These adaptive controller are equivalent to linear time variant controllers (LTV) operating on very narrow frequency bands, whose amplitude is a function of the gain K. The narrow band determines a relatively slow transient activation of a few seconds but, however, also helps for the robust stability of the adaptive system.

If the linear plant P has suitable characteristics, i.e. it is a “strictly positive real” system SPR: it behaves as an impedance- according to Brune’s functions properties- of a passive electrical network, (formed only by capacitors and inductors), is possible to apply well known results of adaptive control theory (references to the lemma of Kalman Yakubovic in (P. A. Ioannou) (S. Sastry, 1989)) and the asymptotic stability of the adaptive control loop has been proven.

The adaptive parameters converge to the true values and its possible to determine an exact copy of the torque disturbance knowing the signal model structure. Once the adaptive system transient goes to the end and the adaptive parameters reach their steady state values, the gain K , can be set to 0. The update of adaptive parameters stop and the Figure 3.6 reduce to a feed forward disturbance compensation like (TRC), that’s is open loop.

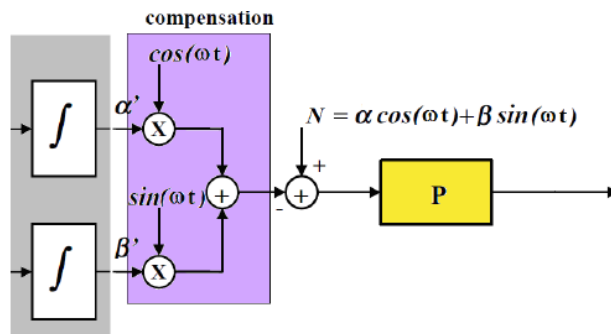


Figure 4.6 Feed forward disturbance compensation

A detailed analysis of the robust stability of adaptive schemes applicable to the control of electromechanical systems and industrial manipulator is in (Bottero A.).

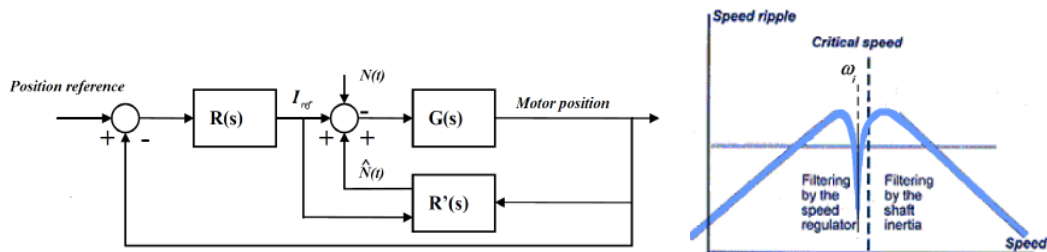


Figure 4.7 The complete architecture of the adaptive compensator

Using and extending some results obtained in a previous work (Bottero A.), it **has been possible to combine a network $R'(s)$ of adaptive compensators (that are** in concept similar to the controller shown in Fig. 4.6) with the position controller of COMAU Robotics C5G Control Unit (see Fig. 4.7).

The block $R'(s)$ represents the parallel of 14 adaptive regulators, being each of them "tuned" to one of the components of the trigonometric series expansion of $N(\alpha, I_{ref})$. With reference to Fig. 6, the plant P output has been chosen as the output of a load torque observer, designed on the nominal model of the motor. It is possible to demonstrate (Bottero A.) that, with this output, the plant P in Fig. 4.5 is always SPR, in a robust way and in presence of uncertainty. The position trajectory, during the estimation procedure, provides a significant change in load torque / current \bar{I}_{ref} . So the conditions for "*persistent excitation*" (PE) are created and it is possible to get parameter estimates for $B_{\sigma_n} A_{\sigma_n} B_{\rho_n} A_{\rho_n}$, with low bias error (estimates tend to be consistent). **The adaptive block $R'(s)$ is active only** during the parameters identification procedure. In normal operation conditions, the torque ripple compensation is assured by TRC, implemented as a part of digital drives software. The identification phase results to be fast, automatic and robust.

5 CASE STUDY: ABNORMAL NOISE ON AXIS 3 DUE TO A BELT-BASED POWER TRANSMISSION SYSTEM

5.1 BELT BASED POWER TRANSMISSION

The Belt analyzed is a BELT GATES 426-3MGT WIDTH=6 the length specified is 426 mm.

5.1.1 Frequency Analysis

The *belt frequency* is given by the formula:

$$\text{Belt frequency} = \frac{\pi \times \text{pulley rpm} \times \text{pulley diameter}}{\text{belt length}}$$

In the single-axis test at the specified velocities the frequency of the belt is given in the following table:

5% of the max. speed 300 rpm	25% of the max. speed 1500 rpm	50 % of the max. speed 3000 rpm	75% of the max. speed 4500 rpm
1,58363615 Hz	7,918180751 Hz	15,8363615 Hz	23,75454225 Hz

Table 2 Frequencies of the belt at different speed of the motor

For the *pulleys* obviously is assumed that the Driver one has the same frequency of the motor and the driven one has a frequency that can be easily calculated knowing the reduction ratio $z=z_1/z_2$ where $z_1=45$ (driver pulley) and $z_2=40$ (driven pulley). The results are shown in the following table:

	5% of the max. speed 300 rpm	25% of the max. speed 1500 rpm	50 % of the max. speed 3000 rpm	75% of the max. speed 4500 rpm
Driver	5 Hz	25 Hz	50 Hz	75 Hz
Driven	5,625 Hz	28,125 Hz	56,25 Hz	84,375 Hz

Table 3 Frequencies of the Driver and Driven Pulley at different speed of the motor

The frequency measured by the The Sonic Tension Meter capable to identify the vibration of the belt span and instantly converts it into belt static tension coincide with a zero placed at the pulsation

$$\omega_{ar} = 2\pi f_{ar} = \sqrt{\frac{K}{J_l}}$$

Case Study: Abnormal noise on Axis 3 due to a belt-based Power Transmission System

Where K is the torsional rigidity of the coupling between the pulleys only, Jr is the inertia of the driven pulley. Far represents the belt frequency tensioning. [Far]=Hz.

The *resonance frequency* that are possible to see from the current and the velocity as vibrations that can generate noises and are index of marginal instability caused by the belt-based transmission are visible in a frequency greater than the tensioning frequency according to the expression:

$$\omega_r = 2\pi f_r = \sqrt{\frac{KJ_t}{J_l(J_m + J_p)}} = \omega_{ar} \sqrt{\frac{J_t}{(J_m + J_p)}}$$

$$J_t = J_m + J_p + \frac{J_l}{n^2}$$

Where Fr is the resonance frequency [Fr] = Hz. Jt is the inertia seen at the motor side and is equal as first approximation at the sum of the motor inertia + Jp the inertia of the driver pulley (fixed to the motor) +the onertia JI/n^2 of the driven pulley expressed at the motor. n is the the transmission ratio between the driven pulley and the driver one.

The resonance frequency of the belt-based transmission are normally higher than 100 Hz. This is valid also for all the Racer. Given the tensioning nominal frequency (far) and the the previous formula where are visible Jt, Jm, and Jp is possible to derive the nominal-resonance frequency of the belt (of the belt-based transmission motor-driven pulley) and the resulti s displayed in Table 5. Oscillation at the tensioning frequency are not visible but only oscillation at the resonance frequency fr greater than far. In the following Tables the Inertia related to the components of the Belt-Based Transmission.

Axis 3 Racer 3 Progettazione Meccanica Trasmissione	Index	z	Inertia about rotation axis Kg*m^2	Inertia trasmission seen at motor side Kg*m^2
Driver Pulley	Jp_dp	45	0,00000996	
Calettatore Driver Pulley	Jp_c		0,00000438	
Sum Jp_dp+Jp_c			0,00001434	
Driven Pulley	Jl	40	0,00001801	
Motor axis 3	Jm		0,0029	
Trasmission ratio (z2/z1)	n	0,888888889		

$J_t = (J_m + J_{p_c} + J_{p_{dp}} + J_l) / (40/45)^2$				0,003711255
--	--	--	--	-------------

Table 4 Inertia of the different components

Asse 3 Racer 3 Progettazione Meccanica Trasmissione	K estimated	Tensioning Frequency Far	Resonance Frequency Fr	war	wr
Belt _ PowerGrip GT3-3MGT	23,81089002	183	206,510152	1149,822911	1297,54155 3

Table 5 Resonance frequency and Tensioning frequency of the belt

5.1.2 Temporal Analysis

Here a change in the characteristics of belt vibration power in response to a change in belt velocity is investigated.

5.1.2.1 Belt Velocity and Transverse Vibration Power

When a belt span vibrates in the transverse direction there occurs a continuous exchange of energy between elastic potential energy and kinetic energy. A measurement of belt displacement over time and the mass of the belt allows one to specify the distribution of energy between the elastic potential form and kinetic form. The average energy dissipated as vibration over time is the vibration power. The average energy dissipated as vibration over time is the vibration power. The energy of the output signal of a vibration transducer averaged over time is a measure of signal power and is a scaled quantification of the vibration power. A measurement of the power of the sampled output signal of any form of transducer is given by equation that specifies the root mean square (r.m.s) value of a series

$$P_y = \sqrt{\frac{1}{I} \sum_{i=0}^{I-1} (y_i)^2}$$

Analysis of Vibration Power

The figure consists of a plot of the maximum velocity assigned knowing that the maximum velocity of the versus vibration r.m.s. power. Each point plotted is derived from a set of vibration data captured by the sensor in term of voltage: the data acquisition rate is 2000 for a duration time of 120 s.

Case Study: Abnormal noise on Axis 3 due to a belt-based Power Transmission System

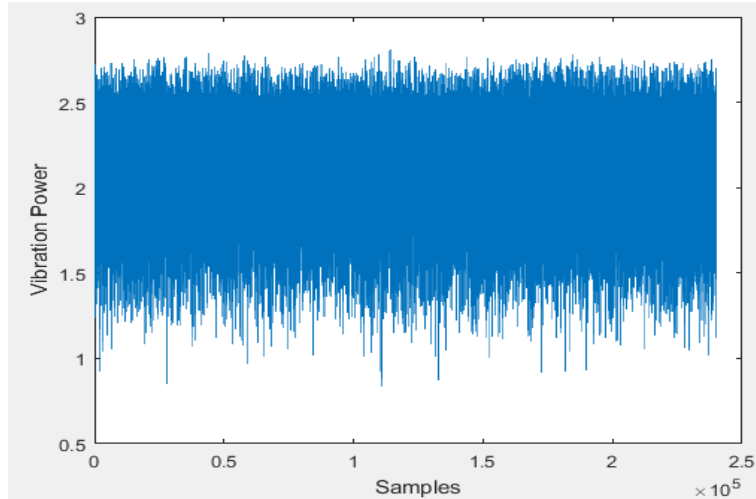


Figure 5.1 Vibration power of the signal coming from the sensor

The following plot shows that the belt vibration power increases with the velocity.

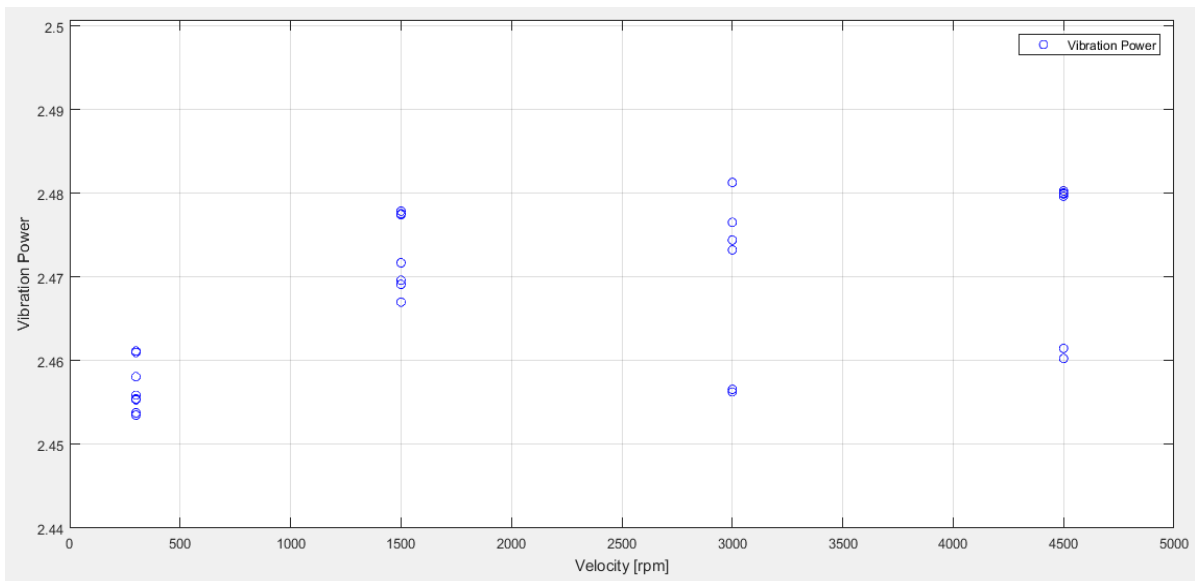


Figure 5.2 Vibration power versus velocity

6 EXPERIMENTAL RESULTS

6.1 EXPERIMENTAL SET UP

The experiments have been made on the industrial robot RACER 3, manufactured by COMAU, endowed with a R1C controller. The Robot RACER3 is a 6 d.o.f, 3 Kg payload manipulator.

The experimental tests are carried out acquiring both signals internal to the controller. Transversal vibration of the belt and axial/radial vibration close to the bearing house are acquired by an infrared displacement sensor and an accelerometer respectively. The experimental test bed comprises a process control board Measuring Computing E-1608 16 bit Multifunction Ethernet DAQ device. A converter is connected to the displacement sensor and is capable to convert 220V AC to 12 V DC.



Figure 6.1: Experimental test bed for displacement sensor

Cheng Ke CT5201 single-channel constant-current adapter acceleration sensor power supply and amplifier with constant current source is used to acquire data from an accelerometer. The excitation source voltage is +24 VDC with a current of 2mA. The upper and lower limit frequency are 100kHz and 0.3 Hz respectively. The output will have a possible gain of x1, x10 according to panel selection and an accuracy $\leq \pm 1.5\%$.



Figure 6.2: Experimental test bed for Accelerometer

6.1.1 High frequency acquisition from a signal controller

The motor shaft position are measured by means of position encoders with a resolution of 21 bits, while currents are coded on a signed 16 bit string. The sampling time of the controller is fixed to 0.004s obtaining a visibility of 125 Hz (Nyquist frequency) this is the frequency that is visible plotting the spectrum of a `moni.log` of type 10.

The interface WinC5G is used to establish by remote a connection, take the `moni.log` data and from the terminal start the acquisition. In order to deal with high order frequency a `moni.log` of type 30 is used obtaining a rate of 4 μ s and so a frequency of 125000 Hz sufficient for the analysis that is carried out.

The diagnostic information related to mechanical problem usually are motor rotational speed and the reference current. For the efficiency of the torque the quadrature current I_q and the deflux current I_d must be compared with their reference value. In theory is always true that:

- $I_d == I_{d_ref} == 0$
- $I_q == I_{q_ref}$ equal to the torque necessary to impose the trajectory of a manipulator. Since the achievement of these two conditions is achieved by two servo system the equality is not perfectly obtained.

The gap from the nominal condition should be evaluated to understand if we are in presence of an acceptable control limit or the tracking error is not normal.

6.1.2 Acquisition from a displacement sensor

The sensor used for the transversal vibration of the belt is a CMOS type Micro Laser Distance Sensor HG-C. The Measurement center distance is 50 mm, the

measuring range is $\pm 15\text{mm}$ and the linear mapping is obtained between 0-5 V. At distance of 50mm the sensor display the zero value corresponding to a 2.5 V.

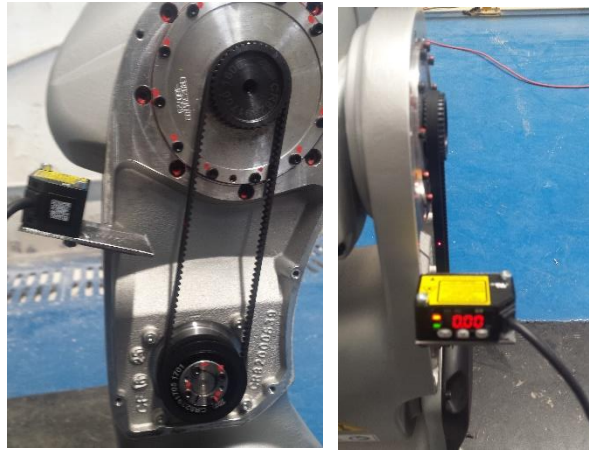


Figure 6.3: CMOS type Micro Laser Distance Sensor HG-C

The interface TracerDAQ® Pro is Out-of-the- box virtual instrument suite with strip chart, oscilloscope, function generator, and rate generator is used to visualize data in Real time. In the following a picture describing the data collected from the sensor: small vibration are visible and close to the zero measurement since the value of the volt plotted is around 2.5V.

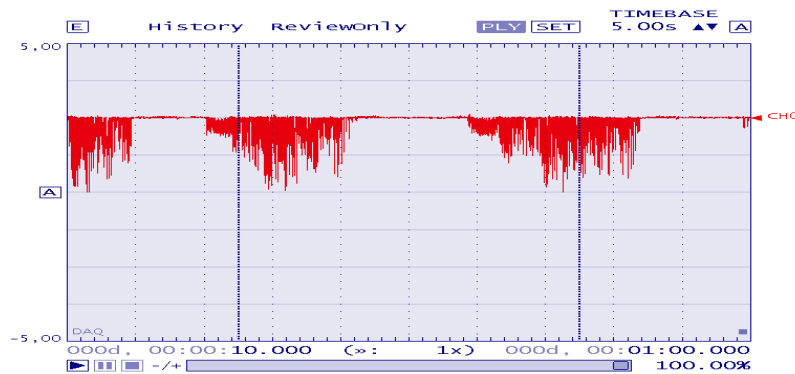


Figure 6.4: The interface TracerDAQ Pro

For vibration analysis MATLAB is used with the connected Moni Library used for the visualization of the Moni.log. Also the Data Acquisition board can be visible Matlab through the Data Acquisition System Toolbox. In the folllowig picture the output

6.1.3 Acquisition from an accelerometer

As for as axial (see picture on the left) and radial vibrations (see picture on the right) is concerned the sensor used is a single axis accelerometer CT1010LC with sensitivity 100 Mv/g and frequency 0-5000 Hz.

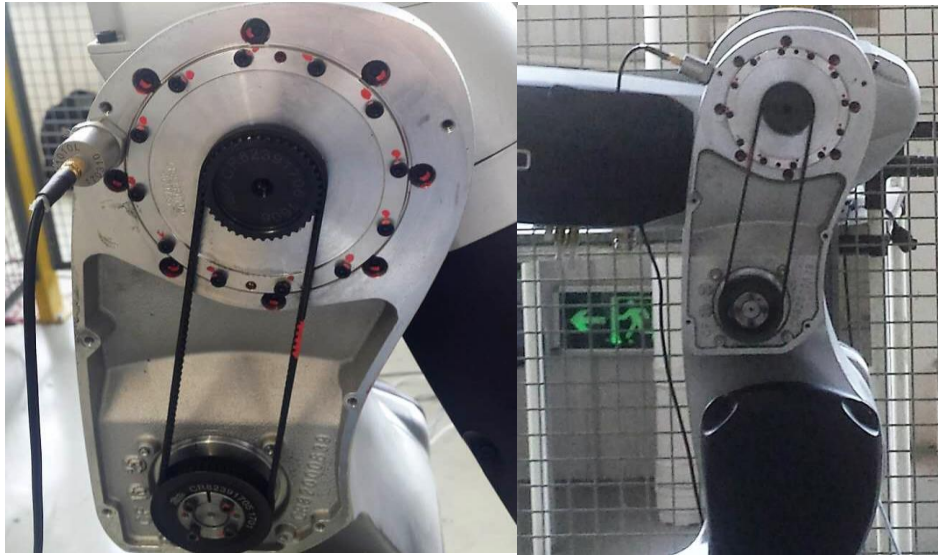


Figure 6.5.a and Figure 6.5.b: Position of the accelerometer in case of Axial and Radial vibration respectively

The interface TracerDAQ® Pro is Out-of-the- box virtual instrument suite with strip chart, oscilloscope, function generator, and rate generator is used to visualize data in Real time. In the following a picture describing axial vibration (in term of voltage)-nominal case with 25% of maximum speed (sensor is positioned as in picture 5.a).

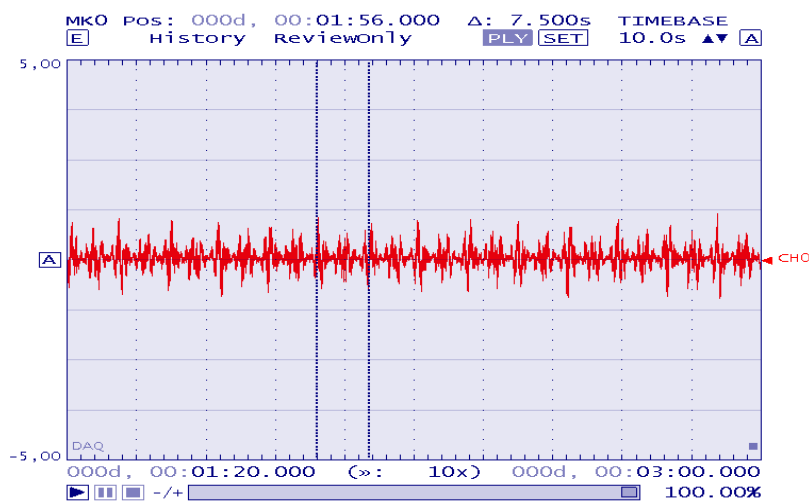


Figure 6.6: Axial vibration in term of voltage in nominal case 25% of the maximum speed

For vibration analysis MATLAB is used with the connected Moni Library used for the visualization of the Moni.log. Also the Data Acquisition board can be visible in Matlab environment through the Data Acquisition System Toolbox. In the following picture the output of the same case seen in Matlab converted in g: the sensitivity is 0.0971v/g.

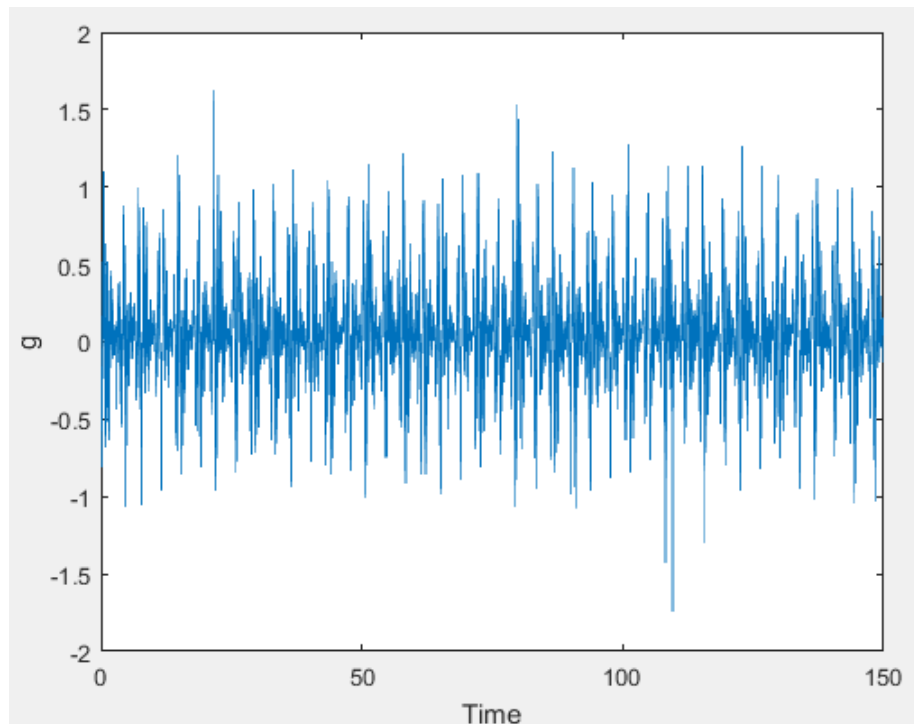


Figure 6.7: Axial vibration in Matlab environment 25% of the maximum speed

6.2 TEST PLAN

Each test that will be performed has a duration of at least two days since in the first day the axis three is evaluated during combined movement of the run in program and in the second day single axis movement are performed at different velocity speed at 5%, 25%, 50% and 75% override speed.

For the Runin Test due to the movement performed obviously the acquisition from the displacement sensor is not carried out but only the signals from the controller will be evaluated.

6.2.1 NOMINAL CASE

In the nominal case is carried out the collection of Moni.log of type 30 (high frequency acquisition) of conditioned type so the point of the program Runin that I have chosen from the acquisition is at 1' 14" of each cycle where combined movement of axis 3 with other axes are performed. In the second day single axis movement are carried out at 5%, 25%, 50% and 75% override speed. The duration of a single-axis acquisition is of 215s in case of three variables (reference position control, position encoder, reference current) and 130s for (position encoder, reference deflux current control, reference quadrature current control, measured deflux current, deflux tension [control output], quadrature tension [control output]).

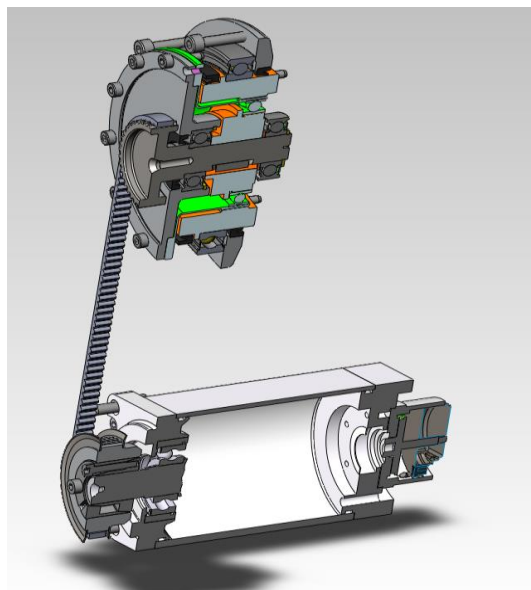


Figure 6.8: Belt-Transmission Based transmission

6.2.2 ANGULAR MISALIGNMENT

To perform this test two Spacers whose thickness is 0.5 mm are added and the inclination obtained is 1.14 degree. From the Manual of the supplier PowerGrip®

GT®3 Belt Drives the Misalignment should not exceed 1/4 degree for all synchronous belt.

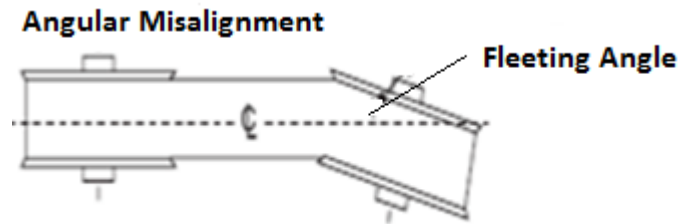


Figure 6.9 Angular Misalignment

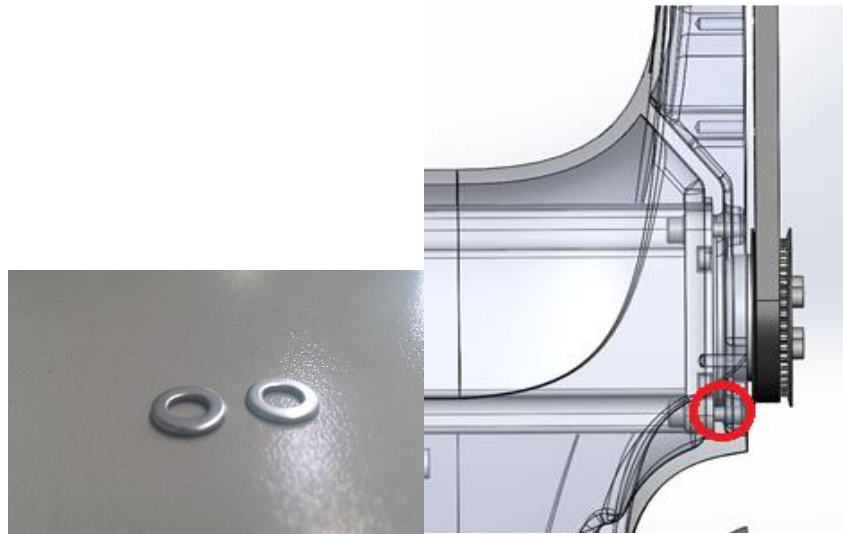


Figure 6.10 Addition of Spacers for the simulation of the Angular Misalignment

Misalignment is rarely seen just as 1× rpm peak. Typically, there will be high axial vibration with both 1× and 2× rpm. However, it is not unusual for 1×, 2× or 3× to dominate. These symptoms may also indicate coupling problems (e.g. looseness) as well (Figure 5.10)

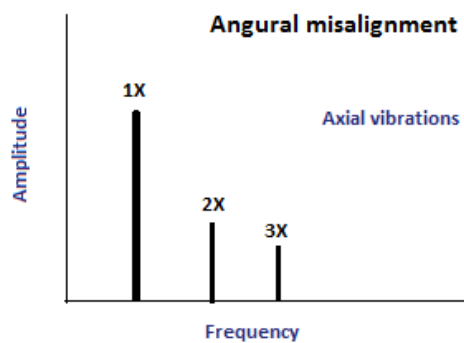


Figure 6.11 FFT in case of Angular Misalignment

After the first acquisition done in the nominal case the data will be evaluated from a single axis test. The tools used for the data acquired from the accelerometer are the DAQTracer and the Data Acquisition Toolbox of Matlab.

6.2.3 PARALLEL MISALIGNMENT

Special pulley attached to the reducer (driven Pulley) is needed to perform this test because the flange must be added in order to avoid that the belt will go out of its race. Due to this mechanical issue this test is not performed because is also far from the real case.

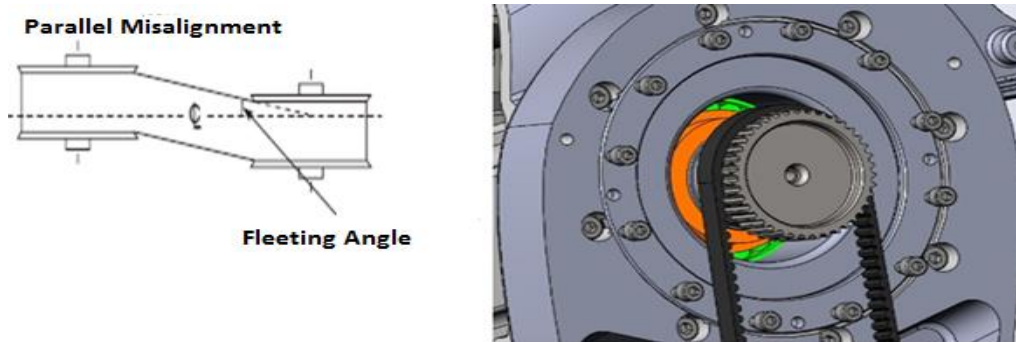


Figure 6.12 Parallel Misalignment

In case of parallel misalignment the vibration will occur at frequency $2x$ rpm, in Radial direction with 180 phase difference across coupling.

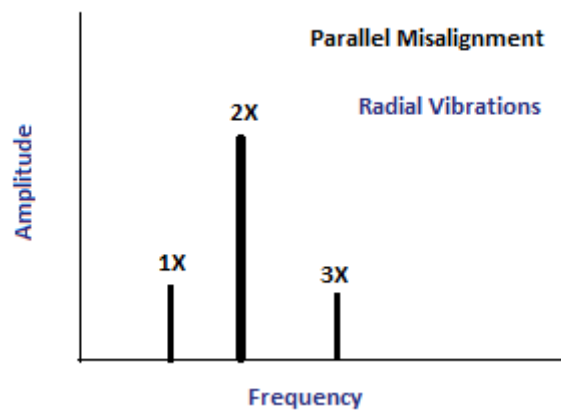


Figure 6.13 FFT in case of Parallel Misalignment

6.2.4 EXCESSIVE LOAD UNBALANCE

To create unbalance an additional mass is added on a rotating element. The formula that estimate the unbalance radial force is

$$F = M \times r \times \omega^2$$

Due to the small space on the rotor shaft is decided to put the additional mass on the driver Pulley.

The inertia of the system transmission+motor is [kg*m²*1E-4] 0.000083.

- Mass of the Driver Pulley is 0.034457 kg.
- **Mass of “callettatore” driver pulley 0.038917 kg.**
- Mass of the Driven Pulley 0.09107 7 kg
- Mass of the motor 0.7 kg.

In order to create a force of 50 N at the velocity of 3000 rpm (half of the max velocity allowed by the motor) on the Driver Pulley a mass of 0.03 Kg is added.

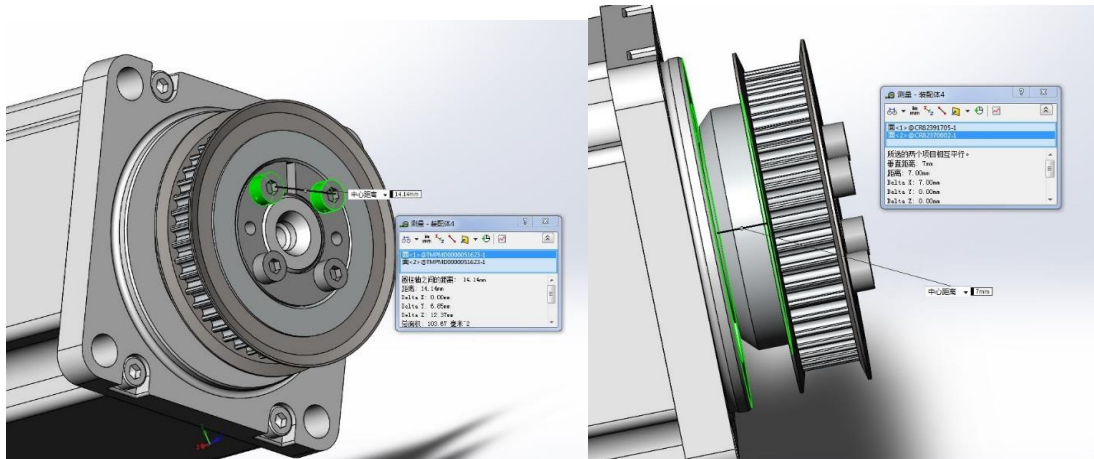


Figure 6.14 Limitations in space considered for the simulation of the fault Unbalance

For all types of unbalance, the FFT spectrum will show a predominant 1× rpm frequency of vibration. Vibration amplitude at the 1× rpm frequency will vary proportional to the square of the rotational speed. It is always present and normally dominates the vibration spectrum

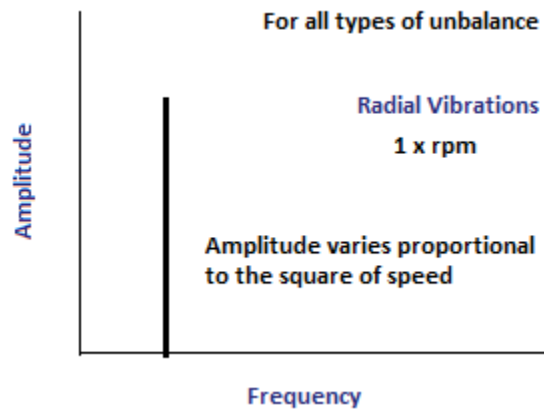


Figure 6.15 FFT of the fault Unbalance

After the first acquisition done during Runin like in the nominal case the Data will be evaluated also from a single axis test according to the data acquired from the displacement sensor through the DAQTracer interface and from Matlab through the Data Acquisition Toolbox.

6.2.5 INTERNAL ASSEMBLY LOSENESS

With the internal assembly looseness we have an improper fit between components part. So is chosen to simulate an assembly problem on the driver pulley and this is done avoiding to fix two screws on the pulley.

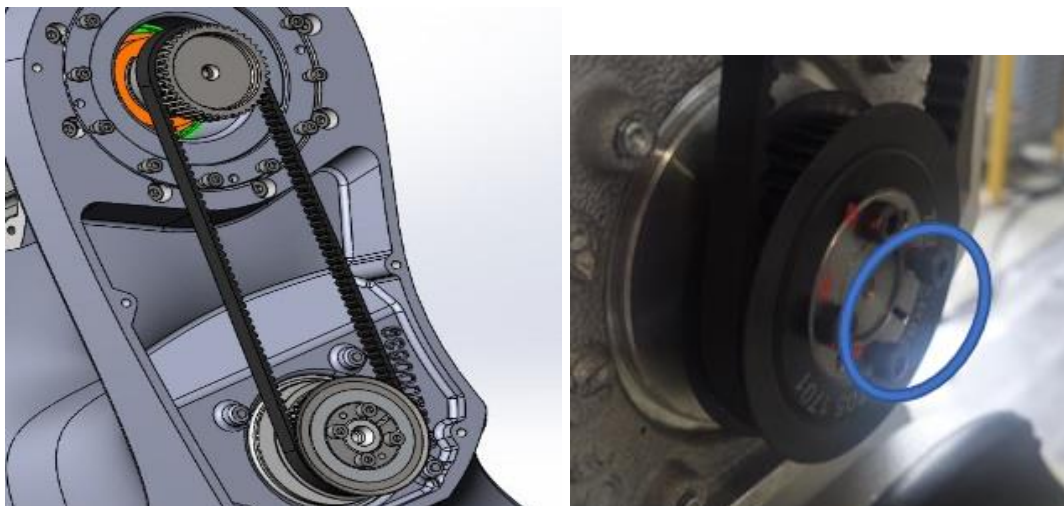


Figure 6.16 Simulation of Looseness

In case of internal assembly looseness the vibration will occur at frequency multiple (1/2,1/3) xrpm, along Radial direction.

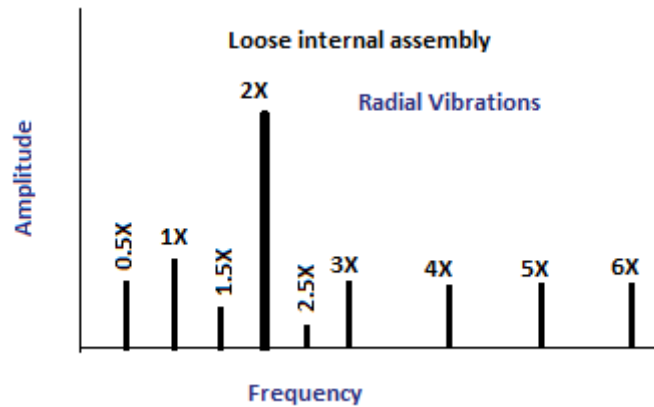


Figure 6.17 FFT in case of Looseness

6.2.6 TOOTH SHEAR

A damaged belt is substituted. The picture on the left shows the damaged belt where two tooth are cut off and the picture on the right instead shows the all transmission with de damaged part signed in red.



Figure 6.19. Damaged Belt



Figure 6.20 Application of a Damaged Belt

6.3 TESTING RESULT

6.3.1 Tooth shear

6.3.1.1 Temporal Analysis performed from the output of the displacement sensor

From the Tracer periodic vibration are detected in tranverse direction as is possible to see in the Figure 6.22 comparing the nominal case (see Figure 6.21). The acquisition is done from a single axis movement at maximum speed of 300 rpm at the rate of 100 Hz. The movement is a simple movement between two points performing a rotation of 270 degree that lasts 15 sec.

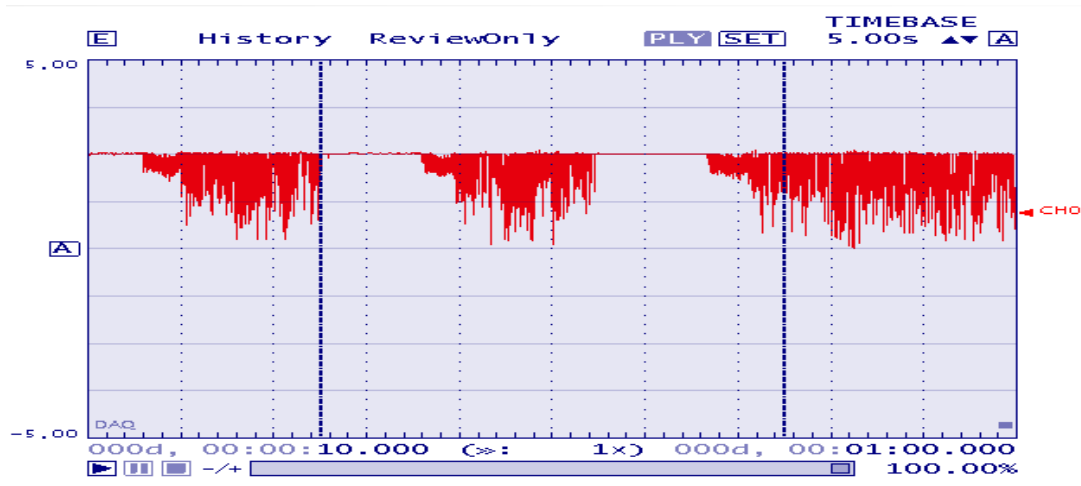


Figure 6.21 Transversal Vibration in Nominal case

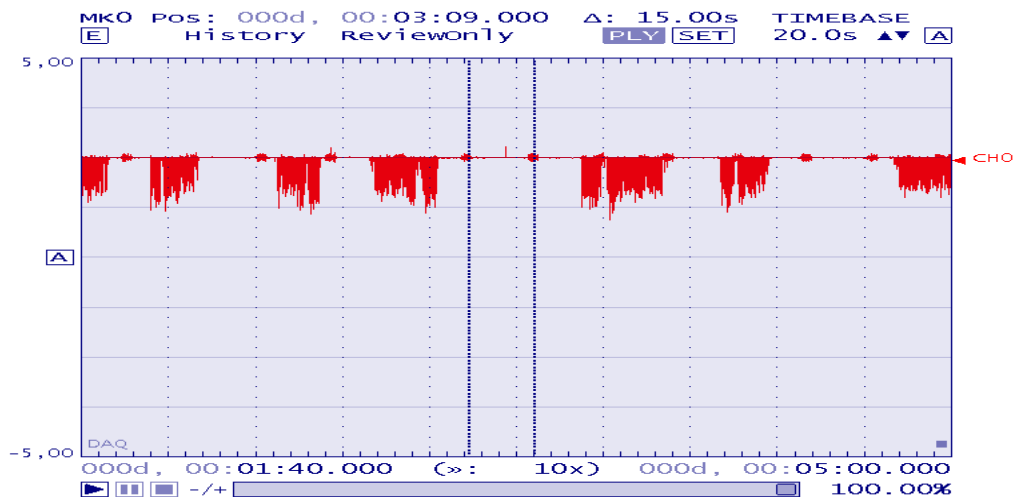


Figure 6.22 Transversal Vibration in case of fault

The oscillation presented shows an interval of 15 sec and is obtained at maximum speed when the acceleration is zero and with duration of 2 s.

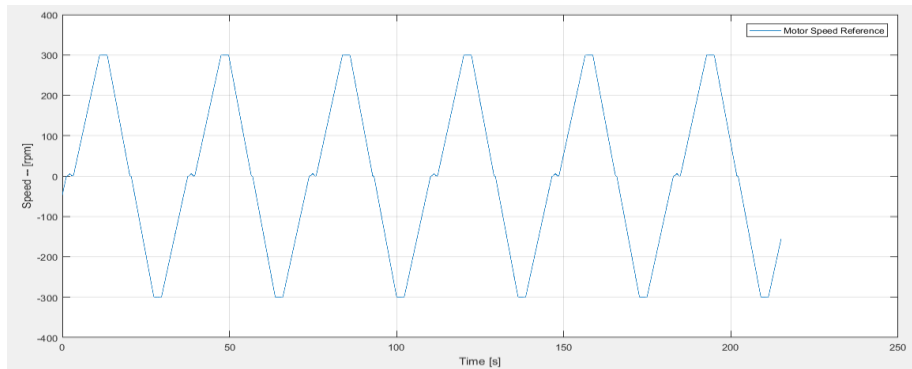


Figure 6.23 Reference Speed of the Motor

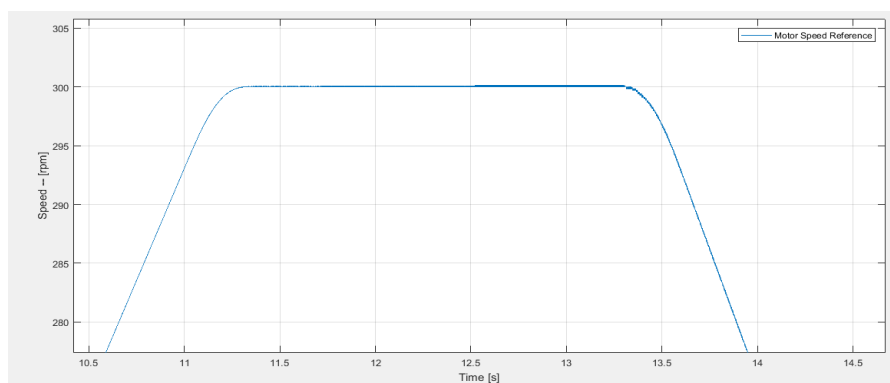


Figure 6.24 Time interval with Constant Velocity

The duration of this vibration can be verified in the scaled trace obtained as shown in the following Figure.

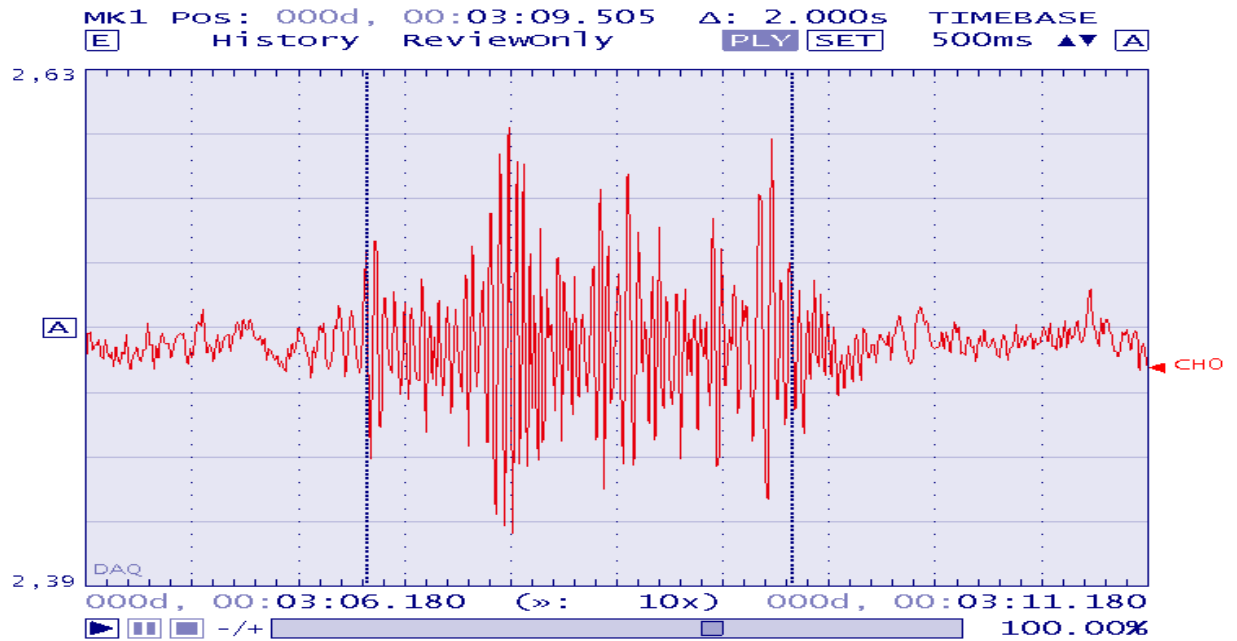


Figure 6.25 Trace of the entire vibration obtained at constant velocity

The temporal analysis is performed considering the interval of time in which the vibration happens in one belt rotation at constant velocity. Knowing that the length of the belt is 426mm is possible to calculate the time interval in which we have oscillations of the belt (in the Figure the two points are A and B).

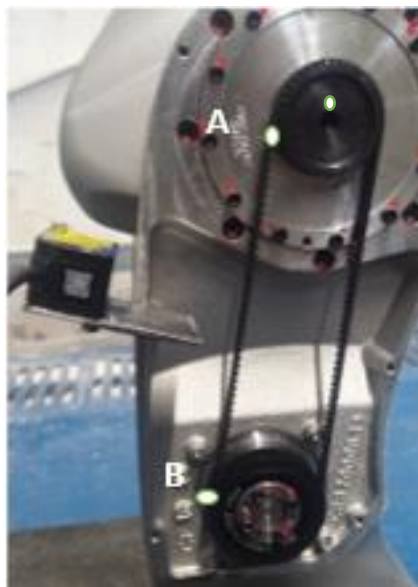


Figure 6.26 Points from which the vibration is recorded

The circumference of the driver pulley can be calculated

$$C_{driven} = 2\pi r = 2\pi \times 24.46\text{mm} = 153\text{mm}$$

If we divide the entire length of the belt by the length of the driver pulley we have the number of times that approximately the driver pulley rotates during one rotation of the belt. Considering constant velocity the time needed for the belt from the point B to the point A whose distance is $d_a = 219$ mm:

$$t_a = \frac{d_a}{R \times \text{RPM} \times 0.10472} = \frac{219}{0.02446m \times 300rpm \times 0.10472} \approx 300ms$$

And the time to run from A to B in clockwise direction is considering $d_b = 149$ mm

$$t_b = \frac{d_b}{R \times \text{RPM} \times 0.10472} = \frac{149}{0.02446m \times 300rpm \times 0.10472} \approx 200ms$$

The total time needed is about 500 ms and can be visible in the Trace shown in the following

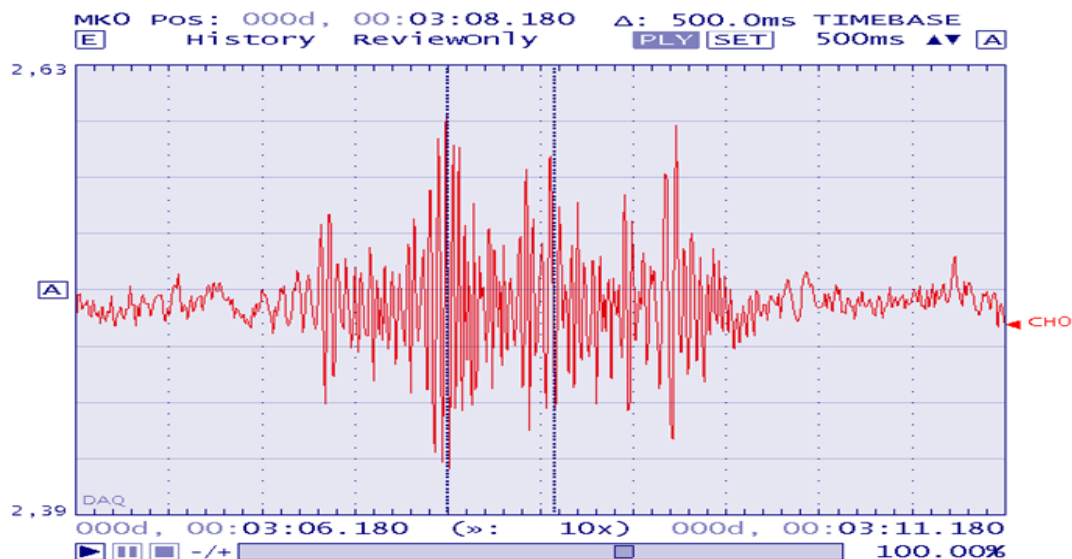


Figure 6.26 Delta of the entire vibration obtained at constant velocity

Is possible to show also the calculated time t_a and t_b where delta is the time between the vertical blue lines

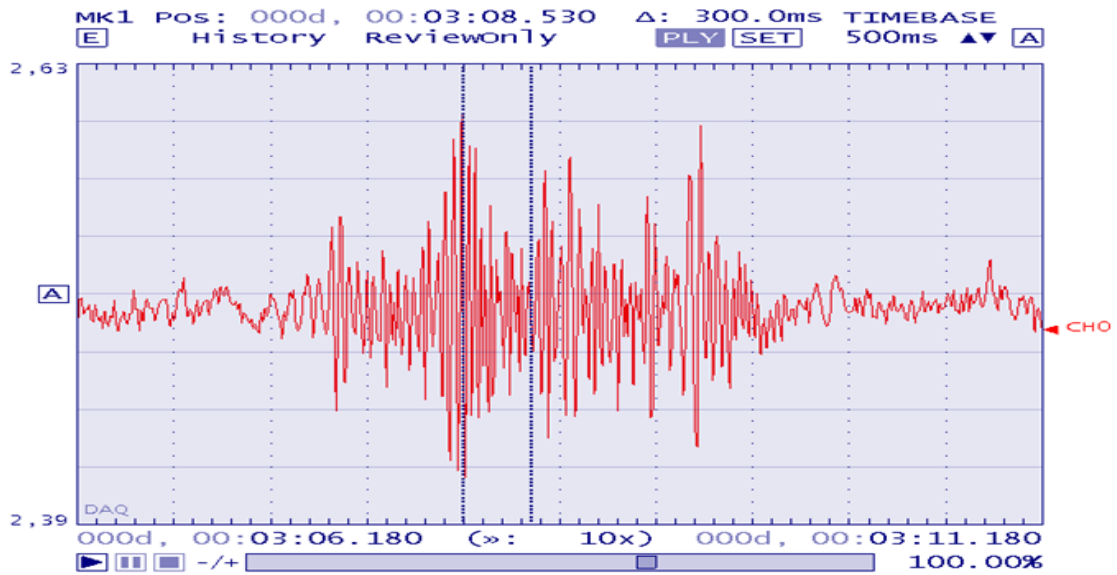


Figure 6.27 Delta of the first vibration obtained at constant velocity

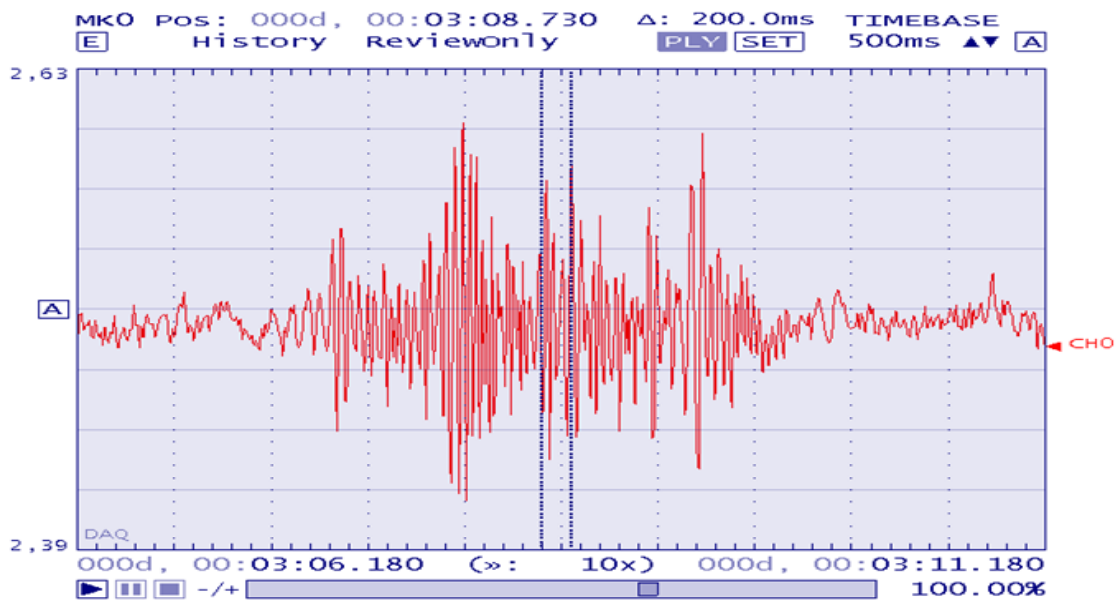


Figure 6.28 Delta of the second vibration obtained at constant velocity

6.3.1.2 An analysis of belt Vibration utilizing the Wavelet Transform

The time interval obtained and the shape of vibration can be seen also using the wavelet transform performing the analysis on the current of axis 3. As is possible to see the number of samples are 5×10^5 and the total time of acquisition is 215 s with a sampling time of 400 us.

As is possible to see the interval of time Δ in which the vibration is visible is 15s like the one seen previously in the trace coming from the sensor.

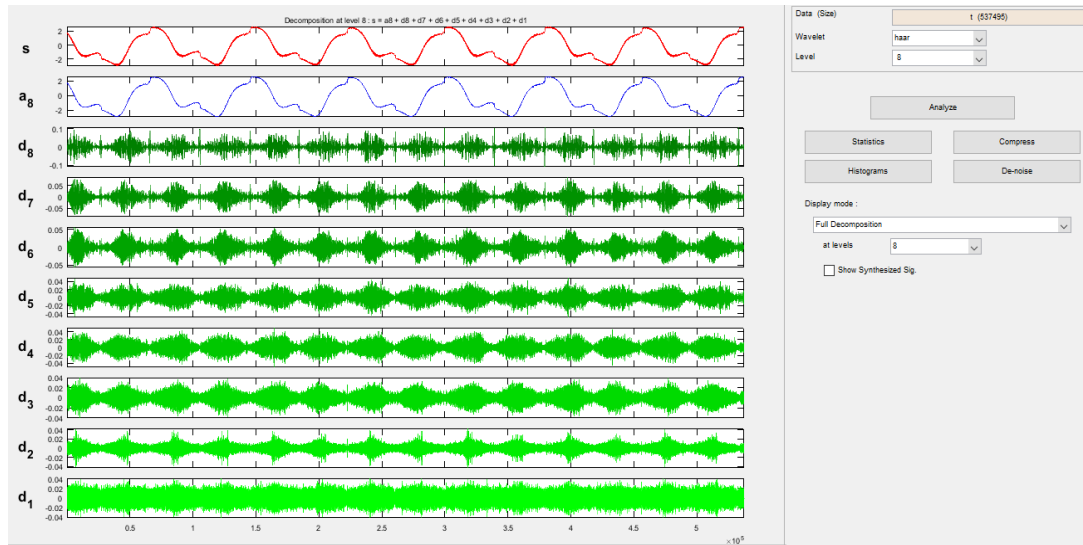


Figure 6.29 Haar 8 level wavelet transform used for the temporal analysis

From 1.22×10^5 until 1.84×10^5 for a sampling time of 400 us the time interval is shown in the following picture.

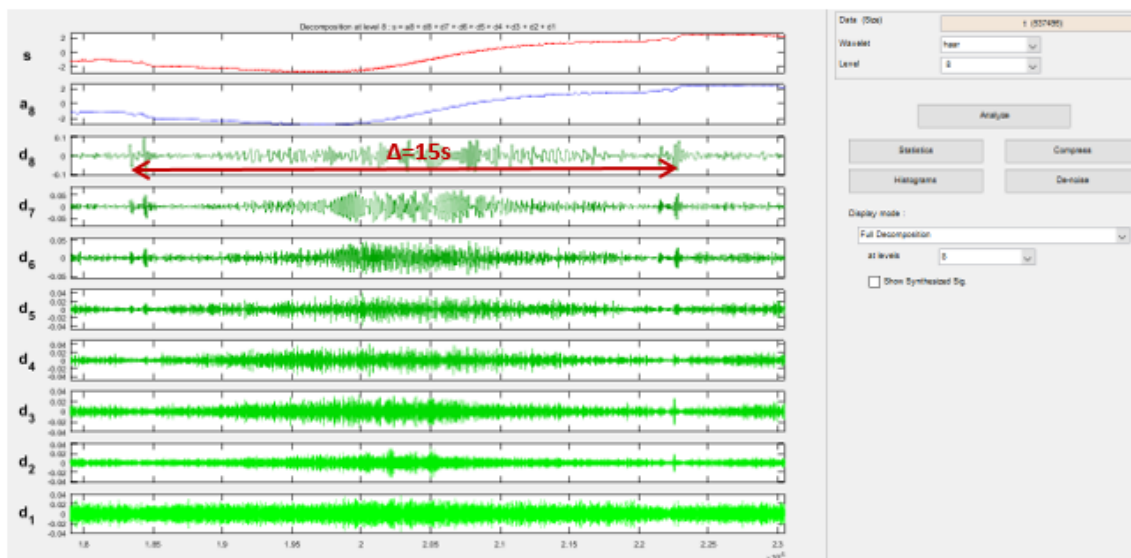


Figure 6.30 Interval of time between vibration confirmed

6.3.2 UNBALANCE

As explained in the test plan this type of fault is performed adding on the Driver Pulley a mass of 0.03 Kg In order to create a force of 50 N at the velocity of 3000

rpm (half of the max velocity allowed by the motor) added as is possible to see in the following pictures.

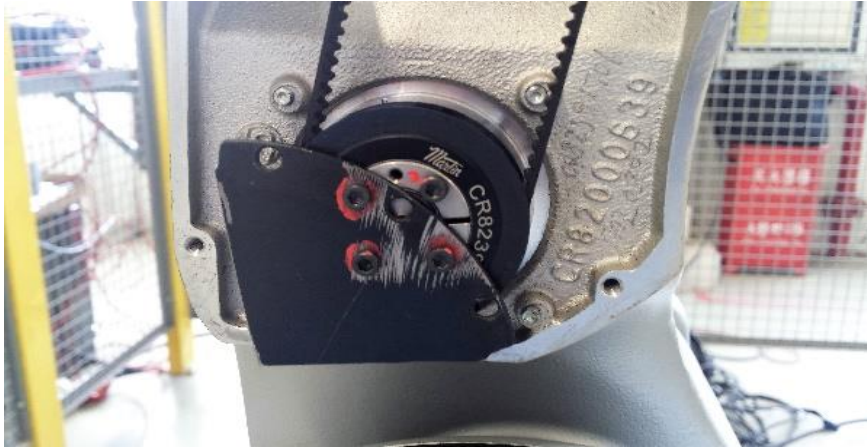


Figure 6.31 Mass added for the simulation of Unbalance

Is possible to see in the spectrum of the speed and of the voltage the effect of the mass added: as defined before. For all types of unbalance, the FFT spectrum will show a predominant $1 \times$ rpm frequency of vibration. Vibration amplitude at the $1 \times$ rpm frequency will vary proportional to the square of the rotational speed. It is always present and normally dominates the vibration spectrum

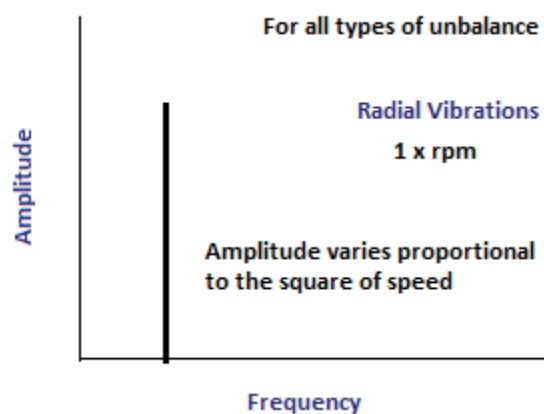


Figure 6.32 FFT in case of Unbalance

In the following picture the comparison in the spectrum of the speed of axis 3 in the first case 300 rpm or 5% of the maximum speed and in the second case 4500

rpm 75% of the maximum speed. In Figure 6.32 in the main frequency 5 Hz is evinced.

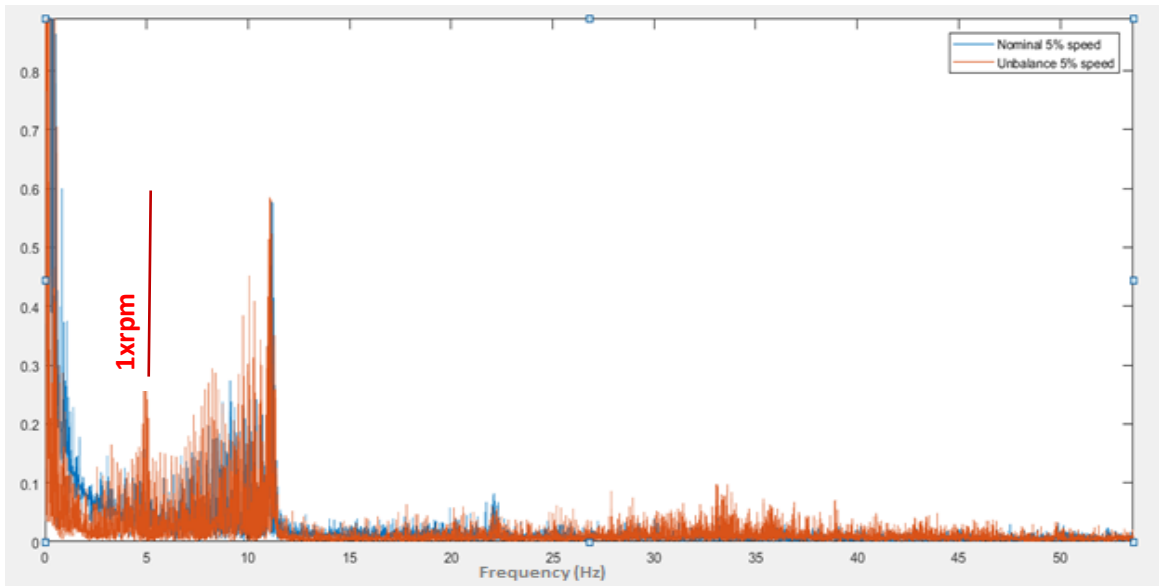


Figure 6.32 Comparison in the spectrum of the speed with 5% of the maximum speed

The same phenomenon is shown in the Figure 6.33 where the maximum speed considered is 4500 rpm and so the frequency 75 Hz is evinced.

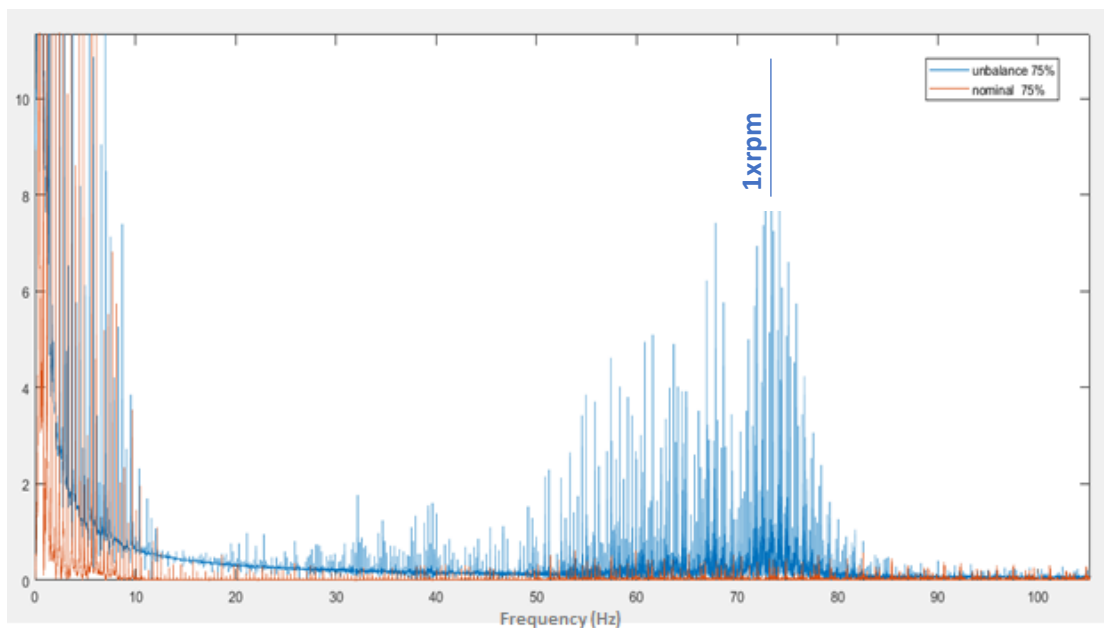


Figure 6.33 Comparison in the spectrum of the speed with 75% of the maximum speed

The radial vibration is also detected from an accelerometer placed in position described in the picture 6.5 b. As is possible to see the fft of the voltage shows the main frequency 5 Hz.

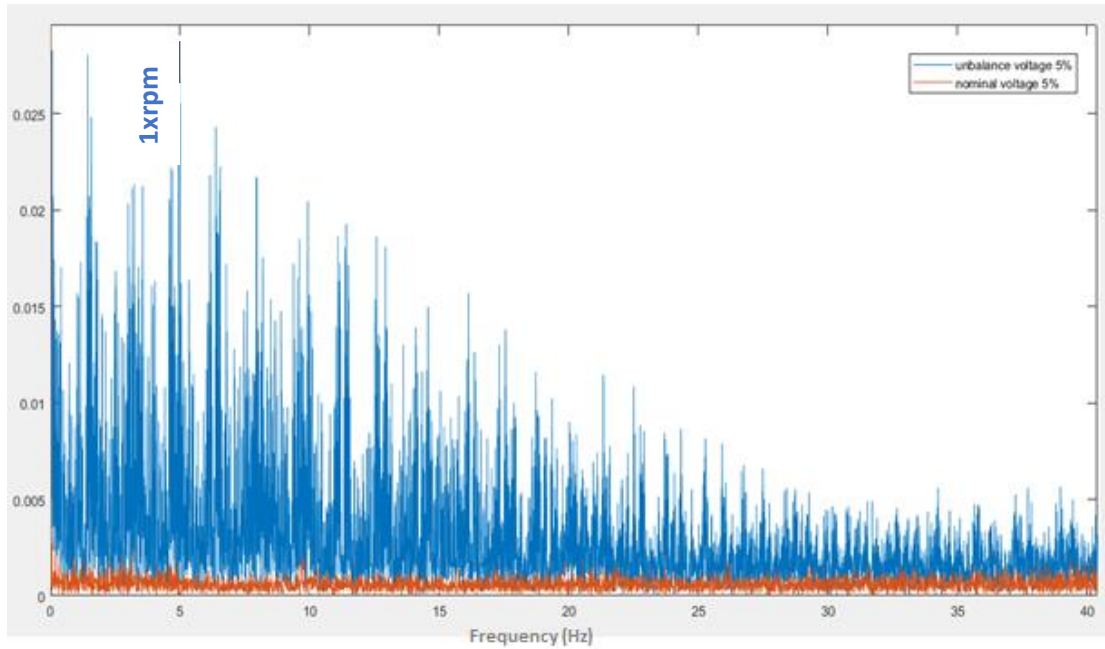


Figure 6.34 Comparison in the spectrum of the voltage with 5% of the maximum speed

In this case we can conclude that the fault can be detected directly from the velocity and can be confirmed by the analysis of the radial vibration carried out by means of the accelerometer.

6.3.3 INTERNAL ASSEMBLY LOSENESS

In case of internal assembly looseness the vibration will occur at frequency multiple $(1/2, 1/3) \times \text{rpm}$, along Radial direction

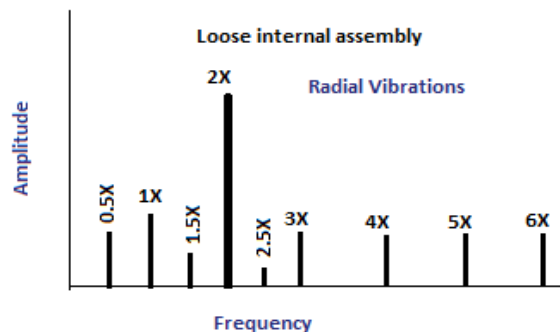


Figure 6.35 FFT in case of Internal Assembly Looseness

so is possible to capture this vibration by means of the accelerometer placed in position described in picture 6.5 b.

The results in the following Figure: in vibration are visible the 1.5, 2x, 2.5x, 4x frequencies.

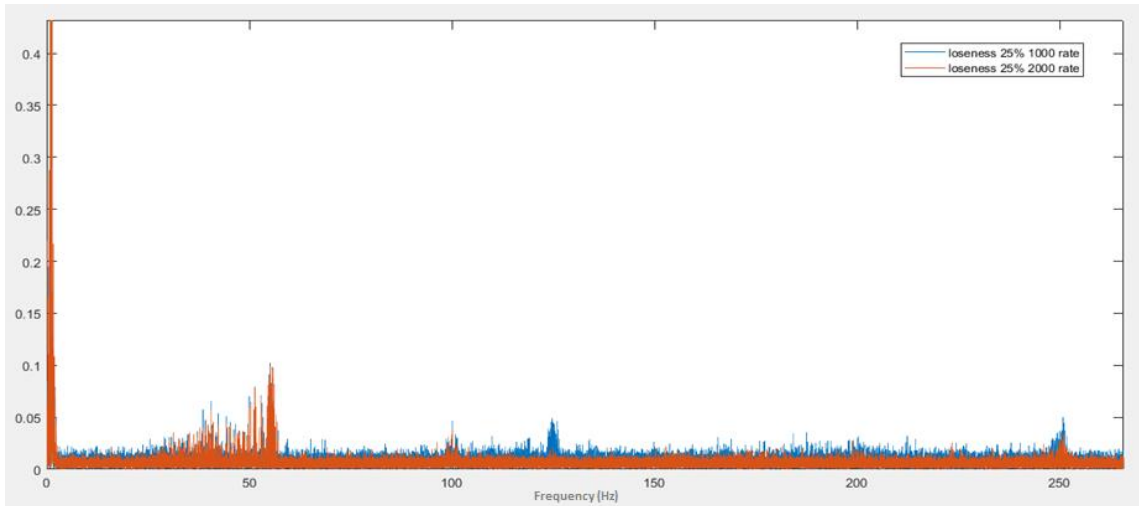


Figure 6.36 FFT of the voltage in case of Internal Assembly Loseness at 25% of the maximum speed: different rate are considered

In speed the behaviour looks like the unbalance case the frequency 1xrpm is visible in the following picture the case in which the speed is 75% of the maximum allowed.

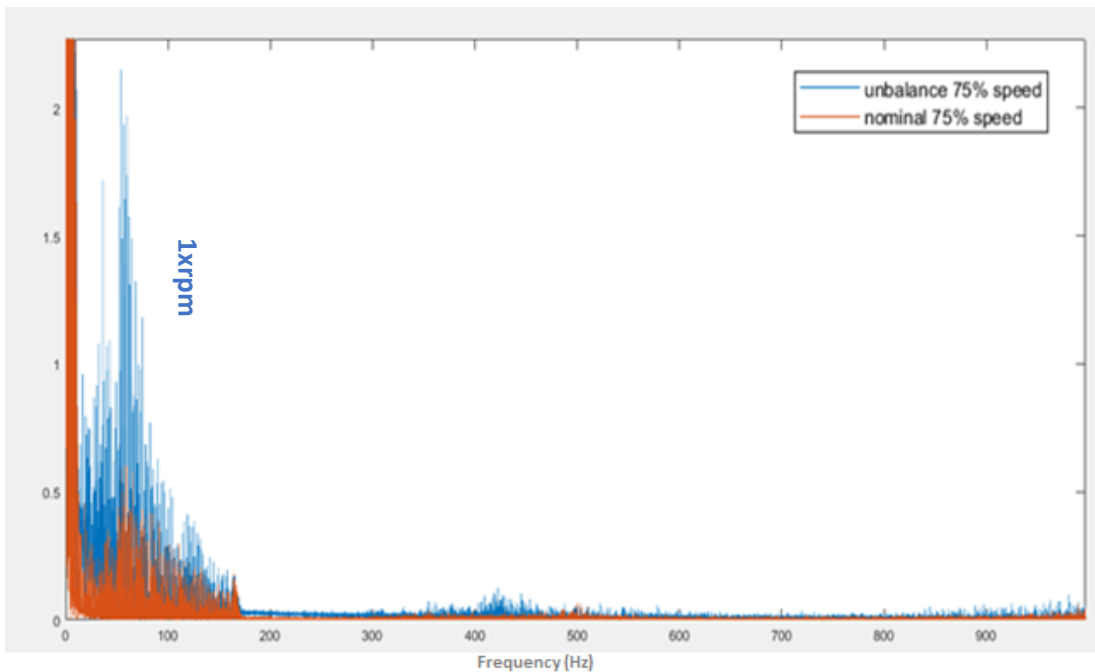


Figure 6.37 FFT of the speed in case of Internal Assembly Loseness at 25% of the maximum speed

7 CONCLUSIONS AND FUTURE WORK

7.1 CONCLUSIONS

In this thesis a data driven approach based on a vibration signature is used to analyze possible faults coming from a belt-based transmission for Comau Racer3 Manipulator.

The Vibration Signature is considered here as a *Feature extracted* used in the diagnostic step of the Health Monitoring Process described in Fig. 1.3.

The main goal achieved is the minimization of the use of sensors like accelerometer and displacement sensor trying to visualize the fault directly from the current and the speed.

As is possible to see in the previous chapter a spectral analysis of the current shows the same fault *Unbalance* detected first taking the data coming from the accelerometer and then analyzing the spectrum of the speed at different rate 5% and 75%.

The same analysis is performed in case of *Looseness* with again in parallel the use of an accelerometer.

In this thesis, a different methodology is used in case of non stationary fault where the FFT is not capable to detect non stationary signal component and the fixed window of the STFT generates a poor frequency resolution.

The trade off between time and frequency resolution is overcome by the use of the Discrete wavelet transform that is helpful for the analysis of a non stationary fault like the *Tooth shear*.

From the use of this Feature is possible to carry out a classification algorithm and start to develop basing on this feature a prognostic module to monitor and track the time evolution (grow) of the fault obtaining an accurate prediction of the remaining useful life (RUL) of a component.

All this process can be carry out loading this feature on the Software MoniCollector developed in Comau s.p.a and installed in China as discussed in the Chapter 1.

7.2 FUTURE WORK

Since early 1980's, various model-based approaches have been introduced to machine condition monitoring (Chen), mainly for the diagnosis of malfunctions in manufacturing and processing equipment. As a future development of this thesis the Model Based or a Model of Signal Based approach instead of the Data driven

one can be used. According to the first approach a comparison between the system output and the model one is performed and a good knowledge of the physics of the system is necessary. The tools used are: Kalman Filter, State Observer and so on.

In the second approach instead is required:

1. Not a perfect knowledge of the physics of the system
2. A parameter estimation algorithm

From the collection of data a possible mathematical model AR, ARX, ARMA, ARMAX can be selected and then the order performing a whiteness test on the error is determined. The following steps are the estimation of the parameter by means of the well known Least Square Method and the Validation of the model.

REFERENCES

- Analog Devices. (1980). In *Synchro and Resolver Conversion*. Boyes Ed.
- Antonino-Daviu, J., Jover, P., Riera, M., Arkkio, A., & Roger-Folch, J. (2007). *DWT analysis of numerical and experimental data for the diagnosis of dynamic eccentricities in induction motor, Mechanical Systems and Signal Processing*.
- Bicker, A. A. (2016). Fault diagnosis of Industrial Robot Bearing Based on Discrete Wavelet Transform and Artificial Neural Network. *International Journal of Prognostic and Health Management*.
- Bottero A., G. G. (s.d.). *Adaptive Control Techniques and Feed Forward Compensation of Periodic Disturbances in Industrial Manipulators*. Torino: Research and Development, COMAU s.p.a. Robotics, Italy.
- Campostrini, S. a. (1994). Identificazione e simulazione del modello dinamico di robot industriali.
- Chen, Y. (. (s.d.). Machine Condition Monitoring by Inverse Filtering and Statistical Analysis. *The Journal of Mechanical System and Signal Processing*, 177-189.
- Ferretti G., G. M. (1994). *Estimation of resonant transfer functions in the joints of an industrial robot*. Budapest.
- G. Ferretti, G. M. (1998, May). Compensation of Motor Torque Disturbance in Industrial Robot. *Proceedings of the IEEE International Conference on Robotics and Automation* , p. 2995-3000.
- Hanselman D. (1991). Techniques for improving resolver to- digital conversion accuracy. *IEEE Transactions on Industrial Electronics*.
- Hanselman D., J. Y. (1990). Resolver signal requirements for high accuracy resolver-to digital conversion. *IEE Transaction on Industrial Electronics*, 501-504.
- Hanselman D., J. Y. (1992). Torque ripple analysis in brushless permanent magnet motor drives. *International Conference on Electric Machines*, (p. 823-827). Manchester.
- P. A. Ioannou, J. (s.d.). *"Robust Adaptive Control"*. Prentice-Hall: Englewood Cliffs, NJ, 1989.

- Jayasal, P. (2008). Machine Fault Signature Analysis. *Article in International Journal of Rotating Machinery*.
- Kostropoulos, T. L. (1992). Utilising the Wavelet Transform in Condition-Based Maintenance: A Review with Application.
- Lewis, G. V. (2006). *Intelligent Fault Diagnosis and Prognosis for Engineering Systems*. John Wiley & Sons.
- Randall, R. B. (2011). *Vibration-Based Condition Monitoring*. Wiley .
- S. Mallat. (1999). *A Wavelet tour of signal processing*. Academic Press.
- S. Sastry, M. B. (1989). *Adaptive Control: Stability, Convergence and Robustness*. Prentice-Hall: Englewood Cliffs, NJ, 1989.
- Spong, M. a. (1989). *Robot Dynamics am*. John Wiley & Sons.
- Vetterli, O. R. (s.d.). Wavelets and signal processing. *IEEE SP Magazine*, p. 14-38.
- Wavelets and signal processing. (s.d.). *IEEE SP Magazine*, p. 14-38.

APPENDIX

Spectrum

```

function [spet,freq] = spettro(segnale,Ts)
%
% function [spet,freq] = spettro(segnale,Ts)
%
% Calcola lo spettro del segnale
%
% Ingressi:
% - segnale : segnale di cui si deve calcolare lo spettro in frequenza
% - Ts      : periodo di campionamento [sec]
%
% Uscite:
% - spet    : spettro del segnale
% - freq    : frequenze alle quali si riferiscono i campioni dello
spettro [Hz]
%
% Esempio d'uso:
% [spet,freq] = spettro(e,Ts);
% plot(freq,spet);

% Controllo degli ingressi
if (nargin < 2)
    fprintf(1,'Misure non sufficienti.\n');
end % if s(1)<s(2)
if (Ts < 0)
    fprintf(1,'Periodo di campionamento non corretto.\n');
end % if (Ts < 0)

% Interpretazione del segnale in ingresso
s = size(segnale);
if s(1)<s(2)
    segnale = transpose(segnale);
end % if s(1)<s(2)

% Calcolo della precisione di calcolo
N = length(segnale);
% N = 2^floor(log(N)/log(2));
% segnale = segnale(1:N);
Tmax = (N-1)*Ts;

% Calcolo dello spettro
spet = abs(fft(segnale));
freq = [0 : 1/Tmax : (N-1)/Tmax];
freq = transpose(freq);
freq = freq(1 : floor(length(freq)/2));
spet = spet(1:length(freq));
spet = spet/N*2;

```

High Frequency acquisition

```

getmoni_400us
%{
    la struttura MonisStruct.Data.value ha 3 vettori colonna che
    rappresentano la struttura creata con get_moni_400.pdl:

    -- grandezze di tipo reale
    vt_local_axmeasureTLP.fai_parIdFlt[1] := 412 -- axPtr->xf_p.posRef
: RIFERIMENTO CONTROLLO DI POSIZIONE
    vt_local_axmeasureTLP.fai_parIdFlt[2] := 422 -- axPtr->xf_p.trqPo-
sizVal : POSIZIONE ENCODER
    vt_local_axmeasureTLP.fai_parIdFlt[3] := 473 -- axPtr-
>xf_v.trqSatCmd : RIFERIMENTO DI CORRENTE

%}
%
close all
Time = (0:MonisStruct.Sampling:(MonisStruct.Samples-1)*MonisStruct.Sam-
pling)';
plot( Time, MonisStruct.Data(1).value)
hold on
plot( Time, MonisStruct.Data(2).value, 'r-')
legend('Motor Position Reference','Motor Position (encoder)')
xlabel('Time [s]'); ylabel('Motor position -- [Motor Rounds]');
grid on
%
figure
%
Time = (0:MonisStruct.Sampling:(MonisStruct.Samples-2)*MonisStruct.Sam-
pling)';
plot( Time, diff(MonisStruct.Data(1).value)/MonisStruct.Sampling*60 )
hold on
plot( Time, diff(MonisStruct.Data(2).value)/MonisStruct.Sampling*60, 'r-
')
legend('Motor Speed Reference','Motor speed (encoder)')
xlabel('Time [s]'); ylabel('Motor speed -- [RPM]');
grid on
%
figure
%
Time = (0:MonisStruct.Sampling:(MonisStruct.Samples-1)*MonisStruct.Sam-
pling)';
plot( Time, MonisStruct.Data(3).value)
legend('Motor Current Reference Iref')
xlabel('Time [s]'); ylabel('Motor Iref -- [Ap]');
grid on
%

```

Acquisition From Accelerometer

```

%% TH_TEST2SENSOR Code for communicating with a data acquisition de-
vice.
%
% This is the machine generated representation of a data acquisition
% session using the session-based interface. The data acquisition ses-
% sion
% comprises all the steps you are likely to take when communicating
% with
% your data acquisition device. These steps are:
%
% # Create a data acquisition session
% # Add channels specified by subsystem type and device
% # Configure properties
% # Run the data acquisition session
% # Disconnect from the device
%
% To run the saved data acquisition session, type the name of the
file,
% th_test2sensor, at the MATLAB command prompt.
%
% The file, TH_TEST2SENSOR.M must be on your MATLAB PATH. For additio-
nal information
% on setting your MATLAB PATH, type 'help addpath' at the MATLAB com-
mand
% prompt.
%
% Example:
%   th_test2sensor;
%
% Created on 18-Jun-2017 17:15:04.

%% Create a data acquisition session
daqSession = daq.createSession('mcc');

%% Add channels specified by subsystem type and device
daqSession.addAnalogInputChannel('Board0','Ai0','Voltage');

%% Configure properties
daqSession.Rate = 100;
daqSession.DurationInSeconds = 150;

%% Run the data acquisition session
[data,time] = daqSession.startForeground();
figure
data=data/0.09971
plot(time,data)

figure

%% Disconnect from the device
daqSession.release();

```



```
delete(daqSession);
clear daqSession;
```

Acquisition From Displacement Sensor

```
%% TH_DISPLACEMENTSENSORFINAL1 Code for communicating with a data ac-
quisition device.
%
% This is the machine generated representation of a data acquisition
% session using the session-based interface. The data acquisition ses-
% sion
% comprises all the steps you are likely to take when communicating
% with
% your data acquisition device. These steps are:
%
% # Create a data acquisition session
% # Add channels specified by subsystem type and device
% # Configure properties
% # Run the data acquisition session
% # Disconnect from the device
%
% To run the saved data acquisition session, type the name of the
file,
% th_displacementsensorfinal1, at the MATLAB command prompt.
%
% The file, TH_DISPLACEMENTSENSORFINAL1.M must be on your MATLAB PATH.
For additional information
% on setting your MATLAB PATH, type 'help addpath' at the MATLAB com-
mand
% prompt.
%
% Example:
%   th_displacementsensorfinal1;
%
%
% Created on 06-Jul-2017 14:50:09.

%% Create a data acquisition session
daqSession = daq.createSession('mcc');

%% Add channels specified by subsystem type and device
daqSession.addAnalogInputChannel('Board0','A1','Voltage');

%% Configure properties
daqSession.Rate = 2000;
daqSession.DurationInSeconds = 120;

%% Run the data acquisition session
[data,time] = daqSession.startForeground();
figure
plot(time,data)

%% Disconnect from the device
daqSession.release();
delete(daqSession);
clear daqSession;
```

